

Konstantin Schaab

---

# Robust Hierarchical Control of Electrical Power Grids with Renewable Energy Sources

kassel  
university



press

**Konstantin Schaab**

**Robust Hierarchical Control of Electrical Power Grids  
with Renewable Energy Sources**

This work has been accepted by the Faculty of Electrical Engineering / Computer Science of the University of Kassel as a thesis for acquiring the academic degree of Doktor der Ingenieurwissenschaften (Dr.-Ing.).

Supervisor: Prof. Dr.-Ing. Olaf Stursberg, University of Kassel

Co-Supervisor: Prof. Dr.-Ing. habil. István Erlich, University of Duisburg-Essen

Defense day: 26<sup>th</sup> January 2018

Bibliographic information published by Deutsche Nationalbibliothek

The Deutsche Nationalbibliothek lists this publication in the Deutsche Nationalbibliografie; detailed bibliographic data is available in the Internet at <http://dnb.dnb.de>.

Zugl.: Kassel, Univ., Diss. 2018

ISBN 978-3-7376-0498-7 (print)

ISBN 978-3-7376-0499-4 (e-book)

DOI: <http://dx.medra.org/10.19211/KUP9783737604994>

URN: <http://nbn-resolving.de/urn:nbn:de:0002-404996>

© 2018, kassel university press GmbH, Kassel

[www.upress.uni-kassel.de](http://www.upress.uni-kassel.de)

Printed in Germany

# Contents

<b>Summary</b>	<b>v</b>
<b>I. General Introduction</b>	<b>1</b>
<b>1. Introduction and Contribution</b>	<b>3</b>
1.1. Introduction . . . . .	3
1.2. Solution Approach and Contribution . . . . .	5
1.3. Outline of the Dissertation . . . . .	8
<b>2. Literature Review on Relevant Control Techniques for Power Systems</b>	<b>9</b>
2.1. Grid Stabilization by Single Components . . . . .	10
2.2. Multi-Component Control for Grid Stabilization . . . . .	14
2.3. Conclusion . . . . .	15
<b>3. Dynamic Models for Power Systems</b>	<b>17</b>
3.1. Grid Equations . . . . .	18
3.2. Synchronous Generator . . . . .	19
3.3. Wind Turbine based on DFIG . . . . .	21
3.4. Photovoltaic System . . . . .	24
3.5. Models of Faults and Exogenous Effects . . . . .	29
<b>II. Synthesis of Local Robust Controllers</b>	<b>31</b>
<b>4. Modeling Power Grids by Linear Parameter-Varying Systems</b>	<b>33</b>
4.1. Transformation into LPV Models . . . . .	34
4.2. LPV Modeling of a Synchronous Generator . . . . .	35
4.3. LPV Representation of a DFIG-based WECS . . . . .	38
4.4. LPV Formulation of a Photovoltaic System . . . . .	41
4.5. Discussion of the LPV Models . . . . .	43
<b>5. Robust Controller Synthesis for Linear Parameter-Varying Systems</b>	<b>47</b>
5.1. Polytopic System-Description . . . . .	47
5.2. Quadratic Stability . . . . .	49
5.3. Quadratic $\mathfrak{D}$ -Stability . . . . .	51

5.4. LMI Formulations for $H_\infty$ -Design . . . . .	52
5.5. LPV Controller Synthesis with Input Saturation . . . . .	53
5.6. Multiobjective Design of the LPV Controller . . . . .	57
5.7. Global Stability of the LPV controlled System . . . . .	57
5.8. LPV Controller Computation and Implementation . . . . .	60
5.9. Conclusions on the LPV-based Controller Synthesis . . . . .	63
<b>6. Simulation Results for Robust LPV Control</b>	<b>65</b>
6.1. Transient Stability of a Grid with WECSs and SGs . . . . .	66
6.2. Transient Stability with Extension to Input Constraints . . . . .	70
6.3. Transient and Voltage Stability by a Photovoltaic System . . . . .	71
6.4. Voltage and Transient Stability by WECSs and SGs . . . . .	76
6.5. Discussion on the LPV-controlled System . . . . .	79
<b>III. Grid-Wide Coordinating Control</b>	<b>81</b>
<b>7. Model Predictive Control for the LPV-Controlled System</b>	<b>83</b>
7.1. Literature Review of MPC . . . . .	84
7.2. Prediction Model . . . . .	88
7.3. MPC for the LPV-Controlled System . . . . .	92
7.4. MPC with Adapted Sampling Times . . . . .	97
7.5. Discussion of the Grid-Wide Coordinating Controller . . . . .	99
<b>8. Simulation Results for the MPC</b>	<b>101</b>
8.1. Voltage Control by MPC . . . . .	103
8.2. Voltage Control by MPC with an Extended Number of Inputs . . . . .	107
8.3. Size of the Optimization problem and Computation Time . . . . .	109
8.4. Conclusion . . . . .	111
<b>IV. Conclusion</b>	<b>113</b>
<b>9. Conclusions and Future Research</b>	<b>115</b>
9.1. Conclusions . . . . .	115
9.2. Future Research . . . . .	117
<b>Appendix A. Simulation Parameters</b>	<b>119</b>
A.1. Parameters of the Simulations in Chapter 6 . . . . .	119
<b>Notation and Acronyms</b>	<b>123</b>
<b>References</b>	<b>131</b>

# Summary

The growing integration of renewable energy sources into power grids increases the fluctuations of quantities such as active and reactive powers, voltages, and frequencies - these fluctuations may eventually lead to instabilities, possibly cursing to shutdown and potentially reduced availability of electrical power. The standard approach to stabilizing control of electrical power grids is to start from the nominal operation mode, linearize the dynamics around this mode, and to design linear standard controllers locally for each generating component. This procedure may become insufficient for larger shares of renewables, since the fluctuations can lead to considerable deviations from nominal operation thus rendering the use of controllers designed for linearized models inadequate. Furthermore, the controllers of the involved energy sources are typically designed separately and without considering the stability of the complete grid.

This work proposes a multi-level controller approach for power systems, which ensures robustness against changing operating points and fluctuating power sources. On the lower level, the system is decomposed into smaller subsystems, each modeled as a linear parameter-varying system (LPVS), i.e. the LPVS representations of synchronous generators, the wind turbines and photovoltaic systems are proposed. With this technique, the fluctuations and nonlinearities of the components are mapped exactly into variations of the parameters of the LPVS. The varying parameters also account for fluctuations of the connected grid components. The LPV technique allows a decentralized synthesis of locally robust controllers stabilizing for considered ranges of parameters. The synthesis is realized by semi-definite programming. Existing techniques for LPV controller synthesis are tailored to decentralized control of power grids and extended to the handling of input constraints in this work. Since the same modeling and controller technique is applied to the three types of grid components, a truly unified controller approach is realized, ensuring the stabilization of the whole grid. The multi-objective approach allows the simultaneous control of the rotor angle stability, as well as the (local) voltage control, while damping grid oscillations.

In order to realize global voltage control, a high level controller is added, which is provided as model predictive controller (MPC) used to coordinate the low-level LPV controllers. Based on the prediction of the system behavior, optimal inputs for a predefined horizon are computed for control objectives formulated in terms of a cost function to be minimized. Due to the use of existing discrete-time models for the prediction, the MPC naturally accounts for physical limits of the system. Furthermore, constraints can be implemented easily into the MPC, providing com-

pliance to e.g., rules stemming from the grid code. To account for differently fast dynamics occurring for power systems, an adapted scheme of sampling times is used.

The effectiveness of the proposed overall approach is demonstrated for several simulations of benchmark systems. It is shown that, compared to conventional control structures, significantly improved performance of the power system can be achieved. By the use of the proposed framework, robustness against diverse fluctuations and grid faults can be realized, while stability of the complete system is ensured.

## **Acknowledgments**

First of all, I thank my supervisor Prof. Dr.-Ing. Olaf Stursberg for the opportunity to do research on the control of electrical power systems. I am grateful for the freedom that he gave me and his great guidance.

I also would like to thank the complete team of the Institute of Control and System Theory, where the research for this thesis was conducted. Especially, I would like to thank Prof. Dr. rer. nat. Arno Linnemann for the fruitful discussions and for his support for all questions regarding control. Furthermore, I am grateful for the financial support by the DFG through the project ROCS-Grid and by the EU through the H2020-project UnCoVerCPS.

Finally, I would like to thank my family for the encouragement and, in particular, I thank my wife Viola for the love and enduring support during the past years.

**Part I.**

**General Introduction**



# 1. Introduction and Contribution

## 1.1. Introduction

Electrical power grids experience, in many countries, a continuous shift from centralized power generation by a few large power sources to decentralized generation through many sources of renewable energy. While a few decades ago the main share of injected powers were generated by the synchronous generator, the share of injected powers using wind and solar irradiation as a power source are rapidly growing. The increasing share of renewable energy leads to an increase of uncertainties of the availability of energy, driving the grids closer to stability limits, and making them more vulnerable to disturbances [2]. An exemplary illustration of a power system considered in this work is given in Fig. 1.1. The blocks represent grid subsystems of different type, i.e. with different dynamics, inputs, states, interconnections, and specifications. Several instances of any shown type of power generators and consumers on different voltage levels typically exist. The transmission grid in between may have a large number of buses, transformers, and transmission links with the generators and consumers. Points of control are marked by  $U$ , the presence of uncertainties (e.g. varying profiles of wind or solar irradiation, or consumption loads) are denoted by  $W$ , and  $S$  indicates possible switches of transmission lines (e.g. in case of failure), or the (de-)activation of a subsystem. The three main generating units are the conventional power plants using the synchronous generator, the wind power plant, and the photovoltaic power plant. Due to their importance, these three units will be in the focus of this work. Growing attention in research is also paid to flexible AC transmission systems (FACTS), and storage devices in order to improve grid stability. With these devices the capability of a grid to transfer power can be improved [21]. However, the focus of this work is the improved control of generating units for grid stabilization, as an alternative to the integration of very costly devices such as FACTS. Thus, FACTS and storage devices will be not further considered.

A large disturbance, like a link failure or the switch to a redundant node / device, may cause electromechanical oscillations propagating through the grid, or even worse, the synchronous generators may lose synchronism requiring a shutdown. Ensuring stability has always been a great concern in power system operation. Due to the complexity of grids, several (interdependent) stability categories were introduced [42]: *frequency*, *rotor angle* and *voltage stability*. The rotor angle stability (also called transient stability) ensures that the synchronous generators remain syn-

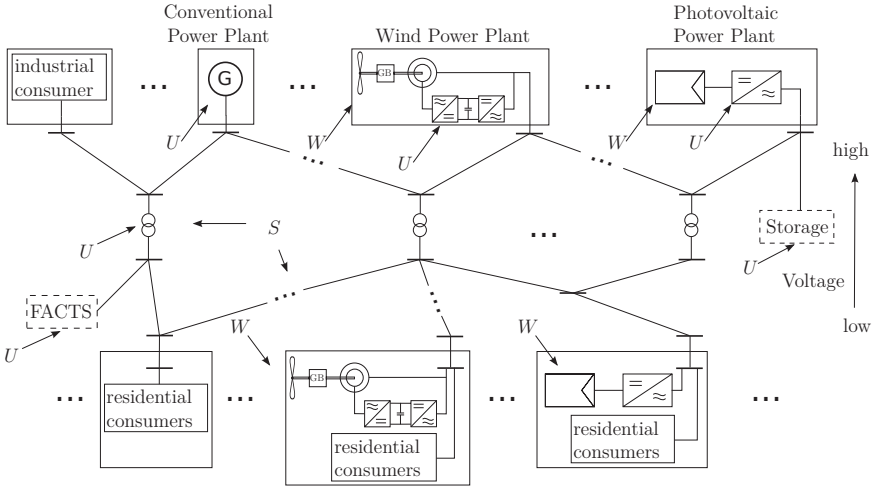


Figure 1.1.: Example of an electrical power grid with distributed generation.

chronous after grid faults and that electromechanical oscillations are damped down in a reasonable time. The frequency stability is concerned with keeping a certain frequency within the grid after e.g. load changes, while voltage stability is concerned with the restoration of a certain voltage level after faults or changing operating conditions.

Although the stability categories are physically interdependent, the respective standard controllers of power system components are often designed individually concerning only one single control objective. Thus, poor coordination between controllers of one system can lead to performance degradation or even to system failure [32]. The rotor angle is a variable commonly associated to synchronous generators. However, sources of renewable energy may have a significant impact on transient stability. These sources do not bear the synchronizing forces of synchronous generators, being the main stabilizing force within a power grid [30, 38]. The standard approach for designing the local controllers attached to the generating units is to: (i) linearize the local dynamics of the generating node around a nominal operating point, (ii) assume that all connected nodes stay in their nominal operating point, (iii) design the local controllers of standard LTI type parametrized for nominal operation. An example following this scheme is the power system stabilizer (PSS) for the synchronous generator. However, the separated local design of controllers for single linearizations of the local dynamics does not provide robustness against transient effects propagating through the grid and against fluctuations arising from the varying power sources of renewables. Furthermore, the controllers for each com-

ponent are designed without regard to each other, while having different impacts on the power system stability.

The separated control of different stability categories, and the different handling of the generating units is motivated by the complexity and variety of power systems. Each of the dynamic components is modeled by first order differential-algebraic equations (DAE). Thus, the complete power system can be represented by collecting the differential and algebraic equations of grid components and the grid, leading to a large system of the form:

$$\dot{x}(t) = f(x(t), z(t), u(t)), \quad (1.1)$$

$$0 = g(x(t), z(t), u(t)), \quad (1.2)$$

where  $x \in \mathbb{R}^{n_x}$ ,  $z \in \mathbb{R}^{n_z}$ , and  $u \in \mathbb{R}^{n_u}$ , are the vectors of  $n_x$  differential variables, of  $n_z$  algebraic variables, and of  $n_u$  inputs. The functions  $f(x(t), z(t), u(t))$  and  $g(x(t), z(t), u(t))$  are often nonlinear (as it will become obvious in Ch. 3, Dynamic Models for Power Systems).

Thus, the challenges of power system control arise from the system size, the structure, and the nonlinear models involving several different timescales. Using one centralized model of a lumped grid model is not amenable to techniques for control and analysis. Thus, the proposed approach developed in this work employs principles of decomposition and hierarchy, and will be sketched next.

## 1.2. Solution Approach and Contribution

As elaborated above, the behavior of future power systems is characterized by a degree of transient behavior and extent of fluctuations, which renders an isolated consideration of the different types of stability and a focus on local disturbance rejection around static operating points unsuitable. In this work, the overall goal of control design for power systems is thus to stabilize the system in the sense of Lyapunov<sup>1</sup>, such that the controlled system reaches steady states for the rotor angle, the frequency, and the voltage in conjunction. However, the control of the voltage to certain voltage levels after changing operating conditions is treated separately in this work. Thus, the terms rotor angle stability and transient stability are used to indicate stability of the power system after grid faults and changing operating conditions. The term voltage stability is used to indicate that the voltages are controlled to predefined values, while grid stability is ensured. The control approach has to explicitly account for differing operating points, while stabilizing the system after severe grid faults and handling the complexity arising from the system size appropriately. These control objectives are to be achieved by multi-objective controllers for the three considered types of subsystems, i.e. synchronous generators (SG), wind energy conversion systems (WECS), and photovoltaic systems (PVS).

<sup>1</sup>The exact mathematical definition of the stability used in this work is provided in Ch. 5

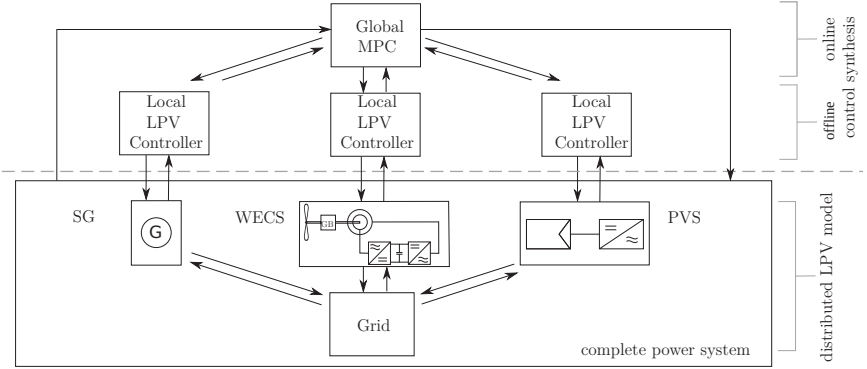


Figure 1.2.: Distributed and hierarchical control structure, to be developed in this work (SG: synchronous generator, WECS: wind energy conversion system, PVS: photovoltaic system).

Fig. 1.2 sketches the solution approach proposed in this work and it is explained next:

- A modularized version of an overall model according to (1.1) and (1.2) is defined by partitioning the grid into subsystems. To enable the synthesis of local controllers for any subsystem contained, the subsystem models are transformed into continuous-time linear parameter-varying system (LPVS) representations. One advantage of the LPVS is its simple structure which is very similar to the linear system description. The varying parameters allow accounting for nonlinear dynamic effects during the transition between different operating points, or for changing values of wind, solar irradiation, or changing power system conditions. Moreover, the LPVS allows handling of subsystem interconnections by parameters which fluctuate within defined ranges. In this work, exact LPV representations of the original nonlinear models of the considered subsystems are derived. The resulting parametrized linear dynamics enables the use of a tailored optimization technique for controller synthesis for the lower layer control, which can be implemented easily.
- For the latter, offline parametrized feedback controllers for stabilizing the subsystems are synthesized for any value of the parameters within the specified ranges. This ensures robustness against the parameter changes. For synthesis, the solution of semi-definite programming problems using linear matrix inequalities (LMIs) for constraint representation is used. The proposed scheme is truly unified for the three types of generating units and allows to conjunctively address rotor angle stability and voltage stability, while achieving good damping of oscillations. Stabilizing the LPVS for all parameters implies the

stabilization of the original nonlinear system. Furthermore, it is shown that by this modularized control, the complete system can be stabilized.

- Typically, for power systems, the inputs have to be constrained. The derived LPV models allow using existing controller synthesis techniques for polytopic system representations. However, the existing technique for the LMI-based controller synthesis has to be extended to tailored handling of inputs constraints.
- The upper layer control aims at accounting for the larger transients arising for power grids. It realizes the necessary adaptations in energy transmission, if the power availability from renewables or changed loads requires the transition into new operating points, i.e. for objectives that can not be controlled locally and are connected to the balance of powers. Voltage control within the complete grid is such an objective and is considered in this work. Control strategies for this purpose are computed online and have to consider the global grid behavior. The use of model predictive control (MPC) appears to be a good choice as it has the advantage that it can be formulated for a variety of different types of systems, including LPVS or systems described by DAEs.

The idea behind MPC is the use of predictions of the system behavior based on existing discrete-time models. An optimal input is computed by solving an optimization problem to minimize performance functions, which measure how well the control objectives are achieved for a future horizon. Thus, the MPC naturally accounts for the question to which extent sources of renewable energy are usable to actively stabilize the grid. One advantage of MPC is that constraints (as e.g. motivated by rules of the grid code) can be implemented easily.

- While many different MPC formulations exist, in this work, an integrating framework is proposed to handle the local control loops, and the coordination between them. The underlying system is modeled by DAEs which explicitly consider the local control loops. The challenge for the global controller is the handling of the different timescales of the control layers, and of the different timescales arising from the different control objectives and components. In this work, a new MPC scheme is proposed that considers the different dynamics by using adapted sampling times for the discrete-time MPC, while accounting for the local LPV-controlled subsystems. Furthermore, the control objectives are formulated in terms of algebraic variables (e.g. the bus voltages of the power system), while guaranteeing stability.

The discussed controller techniques are validated on several simulation scenarios throughout this work.

### **1.3. Outline of the Dissertation**

In the next chapter, existing literature on control techniques for stabilization of power systems by local controllers of the three types of grid components is reviewed, i.e. the local control of the SG, the WECS, and the PVS. The considered control objectives are transient stability and multi-objective control of voltage and transient stability. As it is the aim of this work to introduce a unified controller technique for the three types of components, controller techniques are discussed which use the same approaches for at least two types of components. In Ch. 3, selected existing models for power systems are presented, including models for the three types of components and some controllers, later used for comparison. After that, the exact LPV representations of the SG, the WECS and the PVS are derived in Ch. 4. LMI-based LPV controller synthesis for the derived LPVS is explained in Ch. 5, and extended to the handling of input constraints. The LPV controllers are validated based on simulations for different scenarios in Ch. 6. In order to achieve voltage stability for the complete grid, a centralized MPC for the LPV-controlled system is introduced in Ch. 7, followed by a simulative validation of the multi-level controller in Ch. 8. Finally, a discussion on the derived multi-level controller approach is presented and an outlook on future research is provided in Ch. 9.

## 2. Literature Review on Relevant Control Techniques for Power Systems

Numerous publications exist in the broad field of control of power systems. Most of the results concentrate on the control of one type of component, and on one stability category. In the case of WECS and PVS, many results focus on obtaining maximized active power. For the PVS, for example, most results exist which focus on energy supply by tracking the maximum power point (MPP) [106]. Others focus on the improvement of the capability to withstand critical grid conditions. The active stabilization of the grid by the WECS, or the PVS is usually not in the focus, which implies that this is accomplished by the SG. Thus, the ability of the renewables to stabilize the grid may be not fully exploited. In this chapter, the review is grouped in results in which the SG, the WECS, and the PVS are controlled separately and in results in which the three types of components are controlled conjunctively. The common objective of the two groups is the design of controllers, which are robust against changing operating conditions. For the SG, the considered control objectives are the active stabilization of the grid in terms of transient stability combined with damping of grid oscillations. Furthermore, results on conjunctive control of transient stability and voltage are considered. For the PVS and the WECS, only a small number of results exist in which these components are utilized to actively stabilize the grid. For the two types of components, approaches with improved ability to withstand grid faults, while introducing robustness against changing renewable energy sources are discussed. Irrespective of the named control objectives, approaches using the LPV representation of the components are reviewed. This is motivated by the fact that the unified representation of the SG, the WECS, and the PVS as LPVS is a main contribution of this work.

As already mentioned, one contribution of this thesis is the expansion of existing LPV controller synthesis techniques to handling of input constraints. The review on techniques for handling input constraints is presented in the respective section in Ch. 5. Furthermore, the LPV controllers are coordinated by a centralized controller to control the voltage within the complete grid in the range of seconds and minutes. The approach to ensure global voltage stability is based on the MPC, introducing a new controller technique in Ch. 7. The review on centralized MPC for power systems, for LPVS, and for system described by DAEs is presented in that chapter.

## 2.1. Grid Stabilization by Single Components

### Stabilization through Synchronous Generators

The focus in this section is on rotor angle stability (the so-called transient stability) and on voltage stability. Transient stability refers to the ability of synchronous generators to stay in synchronism after a large disturbance. The standard controller for this purpose and for achieving good damping of electromechanical oscillations is the so-called power system stabilizer (PSS). For the control of the voltage, a so called automatic voltage regulator (AVR) is used. The AVR and the PSS are used as reference controllers for the SG in this work and are detailed in the next chapter. The standard method of designing PSS and AVR is based on modeling synchronous generators as LTI-systems, restricting the operability to close vicinities of a chosen point of operation. Uncertainties arising from changing operating conditions and neglected nonlinearities can deteriorate the control performance and lead to temporary shutdown of grid sections. To reduce these effects, different approaches for robustification have been proposed in the past, see [24] for an overview of handling nonlinearities and parameter changes.

First, robust controllers to improve transient stability while damping oscillations are discussed: Measures to include damping of power systems by pole placement and LMI-based design are reported in [77, 76, 104], where the first reference is on synthesis of state feedback controllers, and the latter two on synthesizing output feedback controllers. The three approaches determine single robust controllers for the whole space of uncertainties, what can lead to rather conservative results. In addition, it is a drawback of these methods that they are based on linearization (and thus approximation) of the DAEs rather than formulating matrix polytopes by analytic expressions over the parameter space – [77] classifies finding a system description as matrix polytope containing all uncertainties as a difficult task, which is accomplished in this thesis. Furthermore, permanent faults or the change of operating points are not considered. In [59], partial feedback linearization (PFL) is used to achieve transient stability. First, the power system is partitioned into dynamic subsystems, i.e. only SGs are considered. Then, according to the PFL technique, each of the subsystems is partitioned in one internal and stable autonomous part, and in one part which can be controlled. The nonlinearities of the controlled subsystem are linearized (exactly) using feedback linearization. A linear controller is designed by using the technique of linear-quadratic regulators (LQR). In [58], the technique is extended to the handling of uncertainties of the parameters of the SG, as well as to grid uncertainties. Thus, the resulting decentralized controller is robust against grid changes, while ensuring transient stability. If all SGs are controlled by this technique, stability of the complete power system is ensured. However, other types of components than the SG and damping of oscillation are not considered.

Combined control for transient and voltage stability based on the technique of direct feedback linearization (DFL) is realized in [32]. One controller is designed

to control the rotor angle stability during a fault. In the post-fault period a global controller activates the voltage regulator. This type of controller cannot be designed flexibly enough to work sufficiently well for all grid structures, and asymptotic stability for the whole grid is not proven. While the coupling of the generator to the grid was modeled by bounded uncertain parameters, the damping of oscillations was not considered. In [28], the voltage controller loop restores the pre-fault voltage value and another loop ensures synchronism. However, the system performance is strongly dependent on estimation of system parameters and global stability is not discussed. In [51], excitation control based on the DFL technique is described and asymptotic stability is ensured based on Lyapunov functions. Other criteria, such as robustness, are not discussed.

As already mentioned, one promising technique to ensure robust operation of the controller is the synthesis based on LPVS, which is used in the course of this work and will be discussed next. The idea behind LPVS is to transform the nonlinearities and the system variabilities into varying parameters of the LPVS. Stabilizing the LPVS leads to a stabilization of the original nonlinear system.

In [74, 53, 52] the LPV technique is used to design robust controllers for the SG (and FACTS) to enhance rotor angle stability. The LPV model is derived using sets of linearized models around several operating points and interpolation in between. The success of this approximative method to gain LPVS of the SG and the FACTS is highly dependent on the gridding process as the models do not represent the exact original dynamics. In [34, 33], an exact polytopic model of the SG is derived by using analytic transformations, only. The derived model comprises the grid equations of a small example of the grid. Stability is guaranteed as long as the parameters stay in the prescribed ranges, making this concept robust against sudden and permanent changes. An application to larger grids does not appear possible, as the LPV model includes the algebraic equations of the complete grid, which can be complex for large grids. While all discussed LPV-based approaches only consider transient stability, none of the discussed papers includes control of WECS or PVS as well.

### **WECS as grid-stabilizing Component**

The results mentioned so far, focus only on control of SG. Results investigating the impact of WECS on transient stability show that WECS can withstand larger grid faults, or even stabilize the grid and attenuate oscillations [70, 30]. This work, is focussed on WECS based on doubly-fed induction generators (DFIG), being the type of WECS which represents a share of close to 50% of the wind energy market (at 2013) [14]. For this case, power system stabilization can be realized through control of the mechanical components (blade system, pitch system, and drive train) as well as the electrical parts (converter of the generator). It is well known that the latter approach is faster, as e.g. documented in the survey of techniques for power system damping in [20]. Existing approaches for damping oscillations for grids with WECS include the introduction of additive signals on the active and reactive power control

loop of the converter controllers [39, 25]. Such active and reactive power control loops are used as reference controllers for the WECS in this work and are detailed in the next chapter. Results exist in which the controllers for WECS are presented to improve rotor angle stability in case of system disturbances and to damp electromechanical oscillations. Due to faster reaction of the electrical components [20], only control techniques based on control of the electrical components rather than of the mechanical ones are reviewed. With the focus on DFIG-based WECS, the signal of the designed controller is added in [39] to the active power control loop of the standard DFIG converter controller to damp system oscillations. The signal is determined based on a controller which is strongly oriented to the PSS of an SG, including filters and PI controllers (see Ch. 3.2). Using an additive signal to the standard control loops as well, a good damping was achieved in [62] and [64] by the pole-placement technique. In all three cases, voltage control was not considered in particular, but is included in the standard control loops for reactive power. These techniques have the advantage of introducing only a single control signal added to the standard DFIG controllers, but the design is based on linearization and does not provide robustness against grid changes.

Again, the LPV-based technique may ensure robustness and has already been used in the context of WECS. Most of the LPV-based results in the literature are concerned with the damping of the inner mechanical oscillations, or focus on aerodynamic phenomena. Examples are the reduction of the fatigue load or the maximization of aerodynamic efficiency for fluctuating wind (e.g.[65]), rather than stabilization of the power system. An overview of LPV-techniques for WECS control is provided in [40]. Some results will be discussed nevertheless, considering the used LPV models of the WECS and their applicability to control for transient stability. The authors of [40] introduce an LPV-based anti-windup pitch control for a considerably simplified version of the DFIG dynamics. However, for transient stability, the dynamics of the DFIG can play a major role with potentially fast control responses in case of grid faults. The mechanical system of the WECS and active support of the grid by the WECS is not considered. In [98], an LPV controller of the rotor side converter is designed in order to control the electrical torque and the power factor of the DFIG-based WECS. The LPV controller is synthesized by using LMIs such that the closed-loop system is robust against the varying rotor speed and voltage dips at the point of connection to the grid. In [97], this approach is applied on a test platform, with a slightly different control objective, i.e. the electrical torque and the reactive powers are controlled. The closed-loop system can withstand certain grid faults but can not actively damp oscillations. Furthermore, the derived LPV model does not account for permanent changes within the grid. A robust (grid) frequency controller is presented in [102] and detailed LPV models of the mechanical parts and the electrical parts are derived. A robustification against grid changes is introduced by using  $H_\infty$  controller design with an auxiliary disturbance input. However, the model used for controller design comprises only the electrical parts of the WECS, ignoring the mechanical parts. Thus, a switching mechanism for

the controller is introduced to prevent the rotor speed of falling too low. Similarly, in [66] two LPV models for the mechanical and electrical parts are presented. One control loop for each set of equations is designed to minimize fatigue loads and to damp the electrical torque fluctuations. The controllers are synthesized by using an LMI-based  $H_\infty$ -technique. To the best of the authors knowledge, a unified LPV model of the WECS comprising electrical and mechanical parts for robust control of the power system in response to grid faults and for voltage control at the same time has not been presented so far.

### **Enhancement of Grid Stability through PVS**

A discussion on the impact of the PVS on the transient and voltage stability is discussed in [86] by reviewing existing results on this topic. In the case of voltage stability, no clear conclusion can be drawn whether the effect of a grid connected PVS is positive or rather negative. Concerning the transient stability, the impact appears to be rather negative [86]. This is not a surprise as most results focus on energy supply aiming at injecting the maximum available active power into the grid, following the MPP. Results on tracking the MPP represent the majority of the existing results on PVS control [106]. This control objective is often combined with controlling the injected reactive power to zero, i.e. control of the power factor close to unity. From the point of view of the PVS operator, this is the most cost-effective way. However, stabilizing effects of the PVS may be not fully exploited. Due to lack of results with the focus on (active) grid stabilization, results aiming at a reduced impact on the grid and robustness against changes of the grid, of solar irradiation and temperature are reviewed, as well. This review is focused on large-scale photovoltaic systems.

Many results aiming at the grid support by the PVS involve the use of a device for energy storage. In [93], for example, the PVS is combined with a battery. The DFL technique is used to linearize the system exactly, allowing the use of linear PI controllers. The bus voltage and the frequency of the grid can be controlled with this system. However, in this work, only results are considered, in which no additional devices are integrated. A control strategy for the PVS aiming at increased damping of power system oscillations is presented in [87]. The authors reuse existing controllers of the PVS (PI controllers for active and reactive power control) and introduce an additional signal to damp oscillations. The control is designed by using a minimax linear quadratic Gaussian control design based on the solution of Riccati equations. The model used for the controller synthesis is a linearized model of the complete considered power system around one operating point. Thus, stability is not guaranteed for changing operating conditions. Furthermore, due to the use of the complete power system for the controller design, a completely decentralized scheme with a set of local controllers is not realizable with this approach. To avoid linearizations around one or a few operating points, the DFL technique is used for the PVS in [47]. A robust state feedback controller is synthesized, which is robust

against changes of the solar irradiation and temperature. Robustness against grid changes and active support of grid stability are, however, not considered. In [60], the PFL approach is used for the PVS, leading to an exact system representation, which allows the use of linear controllers. The control objectives are the control of the DC-voltage and the grid current (aiming at the control of the reactive power to zero). This approach requires the exact knowledge of system parameters. This drawback is overcome by the same group in [61], by extending the PFL approach to modeling the parameter uncertainties. The resulting (linear) controller is robust against uncertain PVS parameters and changed solar irradiation and temperature. Furthermore, the approach can withstand large grid faults, demonstrated with a short circuit at the point of connection of the system. However, changing operating points of the grid (e.g. permanently changed line impedances) and interactions with other components are not considered. In [106], PVS are linearized using feedforward control. This resulting model is an exact and linear representation of the original PVS. The designed controller comprises PI controllers, which are robust against grid changes. The approach presented in [106] is used as the reference controller for PVS in this thesis and is detailed in the next chapter.

In all discussed (local) approaches for the control of the PVS, the active grid stabilization is not considered, i.e. grid oscillation are not actively damped by the PVS. To the best of the authors knowledge, approaches by other authors in which an LPVS representation of the PVS is used, comprising the panel and the inverter, do not exist.

## 2.2. Multi-Component Control for Grid Stabilization

As already mentioned, one of the objectives of this work is the use of unified robust controllers for different types of grid components. Important criteria for the review are that these controllers can be used for large power systems in a decentralized manner and that the used models account for the power sources of renewable energy, to be able to fully account for their variabilities. Three research areas exist, which use unified controllers for different types of components but do not fully match the named criteria. However, due to the large number of publications focusing on these areas and for the sake of completeness, they are mentioned next, without a review. After that, results which match the criteria are discussed.

One possibility for handling two different energy sources is by treating them as one energy system - often called a hybrid energy system. Such a system often comprises WECS and PVS. A review on hybrid energy systems can be found in [57]. As an example, the authors in [73] use MPC to control a system comprising the WECS and the PVS. The objective is to control the two devices such that the power demand is met. The controller outputs of the MPC are the injected active powers of the devices, which in turn are controlled by standard PI controllers to their nominal values. The use of hybrid systems does not allow a decentralized

operation of the WECS and the PVS as independent systems as they are treated as one system.

Numerous results consider the control of different units within small grids, the so called micro-grids. For example in [36], a micro-grid comprising PVS, WECS, batteries, transmission lines, and (dynamic) loads is controlled. The approach is designed such that the micro-grid can be operated in islanded mode, or connected to a large grid. In this example, a two level controller is proposed: the high level controller balances the active and reactive powers by defining the reference values for the WECS and the PVS. The low level controllers are used to control the desired reference values. The desired powers are mainly injected through the integrated batteries. The control strategy is based on a detailed model of the micro-grid. An application of the micro-grid approaches to large grids is not possible as they are tailored to only a small number of components.

Other groups concentrate on control of inverters, in general, as in [1] or [71]. Although, inverters are needed for the control of the WECS and the PVS, this general view on inverter control does not comprise models of the renewable energy sources, ignoring effects of changed wind or changed solar irradiation. The resulting simplified view on the WECS and the PVS does not allow to account for fluctuating energy sources.

Mahmud et. al used the same approach, i.e. the robust PFL technique, for the control of the SG (in [59] and [58]) and of the PVS (in [60] and [61]). The group shows that unified robust control with the same technique is possible. The PFL was also used in the context of a DFIG-based WECS by the authors of [16], showing the applicability of the technique to three different types of components. However, in the case of the WECS, the control objective is the damping of sub-synchronous control interactions, rather than transient stability. Changing the control objective to transient stability may require a different model. The existence of an autonomous part of the resulting model is not granted and has to be evaluated. Furthermore, the PVS is controlled only as an isolated system, without any transmission lines or loads involved in the simulation. Thus, interaction with other dynamic components and, in particular, effects caused by changing grid parameters are not considered.

To the best of the authors knowledge, these are the only results which aim at applying the same technique for the control of the considered three types of energy sources.

## 2.3. Conclusion

Most of the discussed results focus on control of one type of grid component, only, often based on simplified or approximative models. A multi-objective control approach for grid stabilization based on exact models which comprises robustness against grid changes, while ensuring grid wide stability, does not exist so far. These findings apply to the control of the SG, the WECS, and the PVS. Because a com-

pletely unified approach for the three components with the relevant control objectives does not exist, the grid wide stability can not be guaranteed by existing approaches for a power system comprising all three types of components.

Lastly, exact (not approximative) LPVS representations of the three types of components, which comprise all relevant dynamics of the systems do not exist. A unified modeling of the system as LPVS allows a unified robust control and is presented in Ch. 4.

# 3. Dynamic Models for Power Systems

A power system model comprises many different elements where even one single component can have dynamics with several different time constants. To handle the complexity of such a system, the phenomena to observe must be specified. Typically, very slow dynamics are considered constant and very fast dynamics are modeled with algebraic equations, while the most relevant dynamics are kept as states. The decision on how to treat these variables depends on the phenomena which are in the focus of the analysis. In this work, the stability categories transient stability and voltage stability are addressed. Thus, the power system model must include electromechanical phenomena [42]. The related models and equations are standard and are typically described in dq-coordinates (indicated by the indices  $d$  and  $q$  throughout this work) and in *per units* representation [41]. Taking the 9-bus system from [5] depicted in Fig. 3.1 as an introductory example, a power system comprises several dynamically modeled grid components such as FACTS, WECS and SGs (indicated by  $G_h$ ) at a bus with the index  $h$ . The remaining grid components of this example are the transformers  $T_h$ , the loads  $A$ ,  $B$ , and  $C$ , and, of course, the connecting lines of the grid. Following the introduced subdivision in very fast and very slow, the dynamically modeled grid components can be described by first order DAEs of the type

$$\dot{x} = f(x(t), z(t), u(t)) \tag{3.1}$$

$$0 = g(x(t), z(t), u(t)), \tag{3.2}$$

where  $x \in \mathbb{R}^{n_x}$ ,  $z \in \mathbb{R}^{n_z}$ , and  $u \in \mathbb{R}^{n_u}$ , are the vectors of  $n_x$  differential variables, of  $n_z$  algebraic variables, and of  $n_u$  inputs. The very slow dynamics appear as constant parameters within the functions  $f$  and  $g$  of these equations. Staying with the example, the fast electromagnetic dynamics of the connection lines and parts of the component dynamics are reduced to algebraic equations, while other variables remain states.

The fast local controllers in this work are decentralized and are applied to the dynamically modeled grid components. The components are coupled through the (algebraic) grid model, which will be discussed first. After that, detailed models of the three considered types of components are presented, i.e. of the synchronous generator (SG), of the wind energy conversion system (WECS) based on a doubly-fed induction generator (DFIG), and of the photovoltaic system (PVS). For each

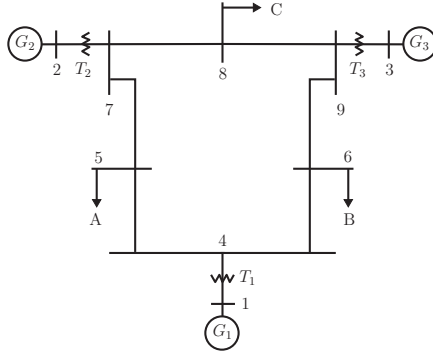


Figure 3.1.: Structure of the 9-bus-system.

plant typical controllers are described, which will be implemented for comparison to the controllers synthesized in this work. While several controllers are established in literature in the case of the SG and the WECS, for the PVS a controller is taken from [106]. The dynamic models and controllers presented in this chapter are only excerpts of a variety of different models and existing controllers (see [41] and [63]). However, the chosen models are well established and are appropriate for the studies of transient and voltage stability, and so are the chosen reference controllers.

Compared to the SG and the WECS, the PVS model is treated differently, due to the fact that the PVS introduce only electromagnetic rather than electromechanical behavior. From this perspective, the PVS can be considered as “very fast”. That is why the PVS is often modeled as a current source in studies of transient stability involving SGs, implying perfect controllers. In this work, however, the objective is the introduction of a unified and modular modeling and controller concept. Thus, a simplification of the PVS to algebraic variables or as a current source is avoided. For brevity, the dependency of the variables on time  $t$  is omitted in the sequel.

### 3.1. Grid Equations

In context of control objectives focusing on electromechanical phenomena, the grid is typically modeled with constant impedances. The grid connections are then encoded by so-called *admittance matrices*  $\bar{Y} \in \mathbb{R}^{r \times r}$ , where the bar  $\bar{\bullet}$  indicates a phasor. Thus,  $\bar{Y}$  represents the grid structure and can be used to calculate the four variables that characterize a bus with the number  $h$ : the voltage  $v_h$  and its phasor  $\varphi_h$ , and the active and reactive powers  $p_h$  and  $q_h$ . The admittance matrix is symmetric and the diagonal entries  $\bar{y}_{hh}$  equal the sum of all shunt and line admittances connected to the bus  $h$ . An off-diagonal entry  $\bar{y}_{hk}, k \neq h$  is set to 0 if the buses  $h$  and  $k$  are not connected. If they are connected,  $\bar{y}_{hk}$  is the

negative value of the sum of admittances connecting  $h$  and  $k$ . The bus voltages will be represented in a matrix  $\bar{V}$ , or in a vector  $\bar{v}^*$  respectively, where an asterisk  $\bullet^*$  represents the conjugate complex of the respective variable. Then, the complex-valued power  $\bar{s}_h = p_h + jq_h$ , consisting of active power  $p_h$  and reactive power  $q_h$ , can be calculated according to [63] from:

$$\underbrace{\begin{bmatrix} \bar{s}_1 \\ \bar{s}_2 \\ \vdots \\ \bar{s}_r \end{bmatrix}}_{\bar{s}} = \underbrace{\begin{bmatrix} \bar{v}_1 & 0 & \dots & 0 \\ 0 & \bar{v}_2 & \dots & 0 \\ \vdots & \vdots & \ddots & \vdots \\ 0 & 0 & \dots & \bar{v}_r \end{bmatrix}}_{\bar{V}} \underbrace{\begin{bmatrix} \bar{y}_{11}^* & \bar{y}_{12}^* & \dots & \bar{y}_{1r}^* \\ \bar{y}_{21}^* & \bar{y}_{22}^* & \dots & \bar{y}_{2r}^* \\ \vdots & \vdots & \ddots & \vdots \\ \bar{y}_{r1}^* & \bar{y}_{r2}^* & \dots & \bar{y}_{rr}^* \end{bmatrix}}_{\bar{Y}^*} \underbrace{\begin{bmatrix} \bar{v}_1^* \\ \bar{v}_2^* \\ \vdots \\ \bar{v}_r^* \end{bmatrix}}_{\bar{v}^*}. \quad (3.3)$$

The quantities  $p_h$  and  $q_h$  also appear in the equations of the dynamically modeled grid components and have values which are consistent with them, see below. To simplify notation, the index  $h$  is only used for those variables, which identically appear in the bus equations (3.3) to connect the respective components to the grid. Loads and transformers are typically modeled as constant impedances.

## 3.2. Synchronous Generator

Several well established and detailed models exist for SG with up to eight states. Regarding transient stability, the SG connected to a bus  $h$  can be modeled using the three states rotor angle  $\delta$ , the angular velocity  $\omega$ , and the transient voltage  $e'_q$ . The dynamics of  $\delta$  is governed by the difference between  $\omega$  and the reference frequency  $\omega_b$ , while  $\omega$  is determined by the difference between the mechanical torque  $\tau_m$  and the electrical torque  $\tau_e$  (an algebraic variable). When focusing on transient stability, the dynamics of the SG is very fast and  $\tau_m$  can be considered to be quasi-stationary compared to changes of the other variables. The remaining machine parameters  $\Omega_b$ ,  $D$ ,  $H$ ,  $r_a$ ,  $x_d$ ,  $x'_d$ , and  $T'_{dO}$  are the base synchronous frequency, the damping coefficient, the inertia constant, the armature resistance, the d-axis synchronous reactance, the d-axis transient reactance, and the d-axis open circuit transient time constant. The differential equations of the states then follow to [63]:

$$\dot{\delta} = \Omega_b(\omega - \omega_b), \quad (3.4)$$

$$\dot{\omega} = \frac{1}{2H}(\tau_m - \tau_e - D(\omega - \omega_b)), \quad (3.5)$$

$$\dot{e}'_q = \frac{1}{T'_{dO}}(-e'_q - (x_d - x'_d)i_d + v_f). \quad (3.6)$$

The field voltage  $v_f$  is the input of the machine, while the algebraic variables are the machine voltages (dq-transformed)  $v_d$  and  $v_q$  as well as the machine currents  $i_d$

and  $i_q$ . These quantities are determined by the following equations:

$$0 = \tau_e - (v_d + r_a i_d) i_d - (v_q + r_a i_q) i_q, \quad (3.7)$$

$$0 = v_q + r_a i_q - e'_q + x'_d i_d, \quad (3.8)$$

$$0 = v_d + r_a i_d - x_q i_q, \quad (3.9)$$

$$0 = v_d - v_h \sin(\delta - \varphi_h), \quad (3.10)$$

$$0 = v_q - v_h \cos(\delta - \varphi_h), \quad (3.11)$$

$$0 = p_h - v_d i_d - v_q i_q, \quad (3.12)$$

$$0 = q_h - v_q i_d + v_d i_q. \quad (3.13)$$

The algebraic variables assigned to bus  $h$  (namely the powers  $p_h$  and  $q_h$ , the bus voltage  $v_h$  and its phasor  $\varphi_h$ ) appear as introduced above.

### Standard Controllers - PSS and AVR

Many different controller schemes were proposed for synchronous generators (e.g. in [41], [63], [23]). Typically, the different types of controllers are synthesized for the control of one specific type of stability and are jointly operated. In the case of transient stability, a so called power system stabilizer (PSS) is used to stabilize the grid after faults and to damp oscillations. The input of the PSS may be the voltage  $v_h$ , the active power  $p_h$ , or the rotor speed  $\omega$ , which all may map oscillations - the latter is used in this work. The output of the PSS is the offset for the input of the so called excitation system which contains the so called automatic voltage regulator (AVR). The AVR controls the voltage of the bus the SG is connected to. The output of the excitation system is the field voltage  $v_f$ .

The resulting controller structure is depicted in Fig. 3.2. The washout filter of the PSS has the gain  $K_w$  and time constant  $T_w$ . The lead lag part for enhancing the frequency response has the time constants  $T_1$ ,  $T_2$ ,  $T_3$ , and  $T_4$  (PSS Type II in [63]). The simplified model of the excitation system consists of the regulator gain  $K_A$  and the regulator time constant  $T_A$  [90]. These controllers are synthesized based on linearizations around one operating point, with no guarantees for stability for changing operating conditions of the system.

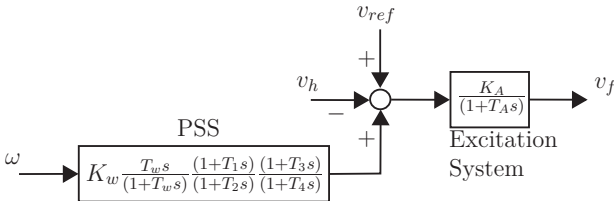


Figure 3.2.: Controller structure of the AVR and the PSS.

### 3.3. Wind Turbine based on DFIG

The three generators that are typically used in large WECS are doubly-fed induction generators, squirrel-cage induction generators and the direct drive synchronous generators. Even though the share of the latter generator type for large WECS is growing (especially for offshore applications) [50], in this work, the DFIG-based WECS is analyzed due to its actual share of close to 50% of the wind energy market (at 2013) [14]. Despite the different designs of the generators of the WECS, the modeling and controller technique presented in the subsequent chapters is, in principle, applicable to them. This is indicated and demonstrated by the application of the technique to the SG and the PVS, having some similarities in their dynamic equations with the different types of the WECS.

A WECS based on the DFIG, as depicted in Fig. 3.3, is typically described by the equations of the turbine aerodynamics, the pitch system, the drive train, the generator, and the converter (protection devices are neglected in this work). The turbine model can be represented by a power curve for the mechanical input  $P_m$ . With the air density  $\rho$ , the base power (for the per unit representation)  $P_B$ , the area covered by the rotor  $A_r$ , the pitch angle  $\beta$ , the tip speed ratio  $\lambda$ , and the performance coefficient  $C_p(\lambda, \beta)$ ,  $P_m$  can be described by the following algebraic equation [63]:

$$P_m = \frac{\rho}{2P_B} A_r C_p(\lambda, \beta) v_w^3. \quad (3.14)$$

Because the tip speed ratio is the ratio between the blade tip speed and wind speed,  $P_m$  is a function of the wind speed  $v_w$ , the shaft speed  $\omega_{sh}$ , and the pitch angle  $\beta$ . For studies of transient stability, the assumption is used that the wind speed and the pitch are constant since during the considered faults the other variables change with orders of magnitude faster than wind speed and pitch [30]. However, in this work, the pitch system is neglected but the controllers designed in the subsequent parts are synthesized and simulated such that wind fluctuations are addressed properly.

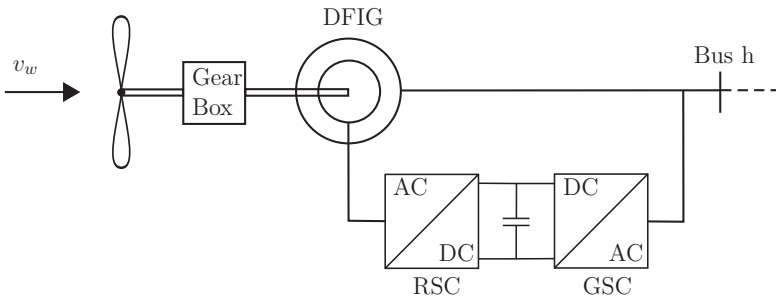


Figure 3.3.: DFIG-based WECS as a one line diagram.

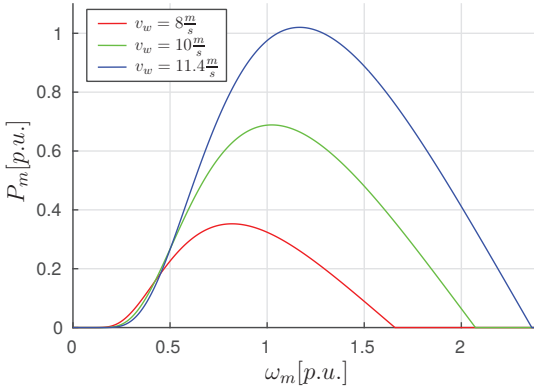


Figure 3.4.:  $P_m(v_w, \beta, \omega_m)$  exemplary for different wind speeds and a constant pitch angle  $\beta = 0$ .

For a rigid shaft, the generator rotor speed  $\omega_m$  equals the shaft speed  $\omega_{sh}$ , and the power curve (which represents the resulting turbine model) is then a function of  $\omega_m$  only, see Fig. 3.4 for different wind speeds. It is obvious, that for each specific wind speed, one equivalent value for the rotor speed exists, where the maximum mechanical power is extracted from the wind - the so called *Maximum Power Point* (MPP). While the tracking of the MPP is not in the focus of this work, the control of  $\omega_m$  has to be considered for transient stability studies. The mechanical torque is calculated by  $T_m = P_m/\omega_m$ .

Assuming a loss-less converter and a synchronous (idealized) operation of the grid side converter (GSC), the active power of the GSC  $p_c$  equals the active power of the rotor side converter (RSC)  $p_r$  and the reactive power of the GSC is then  $q_c = 0$ . Consequently, the variables of the GSC are neglected and only rotor and stator variables are considered in the model. The main electrical variables of the DFIG are then the currents  $i_r$  and  $i_s$ , the voltages  $v_r$  and  $v_s$  as well as the fluxes  $\psi_r$  and  $\psi_s$  of the rotor and stator, indicated by the indices  $r$  and  $s$ . Furthermore, the indices  $d$  and  $q$  will be used for dq-transformed quantities. According to [26], a third order model is sufficient to investigate transient stability. This implies that stator transients are negligibly small, thus  $\frac{d\psi_s}{dt} = 0$ , since the DFIG is connected to the grid through the stator while the grid is modeled through algebraic equations [63, 23]. The three remaining states of the model are  $\omega_m$ , and the two dq-transformed rotor fluxes  $\psi_{r,d}$  and  $\psi_{r,q}$ . The mechanical machine parameter is the sum of the turbine and rotor inertia  $H_m$ . The electrical parameters of the stator and rotor are the resistances  $r_s$  and  $r_r$ , and the reactances  $x_s$  and  $x_r$ . The remaining electrical parameters of the system are the sums of the reactances  $x_{s,\mu} = x_s + x_\mu$  and  $x_{r,\mu} = x_r + x_\mu$ , where  $x_\mu$

is the magnetizing reactance (to consider the air gap between the stator and the rotor). The system inputs are rotor voltages  $v_{r,d}$  and  $v_{r,q}$ . The slip  $s = \left(\frac{\omega_s - \omega_m}{\omega_s}\right)$  is the relation between the angular velocities of the stator and rotor. Similar to the SG, the angular velocity  $\omega_m$  is governed by the difference between the mechanical torque  $T_m$  and the electrical torque  $T_{el}$ :

$$\dot{\omega}_m = \frac{1}{2H_m}(T_m - T_{el}), \quad (3.15)$$

$$\dot{\psi}_{r,d} = v_{r,d} + r_r i_{r,d} + \omega_s s \psi_{r,q}, \quad (3.16)$$

$$\dot{\psi}_{r,q} = v_{r,q} + r_r i_{r,q} - \omega_s s \psi_{r,d}. \quad (3.17)$$

In contrast to the SG,  $T_m$  can not be assumed constant as it depends here on  $\omega_m$ , as defined by the power curve for  $P_m$ . The remaining algebraic variables are determined by:

$$0 = T_{el} - x_\mu (i_{r,q} \dot{i}_{s,d} - i_{r,d} \dot{i}_{s,q}), \quad (3.18)$$

$$0 = -s + \left(\frac{\omega_s - \omega_m}{\omega_s}\right), \quad (3.19)$$

$$0 = v_{s,d} + r_s \dot{i}_{s,d} + \omega_s \psi_{s,q}, \quad (3.20)$$

$$0 = v_{s,q} + r_s \dot{i}_{s,q} - \omega_s \psi_{s,d}, \quad (3.21)$$

$$0 = \psi_{r,d} + (x_{r,\mu} \dot{i}_{r,d} + x_\mu \dot{i}_{s,d}), \quad (3.22)$$

$$0 = \psi_{r,q} + (x_{r,\mu} \dot{i}_{r,q} + x_\mu \dot{i}_{s,q}), \quad (3.23)$$

$$0 = \psi_{s,d} + (x_{s,\mu} \dot{i}_{s,d} + x_\mu \dot{i}_{r,d}), \quad (3.24)$$

$$0 = \psi_{s,q} + (x_{s,\mu} \dot{i}_{s,q} + x_\mu \dot{i}_{r,q}), \quad (3.25)$$

$$0 = v_{s,d} + v_h \sin \varphi_h, \quad (3.26)$$

$$0 = v_{s,q} - v_h \cos \varphi_h, \quad (3.27)$$

$$0 = p_h - v_{s,d} \dot{i}_{s,d} - v_{s,q} \dot{i}_{s,q} - v_{r,d} \dot{i}_{r,d} - v_{r,q} \dot{i}_{r,q}, \quad (3.28)$$

$$0 = q_h - v_{s,q} \dot{i}_{s,d} + v_{s,d} \dot{i}_{s,q}. \quad (3.29)$$

Similarly to the SG, the last four equations represent the network interface to the bus  $h$ .

The injected powers for transient stability studies are typically too high for one WECS. To circumvent this problem, and assuming same wind conditions for all turbines, an aggregated model of several wind turbines can be used. The aforementioned equations and the parameters in p.u. remain valid [26]. The rated power is then equal to the sum of the rated powers of all wind turbines, i.e. only the power curve has to be scaled, and the power  $P_m$  is injected into the system through  $T_m$ .

### Active and Reactive Power Controllers

The controllers presented next, are widely used in literature and consist of two controllers for the injected active power  $p_h$  and the injected reactive power  $q_h$  at

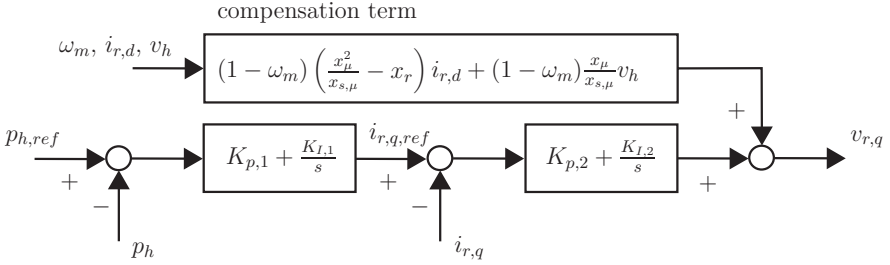


Figure 3.5.: Controller structure of the WECS for the active power [26].

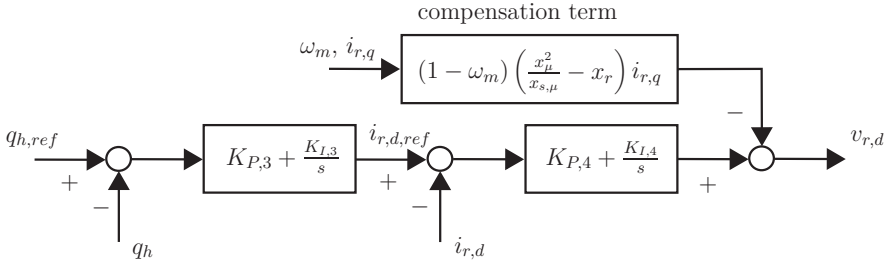


Figure 3.6.: Controller structure of the WECS for the reactive power [26].

the bus  $h$  (e.g. in [26] or [23]). By using compensation terms, the control of the two variables  $p_h$  and  $q_h$  is decoupled such that each of the inputs of the WECS  $v_{r,q}$  and  $v_{r,d}$  is used to control one variable. As depicted in Fig. 3.5 and Fig. 3.6, each controller has an outer loop to regulate the power and an inner loop to regulate the rotor current. All controllers have proportional and integral terms (with the gains  $K_{P,i}$  and  $K_{I,i}$ ) and reach steady-state accuracy for  $p_h$  and  $q_h$ , respectively. Similar to the classical controllers of the SG, these controllers are synthesized based on (Taylor) linearizations around one operating point. Thus, their operation for changing condition is not guaranteed.

### 3.4. Photovoltaic System

The photovoltaic system (PVS) described in this chapter is based on the benchmark system presented in [108]. In contrast to the SG and the WECS, PVS has no mechanical parts and its dynamics is governed by electromagnetic transients only. Following the argumentation from this chapter so far, i.e. that the electromagnetic transients of the transmission lines are modeled by algebraic equations, the dynamics of the PVS must be modeled by algebraic equations as well. This is e.g. done

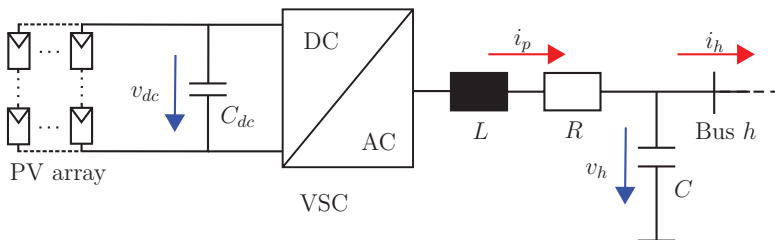


Figure 3.7.: Photovoltaic system as a one line diagram.

in [63] for the voltage source converter (VSC), where the AC-side is modeled by (simplified) injected active and reactive powers, including the descriptions of the assumed controllers. The AC-phase reactor and shunt capacitor dynamics are neglected. In general, it is feasible to combine an PVS model with electromagnetic dynamics with the algebraic description of the grid as in in Ch. 3.1. However, this contradicts the assumption of the neglected electromagnetic transients. Furthermore, the fast PVS dynamics and the swings within the PVS are hardly visible on the timescales needed for the simulation of SG and WECS dynamics (both including the mechanical equations of rotating masses). However, as it is the objective of this work to introduce the LPV modeling and control technique to the PVS, a state space description of the PVS is required. Consequently, the model described next, will be simulated in the context of a grid described by differential equations. The detailed simulation environment will be introduced in Ch. 6.3.

A PVS consists of the PV-array, the voltage source converter (VSC) and the filter as depicted in Fig. 3.7. The PV-array plant consists of a PV-array with  $n_{pv,p}$  PV-strings in parallel, and  $n_{pv,s}$  PV-cells per string in series. The current of the overall PV-array  $i_{pv}(S, \vartheta, v_{dc})$  is a function of the solar irradiation  $S$ , the  $p$ - $n$  junction temperature  $\vartheta$ , and the dc-link voltage  $v_{dc}$ .  $S$  is normalized, where  $S = 1$  references to the solar irradiation  $1000\text{W/m}^2$  and  $\vartheta$  is assumed to be constant at  $\vartheta = 300\text{K}$  in the course of this work.  $I_s$  is the reverse saturation current caused by the  $p$ - $n$  junction and  $I_{ph}(\vartheta)$  is the temperature adjusted short-circuit current of one string and is weighted by  $S$ . The photovoltaic cell coefficient, which describes the PV characteristic, is denoted by  $\beta_{pv}(\vartheta)$ . With the relation between the current  $i_{pv}$  and the power injected by the PV-array as  $p_{pv} = i_{pv}v_{dc}$ , the two quantities can be described as follows:

$$i_{pv}(S, \vartheta, v_{dc}) = n_{pv,p}I_{ph}(\vartheta)S - n_{pv,p}I_s \left( e^{\beta_{pv}(\vartheta)\frac{v_{dc}}{n_{pv,s}}} - 1 \right), \quad (3.30)$$

$$p_{pv}(S, \vartheta, v_{dc}) = n_{pv,p}I_{ph}(\vartheta)Sv_{dc} - n_{pv,p}I_s v_{dc} \left( e^{\beta_{pv}(\vartheta)\frac{v_{dc}}{n_{pv,s}}} - 1 \right), \quad (3.31)$$

Exemplary courses for  $p_{pv}(S, \vartheta, v_{dc})$  for different values of solar irradiation are shown in Fig. 3.8. Similarly to the role of the angular velocity  $\omega_m$  of the power curve of

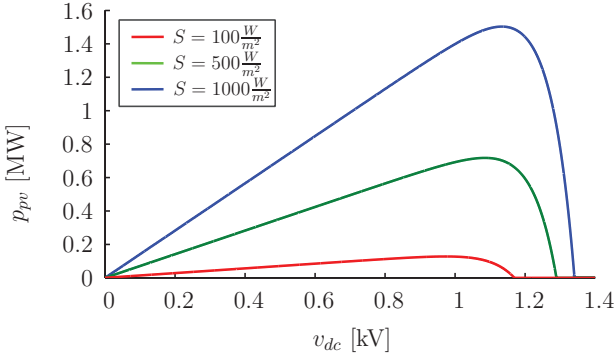


Figure 3.8.: Exemplary power curve of a PVS as a function of  $v_{dc}$  for different values of solar irradiation.

the WECS, the extracted power  $p_{pv}$  can be changed by variation of  $v_{dc}$ , e.g. for maximum power point tracking (MPPT). The DC interface dynamics can be derived from the balance of the power generated by the PV array  $p_{pv}$  and the DC real power output of the VSC  $p_{dc}$  (by neglecting losses). This is indicated in (3.32), using the squared DC voltage  $v_{dc}$  as a state variable [106], where  $C_{dc}$  is the DC-side capacitor. The AC interface comprises the VSC LC-output filter and the differential equations for the filter-inductance  $L$  and the filter-capacity  $C$  can be deduced from Kirchhoff's Laws. The states of the PVS are then the dq-transformed AC side currents  $i_{p,d}$  and  $i_{p,q}$ , and the voltages  $v_{h,d}$  and  $v_{h,q}$  at the capacitor  $C$  at the point of connection at bus  $h$ . The AC-side terminal voltages of the VSC can be represented by  $e_d = K_d \frac{v_{dc}}{2}$  and  $e_q = K_q \frac{v_{dc}}{2}$ . In order to get a representation with the control inputs  $K_d$  and  $K_q$ ,  $e_{\{d,q\}}$  are inserted directly and are only indicated in the following equations. The PVS as depicted in Fig. 3.7 can then be described by [71, 106]:

$$\frac{d(v_{dc}^2)}{dt} = \frac{2}{C_{dc}} \underbrace{i_{pv} v_{dc}}_{p_{pv}} - \frac{2}{C_{dc}} \underbrace{\left( i_{p,d} K_d \frac{v_{dc}}{2} + i_{p,q} K_q \frac{v_{dc}}{2} \right)}_{p_{dc}}, \quad (3.32)$$

$$\dot{i}_{p,d} = -\frac{R}{L} i_{p,d} + \omega i_{p,q} + \frac{1}{L} \left( \underbrace{K_d \frac{v_{dc}}{2}}_{e_d} - v_{h,d} \right), \quad (3.33)$$

$$\dot{i}_{p,q} = -\frac{R}{L} i_{p,q} - \omega i_{p,d} + \frac{1}{L} \left( \underbrace{K_q \frac{v_{dc}}{2}}_{e_q} - v_{h,q} \right), \quad (3.34)$$

$$\dot{v}_{h,d} = \omega v_{h,q} + \frac{1}{C} i_{p,d} - \frac{N}{C} i_{h,d}, \quad (3.35)$$

$$\dot{v}_{h,q} = -\omega v_{h,d} + \frac{1}{C} i_{p,q} - \frac{N}{C} i_{h,q}, \quad (3.36)$$

where  $N$  is the transformer ratio. During operation, the inputs  $K_{\{d,q\}}$  are converted into the duty cycles for the power electronic switches in the VSC. In classic transient analysis of power grids, the voltage at a grid node with index  $h$  is normally defined in terms of the voltage amplitude  $v_h$  and the voltage angle  $\varphi_h$ . These quantities are formulated in  $dq$ -representation and as algebraic equations. As mentioned in the introduction of this section, the PVS is simulated in the subsequent chapter in the context of a grid modeled by differential equations only. The coupling of the presented PVS is then realized through the currents  $i_{h,d}$  and  $i_{h,q}$ , which are the currents of the transmission line connecting the PVS to the bus  $h$  of the grid. Instead of the algebraic representation of the voltage  $v_h$  at the bus  $h$  and its phasor  $\varphi_h$ , the voltage and the phasor are indirectly represented as dq-transformed states  $v_{h,d}$  and  $v_{h,q}$ . This is advantageous, when it comes to the control of the bus-voltage, making a derivation by differentiation of  $v_h$  (as it has to be done for the SG and the WECS) obsolete.

### Reference Controllers for the PVS

Conventional controllers for the PVS are often designed to control the power factor and the dc-link voltage  $v_{dc}$ . The tracking of the MPP is realized by variation of  $v_{dc}$ . Based on the conventional controller, a more sophisticated controller is designed in [106] and [107]. This controller is used for comparison in Ch. 6 and is presented next. It comprises a phase-locked-loop (PLL), an outer control loop for  $v_{dc}$  and an inner control loop for  $i_{p,d}$  and  $i_{p,q}$ .

### Phase-Locked-Loop

The PLL is designed to control the  $q$ -component of  $v_h$  to zero and it also provides the actual value of the grid frequency. The aim  $v_{h,q} = 0$  is achieved by i) synchronizing the rotational speed of the  $dq$ -frame with the grid frequency  $\omega_0$  and by ii) aligning the  $dq$ -frame with the grid voltage vector, i.e.  $\tilde{\varphi}_h = \varphi_h$ , see Fig. 3.9. Thus, the transfer-function of the first block consists of a PI-controller and a low-pass filter (with the parameters  $\xi_1$ ,  $\xi_2$ , and  $\xi_3$ ) and, additionally, integrating behavior for  $\omega$  is introduced.

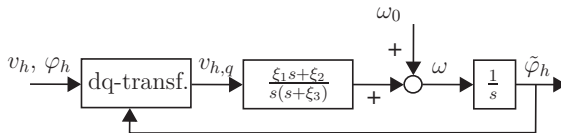


Figure 3.9.: Controller structure of the PLL of the PVS [107].

### Current Controllers

In the current control scheme of [106], Eqs. (3.33) and (3.34) are linearized by introducing two auxiliary inputs  $u_d$  and  $u_q$  with the following connection to the original inputs  $K_d$  and  $K_q$ :

$$K_d = \frac{1}{v_{dc}}(u_d - L\omega i_{p,q} + v_{h,d}), \quad (3.37)$$

$$K_q = \frac{1}{v_{dc}}(u_q + L\omega i_{p,d} + v_{h,q}). \quad (3.38)$$

By inserting Eqs. (3.37) and (3.38) in (3.33) and (3.34), the resulting linear system with two identical equations can be controlled by the identical PI-controllers as depicted in Fig. 3.10. The control parameters  $k_p$  and  $k_i$  can be chosen as  $k_p = \frac{L}{\tau_i}$  and  $k_i = \frac{R}{\tau_i}$  [106]. The time constant  $\tau_i$  must have a small value to achieve fast current control but has to be large enough, so that  $\frac{1}{\tau_i}$  is smaller than the switching frequency of the VSC -  $\tau_i = 0.5ms$  is proposed in [106].

### DC-Voltage Controller

For the (outer) control loop for  $v_{dc}$ , a new control input  $u_v$  is introduced which is defined by a transfer function comprising a PI-controller and a low-pass filter (with the parameters  $\rho_1$ ,  $\rho_2$ , and  $\rho_3$ ) as depicted in Fig. 3.11 [106]. A feed-forward compensation is added to  $u_v$  to calculate  $i_{p,d,ref}$ , the input of the current controller.  $\gamma_p$  is a gain with  $\gamma_p \in [0, 1]$ . The connection between the Eq. (3.32) for  $v_{dc}^2$  and the equation for  $v_{dc}^2$  as used to design the controller in Fig. 3.11 is drawn by the assumption that with a loss-less system  $p_{dc} = i_{p,d}e_d + i_{p,q}e_q = i_{p,d}v_{h,d} + i_{p,q}v_{h,q}$ .

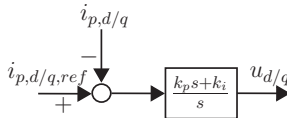


Figure 3.10.: Controller structure of the current controllers of the PVS.

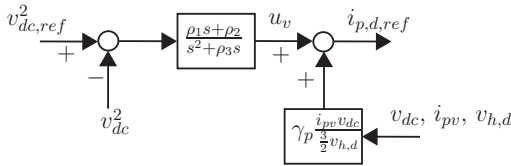


Figure 3.11.: Controller structure of the  $v_{dc}$ -controllers of the PVS.

## 3.5. Models of Faults and Exogenous Effects

In order to verify the controllers designed in the following chapters, the tested grids and their configurations will be subject to the following (symmetric) faults and exogenous effects:

- changes of the wind speed  $v_w$  penetrating the WECS
- changes of the solar irradiation  $S$  penetrating the PVS
- permanent line switches within the grid, i.e. a line admittance is changed permanently
- large voltage drops of a bus within the grid

While the changes of  $v_w$  and  $S$  are implemented naturally by introducing an offset at the (fault) time  $t_f$ , the modeling of the other two faults within the grid is explained next.

### Permanent Grid Fault

A permanent grid fault is introduced as a permanent change of the grid impedance between one line connecting the buses  $h$  and  $k$ , i.e. the changed line is multiplied by the factor  $s_f$ . The relevant elements of the admittance matrix change to  $\bar{y}_{hk,new}$  and  $\bar{y}_{kh,new}$  with:

$$\begin{aligned}\bar{y}_{hk,new} &= s_f \cdot \bar{y}_{hk} \\ \bar{y}_{kh,new} &= s_f \cdot \bar{y}_{kh}\end{aligned}\tag{3.39}$$

The respective diagonal elements of the admittance matrix  $\bar{y}_{hh}$  and  $\bar{y}_{kk}$  have to be recalculated with the new values  $\bar{y}_{hk,new}$  and  $\bar{y}_{kh,new}$ , as well. Similar permanent changes of the grid can be caused by abrupt disconnection of large loads or other devices.

### Bus-Voltage Drop

For transient stability studies, a large three phase fault is introduced. This fault can be modeled by a shunt conductance  $g_f$  and a susceptance  $b_f$ , and interpreted as powers flowing to ground at the fault time  $t_f$  until the fault is cleared at  $t_c$  [63]:

$$\begin{aligned}0 &= -p_h - g_f v_h^2 \\ 0 &= -q_h - b_f v_h^2\end{aligned}\tag{3.40}$$

$$[g_f, b_f] = \begin{cases} [g_f, b_f] & \text{if } t_f \leq t \leq t_c \\ [0, 0] & \text{if } t < t_f \text{ or } t \geq t_c \end{cases}$$

These faults typically appear for short period of times, causing protection devices to react. By choosing certain values for  $g_f$  and  $b_f$ , bus voltage drops e.g. by 20% can be caused.



**Part II.**

**Synthesis of Local Robust  
Controllers**



## 4. Modeling Power Grids by Linear Parameter-Varying Systems

All of the previously presented dynamic systems have nonlinearities making robust control a challenging task. The techniques of the presented reference controllers (of standard LTI type) are all based on linearizations around one operating point, with the assumption that all connected nodes stay close to their nominal operating point. This procedure is not sufficient for larger shares of renewables which can introduce fluctuations and considerable deviations from nominal operation. Robustness against transient effects propagating through the grid is not provided.

One way to handle the nonlinearities is the use of the LPV technique. The dynamically modeled components are transformed into their LPVS representations by analytic transformations in a modular way. The nonlinearities are transferred into the parameters and interdependencies between the modules are mapped into the parameter ranges. The resulting model structure is similar to a linear representation and robustness against fluctuations caused by (grid) faults or exogenous effects can be introduced by the subsequent controller design.

The results presented in the Ph.D. thesis by J. Shamma [88] and in his publication with M. Athans [89] are widely seen as the starting point for the LPV modeling and control technique as it is used in this work (e.g. [11], [35], or [65]). Since then, the LPVS framework has evolved rapidly. There are two ways of finding an LPV model such as using Taylor linearizations for several operating points or by analytic transformations of the nonlinear systems. As already mentioned, the latter approach is used in this work. The general structure of an LPV model is similar to the one of a linear model. The distinguishing factor is the encoding of the parametric variabilities, and to hide the nonlinearities in the parameters of the system matrices. The resulting system description is then given as follows [8, 65]:

$$\dot{x}(t) = A(\theta(t))x(t) + B(\theta(t))u(t) \quad (4.1)$$

$$y(t) = C(\theta(t))x(t) + D(\theta(t))u(t) \quad (4.2)$$

where  $x \in \mathbb{R}^{n_x}$  is the state-vector,  $y \in \mathbb{R}^{n_y}$  are the outputs,  $u \in \mathbb{R}^{n_u}$  are the inputs, and  $\theta \in \mathbb{R}^{n_p}$  is the vector of parameters. If the parameters depend not only on external signals but on internal signals as well, the respective system is called quasi-LPV [99]. However, very often the distinction between LPV and quasi-LPV is not made, as it is done in this work. Here, all derived LPV models are quasi-LPV, due to their dependency on (internal and external) algebraic variables and

states. One contribution of this work is the unified and modular modeling of the subsystems appearing in a power system. This chapter deals with the modeling of the SG, DFIG, and PVS as continuous-time LPVS, needed for the subsequent robust controller synthesis. Some of the results in this chapter have been previously published in [81] and [82] considering the SG, only, in [83] combining the SG and WECS, and in [96], focusing on PVS. For brevity, the time dependency of  $\theta$  is omitted in the following.

## 4.1. Transformation into LPV Models

The objective now is to find an LPV description of the nonlinear DAE models of the SG, the WECS, and the PVS as described in the previous chapter. In [99] and [44], the idea of hiding the nonlinearities of ordinary differential equations (ODE) in the parameters to find an LPV model description was presented and in [81] and [82] this idea is used by the author for DAE-systems. In contrast to the former named two approaches, the original DAE-system of the power grid is decomposed in subsystems, and the coupling through the algebraic variables is mapped into the parameters. Thus, the parameters comprise states and algebraic variables. Furthermore, the modeling technique is extended by the transformation of an algebraic variable (i.e. the voltage at the point of connection) into a differential description for controller synthesis. Due to the fact that the resulting model is not unique in general, the following requirements determine the choice of a suitable LPV model:

- The resulting LPV model should be an exact representation of the original model, i.e. only analytic transformations are used to preserve the original dynamics of the system.
- The resulting LPV model of each subsystem must be local, modular, and remain consistent with the complete DAE-system, i.e. the algebraic grid equations (presented in Eq. (3.3)) must not be used for the transformations, but only equations from the Sections 3.2, 3.3, and 3.4 are used for the respective LPV models of the SG, WECS and PVS.
- The resulting parameters have to be measurable or computable from measurable quantities to ensure applicability.
- The LPV transformed system should remain controllable in the relevant parameter ranges.

The latter point is difficult to prove while modeling, because the parameters have dependencies to other signals and to other parameters. Ignoring this might disqualify well suitable LPV models for controller synthesis. As an illustrative example,

consider a system with a matrix  $A(\theta)$ :

$$A(\theta) = \begin{bmatrix} \theta_1 & 1 \\ \theta_2 & 1 \end{bmatrix}. \quad (4.3)$$

Assuming the parameter ranges  $\theta_1 \in [-1, 1]$ ,  $\theta_2 \in [-1, 1]$ , and the case that  $\theta_1 = \theta_2 = 0$  leads to a rank loss of 1, disqualifying this model due to the controllability requirement. With the additional information that  $\theta_1 \neq \theta_2$ , the model may be suitable, however. In fact, in this work, the statement about controllability is made in connection to a specified range  $\theta \in [\underline{\theta}, \overline{\theta}]$ . Thus, the final statement about controllability of an LPVS is established during the controller synthesis, which will be presented in Ch. 5, and for to the parameter ranges, which are defined by the considered power system, as will be demonstrated in Ch. 6. Furthermore, considering the controllability requirement, one simple idea of restructuring the LPV model is used by introducing auxiliary matrix entries, while retaining system dynamics.

## 4.2. LPV Modeling of a Synchronous Generator

Two LPV models of the SG will be derived next - one for the enhancement of transient stability and one to realize the control of the bus voltage.

### LPV Model of an SG

For transient stability the original system is reformulated in terms of a state vector  $x := [\delta, \Delta\omega, e'_q]^T$  with  $\Delta\omega := \omega - \omega_b$  and an input  $u := v_f$ .

The dynamic model of the first state as in Eq. (3.4) is linear leading to the description in terms of  $x_1$ :

$$\begin{aligned} \dot{x}_1 &= \Omega_b(\omega - \omega_b) \\ &= \Omega_b x_2 \end{aligned} \quad (4.4)$$

The equations for  $x_2$  and  $x_3$  are nonlinear and transformations are needed to find an LPV description. First, the algebraic variable  $\tau_e$  is reformulated. By inserting  $v_q$  from Eq. (3.8) and  $v_d$  from Eq. (3.9) into Eq. (3.7),  $\tau_e$  is

$$\tau_e = (x_q - x'_d)i_d i_q + e'_q i_q \quad (4.5)$$

Using this description for  $\tau_e$ ,  $x_2$  from Eq. (3.5) can be represented by the LPV description:

$$\begin{aligned} \dot{x}_2 &= \frac{1}{2H}(\tau_m - (x_q - x'_d)i_d i_q - x_3 i_q - D x_2) \\ &= \frac{1}{2H}\theta_1 x_1 + \frac{-D}{2H}x_2 + \frac{-1}{2H}\theta_2 x_3, \end{aligned} \quad (4.6)$$

where the parameter definitions are given by the equations (4.9) below. Finally, the last state equation can be formulated in terms of  $x_3$  and as an LPV description to:

$$\begin{aligned} \dot{x}_3 &= \frac{1}{T'_{dO}}(-x_3 - (x_d - x'_d)i_d + u) \\ &= \frac{-(x_d - x'_d)}{T'_{dO}}\theta_3 x_1 + \frac{-1}{T'_{dO}}x_3 + \frac{1}{T'_{dO}}u \end{aligned} \quad (4.7)$$

The system can now be described as an LPV model:

$$\dot{x} = \underbrace{\begin{bmatrix} 0 & \Omega_b & 0 \\ \frac{1}{2H}\theta_1 & \frac{-D}{2H} & \frac{-1}{2H}\theta_2 \\ \frac{-(x_d-x'_d)}{T'_{dO}}\theta_3 & 0 & \frac{-1}{T'_{dO}} \end{bmatrix}}_{A(\theta)} x + \underbrace{\begin{bmatrix} 0 \\ 0 \\ \frac{1}{T'_{dO}} \end{bmatrix}}_B u \quad (4.8)$$

with the following set of parameters:

$$\begin{aligned} \theta_1 &= \frac{(\tau_m - (x_q - x'_d)i_d i_q)}{x_1}, \\ \theta_2 &= i_q, \\ \theta_3 &= \frac{i_d}{x_1}. \end{aligned} \quad (4.9)$$

Due to the use of only analytic transformations, this model is an exact representation of the original model from Sec. 3.2. The validity of this model is limited to the range  $x_1 \neq 0$ , what, however, is not a practically relevant restriction, since  $\delta = 0$  is not reached for the case of a controlled SG. Furthermore,  $\delta$  appears only in two algebraic equations (3.10) and (3.11) in *sine* and *cosine* functions. Thus,  $\delta = 0$  can be avoided without any effects on the dynamics of the system by initializing the values of all rotor angles of the generators e.g. at  $\delta_0 = 720^\circ$  and resetting  $\delta_0$  every  $\pm 360^\circ$ .

### LPV Model of an SG for Voltage Control

In this section, the control objective is extended by voltage control making a reformulation of the model necessary. The three states of the resulting LPV model are defined as  $x := [\delta, \Delta\omega, v_h]^T$ , where  $v_h$  is the controlled voltage at the connecting bus  $h$ .  $\Delta\omega$  and the input are defined as in the previous section by  $\Delta\omega = \omega - \omega_b$  and  $u := v_f$ . So are the LPV descriptions of the first and second states, while the LPV description of the voltage has to be derived. Being an algebraic variable,  $v_h$  has first to be reformulated as a differential variable. The armature resistance  $r_a$  in Eqs. (3.8) and (3.9) is typically a very small value and it is often chosen to 0 for transient stability studies [32]. Using the definition  $v_h = \sqrt{v_d^2 + v_q^2}$ , inserting  $v_q$  from (3.8),  $v_d$  from (3.9), and setting  $r_a = 0$  leads to:

$$v_h = \sqrt{(x_q i_q)^2 + (e'_q - x'_d i_d)^2}. \quad (4.10)$$

To introduce  $v_h$  as the state  $x_3$ , it is differentiated over time to obtain:

$$\dot{v}_h = \frac{1}{v_h} \left[ x_q^2 i_q \dot{i}_q + (e'_q - x'_d i_d) (\dot{e}'_q - x'_d \dot{i}_d) \right]. \quad (4.11)$$

As introduced in the beginning of this section,  $\dot{e}'_q$  is not treated as a state any more, and its differential equation is directly inserted into  $\dot{v}_h$ . Thus, the dynamics of  $e'_q$  is contained in the dynamics of  $x_3$ , and  $e'_q$  is treated as part of the respective parameter, but not as a state. The LPV description of  $x_2$  can be used as derived in Eq. (4.6), with the difference that  $e'_q$  is transferred into parameter  $\theta_2$  (compare  $\theta_2$  in equations (4.9) and (4.14)).

The LPV description for  $x_3$  is then derived as follows:

$$\begin{aligned} \dot{x}_3 &= \frac{1}{x_3} (x_q^2 i_q \dot{i}_q - (e'_q - x'_d i_d) x'_d \dot{i}_d) + \frac{1}{x_3} (e'_q - x'_d i_d) \cdot \dots \\ &\dots \frac{1}{T'_{d0}} (-e'_q - (x_d - x'_d) i_d) + \frac{1}{T'_{d0}} \frac{e'_q - x'_d i_d}{x_3} u \\ &= \theta_3 x_1 + \frac{1}{T'_{d0}} \theta_4 x_3 + \frac{1}{T'_{d0}} \theta_5 u \end{aligned} \quad (4.12)$$

with the parameters as defined below.

The system can now be described as an LPV model:

$$\dot{x} = \underbrace{\begin{pmatrix} 0 & \Omega_b & 0 \\ \frac{1}{2H} \theta_1 & \frac{-D}{2H} & \frac{-1}{2H} \theta_2 \\ \theta_3 & 0 & \frac{1}{T'_{d0}} \theta_4 \end{pmatrix}}_{A(\theta)} x + \underbrace{\begin{pmatrix} 0 \\ 0 \\ \frac{1}{T'_{d0}} \theta_5 \end{pmatrix}}_{B(\theta)} u, \quad (4.13)$$

where the matrices  $A$  and  $B$  are parameter-dependent. The five parameters are

$$\begin{aligned} \theta_1 &= (\tau_m - (x_q - x'_d) i_d i_q) \frac{1}{x_1}, \\ \theta_2 &= e'_q i_q \cdot \frac{1}{x_3}, \\ \theta_3 &= \frac{x_q^2 i_q \dot{i}_q - (e'_q - x'_d i_d) x'_d \dot{i}_d}{x_3} \cdot \frac{1}{x_1}, \\ \theta_4 &= \frac{(e'_q - x'_d i_d) (-e'_q - (x_d - x'_d) i_d)}{x_3^2}, \\ \theta_5 &= \frac{e'_q - x'_d i_d}{x_3}. \end{aligned} \quad (4.14)$$

Again, the transformations used are analytic, making it an exact representation of the models presented in Ch. 3.2. The additional limitation  $x_3 \neq 0$  is not relevant in practice, as  $v_h = 0$  is not a relevant case for a controller (short-circuit).

The connection of both presented LPV models to the grid is realized through the parameters  $\theta$ , which in turn are governed by the currents  $i_d$  and  $i_q$  and their derivatives. The two variables can be calculated based on locally measurable quantities with the following equations (derived from the algebraic equations (3.7) to (3.13)):

$$\begin{aligned} i_d &= \frac{ph}{x_3} \sin(x_1 - \varphi_h) + \frac{qh}{x_3} \cos(x_1 - \varphi_h) \\ i_q &= \frac{ph}{x_3} \cos(x_1 - \varphi_h) - \frac{qh}{x_3} \sin(x_1 - \varphi_h) \end{aligned} \quad (4.15)$$

The derivatives  $\dot{i}_q$  and  $\dot{i}_d$  can be estimated based on these equations.

For the second LPV model, voltage  $e'_q$ , occurring in  $\theta_2$  in (4.14), can be calculated by:

$$e'_q = x'_d i_d + x_3 \cos(x_1 - \varphi_h). \quad (4.16)$$

### 4.3. LPV Representation of a DFIG-based WECS

The controller objectives concerning the grid stability for the WECS are the same as for the SG, i.e. transient and voltage stability. However, to assure the correct point of operation along the power curve, the angular velocity  $\omega_m$  is controlled as well. While  $\omega_m$  is already formulated as a state in the original nonlinear model, a description of  $v_h$  in form of a differential equation has to be found.

#### LPV Model of a WECS

The resulting state vector is defined as  $x := [\omega_m, \psi_{r,d}, \psi_{r,q}]^T$ , and the input vector as  $u := [v_{r,d}, v_{r,q}]^T$ . Due to the fact that all state equations in Sec. 3.3 are nonlinear, the derivation of the LPV descriptions of each state will be given in the course of this section.

Starting from the equation for  $x_1$  in Eq. (3.15), similar to the electrical torque of the second state of the SG, the electrical torque  $T_{el}$  is eliminated from the equation. Transforming equations (3.22) in terms of  $i_{r,d}$ , and (3.23) in terms of  $i_{r,q}$ , leads to the rotor current expressions:

$$i_{r,d} = -\frac{1}{x_{r,\mu}} \psi_{r,d} - \frac{x_\mu}{x_{r,\mu}} i_{s,d}, \quad (4.17)$$

$$i_{r,q} = -\frac{1}{x_{r,\mu}} \psi_{r,q} - \frac{x_\mu}{x_{r,\mu}} i_{s,q}. \quad (4.18)$$

By inserting  $i_{r,d}$  and  $i_{r,q}$  into the Eq. (3.18),  $T_{el}$  is reformulated to:

$$T_{el} = \frac{x_\mu}{x_{r,\mu}} (i_{s,q} x_2 - i_{s,d} x_3). \quad (4.19)$$

By inserting  $T_{el}$  into Eq. (3.15), the following LPV description can be formulated:

$$\begin{aligned}\dot{x}_1 &= \frac{1}{2H_m}(T_m - \frac{x_\mu}{x_{r,\mu}}(i_{s,q}x_2 - i_{s,d}x_3)) \\ &= \frac{1}{2H_m}\theta_1x_1 + \frac{-x_\mu}{2H_mx_{r,\mu}}\theta_2x_2 + \frac{x_\mu}{2H_mx_{r,\mu}}\theta_3x_3,\end{aligned}\quad (4.20)$$

where the definitions of  $\theta_1$ ,  $\theta_2$ , and  $\theta_3$  are given below in Eq. (4.24). The equations of the two states  $x_2$  and  $x_3$  are derived next. The stator frequency is assumed to be close to 1 p.u., i.e.  $\omega_s = 1$ , and the slip simplifies to  $s = (1 - \omega_m)$ . Then, inserting  $i_{r,d}$  defined by (4.17) into Eq. (3.16) leads to:

$$\begin{aligned}\dot{x}_2 &= ((1 - x_1)x_3 - \frac{r_r x_\mu}{x_{r,\mu}}i_{s,d}) - \frac{r_r}{x_{r,\mu}}x_2 + u_1 \\ &= \theta_4x_1 + \frac{-r_r}{x_{r,\mu}}x_2 + u_1.\end{aligned}\quad (4.21)$$

Similarly, inserting  $i_{r,q}$  into (3.17) for  $x_3$  leads to:

$$\begin{aligned}\dot{x}_3 &= -\frac{r_r}{x_{r,\mu}}x_3 + ((x_1 - 1)x_2 - \frac{r_r x_\mu}{x_{r,\mu}}i_{s,q}) + u_2 \\ &= -\frac{r_r}{x_{r,\mu}}x_3 + \theta_5x_1 + u_2.\end{aligned}\quad (4.22)$$

The definitions of the parameters  $\theta_4$  and  $\theta_5$  are described below. Now, the LPV description can be summarized as:

$$\dot{x} = \underbrace{\begin{bmatrix} \frac{1}{2H_m}\theta_1 & \frac{-x_\mu}{2H_mx_{r,\mu}}\theta_2 & \frac{x_\mu}{2H_mx_{r,\mu}}\theta_3 \\ \theta_4 & \frac{-r_r}{x_{r,\mu}} & 0 \\ \theta_5 & 0 & \frac{-r_r}{x_{r,\mu}} \end{bmatrix}}_{A(\theta)} x + \underbrace{\begin{bmatrix} 0 & 0 \\ 1 & 0 \\ 0 & 1 \end{bmatrix}}_B u, \quad (4.23)$$

with the five parameters:

$$\begin{aligned}\theta_1 &= \frac{T_m}{x_1}, \quad \theta_2 = i_{s,q}, \quad \theta_3 = i_{s,d}, \\ \theta_4 &= \frac{(1 - x_1)x_3 - \frac{r_r x_\mu}{x_{r,\mu}}i_{s,d}}{x_1}, \\ \theta_5 &= \frac{(x_1 - 1)x_2 - \frac{r_r x_\mu}{x_{r,\mu}}i_{s,q}}{x_1}.\end{aligned}\quad (4.24)$$

The LPV model represents the nonlinear dynamics with the limitation that  $x_1 \neq 0$ . Since  $x_1$  is the rotor speed  $\omega_m$ , the value 0 refers to conditions (standstill) in which an operation of the WECS is not feasible and is out of the relevant operating range for control. Thus, the applicability of the model is given.

### LPV Model of a WECS for Voltage Control

In order to be able to control the voltage at the bus of the WECS, similarly to the SG, the model has to be extended by the description of the algebraic variable  $v_h$ . The resulting state vector is  $x := [\omega_m, \psi_{r,d}, \psi_{r,q}, v_h]^T$ , and the input vector remains  $u := [v_{r,d}, v_{r,q}]^T$ .

Furthermore, to meet the controllability requirement and to show the non-uniqueness of the LPV formulations, the LPV description of  $x_1$  is reformulated. Starting from the equation for  $x_1$  in (3.15), the equation is expanded by  $x_2 - x_2$  to avoid a zero-row when  $T_m = T_{el}$  for the subsequent choice for the first parameter  $\theta_1$ . The resulting LPV description is:

$$\begin{aligned}\dot{x}_1 &= \frac{1}{2H_m}(T_m - T_{el}) + x_2 - x_2 \\ \dot{x}_1 &= \theta_1 x_1 + x_2\end{aligned}\tag{4.25}$$

where the definition of  $\theta_1$  is given below in Eq. (4.29). Compared to the previous equation for  $x_1$ , only one parameter is introduced instead of three.

While the LPV descriptions for  $x_2$  and  $x_3$ , including their parameters, remain the same as in (4.21) and (4.22), the algebraic variable  $v_h$  has to be introduced as the state  $x_4$ . Thus, the derivative of  $v_h = \sqrt{v_{s,d}^2 + v_{s,q}^2}$  with respect to time has to be built and leads to the following dynamic description:

$$\dot{v}_h = (\dot{v}_{s,d} \cdot v_{s,d} + \dot{v}_{s,q} \cdot v_{s,q}) \frac{1}{v_h}.\tag{4.26}$$

Similarly to  $x_1$ , the equation is expanded by  $x_2 - x_2 + x_3 - x_3$  to ensure controllability, and the LPV description for  $x_4$  is:

$$\begin{aligned}\dot{x}_4 &= x_2 - x_2 + x_3 - x_3 + \frac{\dot{v}_{s,d}v_{s,d} + \dot{v}_{s,q}v_{s,q}}{x_4} \\ &= x_2 + x_3 + \theta_4 x_4\end{aligned}\tag{4.27}$$

where  $\theta_4$  is defined in Eq. (4.29). The LPV model of the DFIG-based WECS can now be summarized as:

$$\dot{x} = \underbrace{\begin{bmatrix} \theta_1 & 1 & 0 & 0 \\ \theta_2 & \frac{-r_r}{x_{r,\mu}} & 0 & 0 \\ 0 & 0 & \frac{-r_r}{x_{r,\mu}} & \theta_3 \\ 0 & 1 & 1 & \theta_4 \end{bmatrix}}_{A(\theta)} x + \underbrace{\begin{bmatrix} 0 & 0 \\ 1 & 0 \\ 0 & 1 \\ 0 & 0 \end{bmatrix}}_B u,\tag{4.28}$$

with the four parameters

$$\begin{aligned}
 \theta_1 &= \left( \frac{T_m - T_{el}}{2H} - x_2 \right) \frac{1}{x_1}, \\
 \theta_2 &= \left( (1 - x_1) x_3 - \frac{r_r x_\mu}{x_{r,\mu}} i_{s,d} \right) \frac{1}{x_1}, \\
 \theta_3 &= \left( (x_1 - 1) x_2 - \frac{r_r x_\mu}{x_{r,\mu}} i_{s,q} \right) \frac{1}{x_4}, \\
 \theta_4 &= \left( \frac{\dot{v}_{s,d} v_{s,d} + \dot{v}_{s,q} v_{s,q}}{x_4} - x_2 - x_3 \right) \frac{1}{x_4}.
 \end{aligned} \tag{4.29}$$

Again, the LPV model represents the nonlinear dynamics. Additionally to  $x_1 \neq 0$ , the limitation  $x_4 \neq 0$  for the voltage  $v_h$  refers to a condition (short-circuit), in which an operation of the WECS is not feasible and is out of the relevant operating range for control.

Regarding both introduced LPV models of the WECS, the connection to the grid is realized through the parameters, and they in turn are influenced by the stator currents  $i_{s,d}$  and  $i_{s,q}$ , the stator voltages  $v_{s,d}$  and  $v_{s,q}$ , and, for the second model, by the derivatives of the voltages  $\dot{v}_{s,d}$  and  $\dot{v}_{s,q}$ . The latter two values can be calculated based on the measurements/calculations of the former four values. In contrast to the SG, the mechanical input - the mechanical torque  $T_m$  - can not be assumed as constant and is influenced by the power curve, i.e. is a function of the wind and  $\omega_m$ . However, due to the fact that  $T_m$  is part of the parameter  $\theta_1$ , the variation of the wind can be considered in the parameter limits needed for the subsequent controller synthesis. Thus, variations from the grid side and from the wind can be considered in the presented model. Other than in [66] and [102], the model of the DFIG and the drive train are unified in one model.

## 4.4. LPV Formulation of a Photovoltaic System

In contrast to the models of the SG and the WECS, the voltage at the point of connection is already formulated in state-space description in d / q coordinates and a derivation by differentiation of  $v_h$  is not needed.  $v_h$  is controlled by using a new state  $v_h^2$ , which is derived in the course of this section. Thus, only one LPV model for the PVS is introduced. The state vector is defined as  $x = [v_{dc}^2, i_{p,d}, i_{p,q}, v_{h,d}, v_{h,q}, v_h^2]^T$ , and the input vector as  $u = [K_d, K_q]^T$ . Starting from Eq. (3.32) for  $v_{dc}^2$ , the LPV model is straightforwardly formulated as:

$$\begin{aligned}
 \dot{x}_1 &= \frac{2}{C_{dc}} p_{pv} - \frac{2}{C_{dc}} x_2 \frac{v_{dc}}{2} u_1 - \frac{2}{C_{dc}} x_3 \frac{v_{dc}}{2} u_2 \\
 &= \frac{2}{C_{dc}} \theta_1 x_1 + \frac{-2}{C_{dc}} \theta_7 u_1 + \frac{-2}{C_{dc}} \theta_8 u_2,
 \end{aligned} \tag{4.30}$$

where  $\theta_1$  contains  $p_{pv}$ , and indirectly variations of the solar irradiation. The LPV descriptions of the second state  $x_2 = i_{p,d}$ , defined by Eq. (3.33), is equivalent to:

$$\begin{aligned}\dot{x}_2 &= -\frac{R}{L}x_2 + \omega x_3 - \frac{1}{L}x_4 + \frac{1}{2L}v_{dc}u_1 \\ &= -\frac{R}{L}x_2 + \omega x_3 - \frac{1}{L}x_4 + \frac{1}{2L}\theta_9 u_1.\end{aligned}\quad (4.31)$$

Similarly,  $x_3 = i_{p,q}$  is described by:

$$\begin{aligned}\dot{x}_3 &= -\frac{R}{L}x_3 - \omega x_2 - \frac{1}{L}x_5 + \frac{1}{2L}v_{dc}u_2 \\ &= -\frac{R}{L}x_3 - \omega x_2 - \frac{1}{L}x_5 + \frac{1}{2L}\theta_9 u_2.\end{aligned}\quad (4.32)$$

The fact that the new state  $x_6 = v_h^2$  does not appear in any of the state equations (3.32)-(3.36) can lead to a zero-column in the matrix  $A(\theta)$ . This can violate the controllability requirement. Therefore,  $v_h^2 - v_h^2$  is added to the state equation of  $x_4 = v_{h,d}$  in Eq. (3.35):

$$\begin{aligned}\dot{x}_4 &= \omega x_5 + \frac{1}{C}x_2 - \frac{N}{C}i_{h,d} + x_6 - x_6 \\ &= \theta_2 x_1 + \frac{1}{C}x_2 + \omega x_5 + x_6,\end{aligned}\quad (4.33)$$

and to the state equation of  $x_5 = v_{h,q}$  in Eq. (3.36):

$$\begin{aligned}\dot{x}_5 &= -\omega x_4 + \frac{1}{C}x_3 - \frac{N}{C}i_{h,q} + x_6 - x_6 \\ &= \theta_3 x_1 + \frac{1}{C}x_3 - \omega x_4 + x_6.\end{aligned}\quad (4.34)$$

To avoid the dependency of the controller performance on the quality of the voltage angle estimation, a PLL is not used (as is typically done in classical approaches). The PLL also controls the voltage  $v_{h,q}$  to zero. By not using the PLL,  $v_h$  consists of both of its dq-transforms  $v_{h,d}$  and  $v_{h,q}$  with  $v_h^2 = v_{h,d}^2 + v_{h,q}^2$ . The dynamic behavior of the new state  $v_h^2$  can be described by:

$$\frac{dv_h^2}{dt} = \frac{dv_{h,d}^2}{dt} + \frac{dv_{h,q}^2}{dt}.\quad (4.35)$$

Using the relation  $\frac{dx(t)^2}{dt} = 2x \frac{dx(t)}{dt}$ , and by multiplying the equations (3.35) by  $2v_{h,d}$  and (3.36) by  $2v_{h,q}$ ,  $\frac{dv_{h,d}^2}{dt}$  and  $\frac{dv_{h,q}^2}{dt}$  can be formulated by the equations:

$$2v_{h,d}\dot{v}_{h,d} = \frac{dv_{h,d}^2}{dt} = 2\omega v_{h,q}v_{h,d} + \frac{2}{C}i_{p,d}v_{h,d} - \frac{2N}{C}i_{h,d}v_{h,d},\quad (4.36)$$

$$2v_{h,q}\dot{v}_{h,q} = \frac{dv_{h,q}^2}{dt} = -2\omega v_{h,d}v_{h,q} + \frac{2}{C}i_{p,q}v_{h,q} - \frac{2N}{C}i_{h,q}v_{h,q}.\quad (4.37)$$

The resulting state-space description of  $v_h^2$  is then:

$$\frac{dv_h^2}{dt} = \frac{2}{C}v_{h,d}(i_{p,d} - Ni_{h,d}) + \frac{2}{C}v_{h,q}(i_{p,q} - Ni_{h,q}) \quad (4.38)$$

with the LPV formulation:

$$\begin{aligned} \dot{x}_6 &= \frac{2}{C}x_4(x_2 - Ni_{h,d}) + \frac{2}{C}x_5(x_3 - Ni_{h,q}) + x_6 - x_6 \\ &= \theta_4x_1 + \frac{2}{C}\theta_5x_4 + \frac{2}{C}\theta_6x_5 + x_6. \end{aligned} \quad (4.39)$$

The LPV description of the PVS can now be summarized as:

$$\dot{x} = \underbrace{\begin{bmatrix} \frac{2}{C_{dc}}\theta_1 & 0 & 0 & 0 & 0 & 0 \\ 0 & -\frac{R}{L} & \omega & -\frac{1}{L} & 0 & 0 \\ 0 & -\omega & -\frac{R}{L} & 0 & -\frac{1}{L} & 0 \\ \theta_2 & \frac{1}{C} & 0 & 0 & \omega & 1 \\ \theta_3 & 0 & \frac{1}{C} & -\omega & 0 & 1 \\ \theta_4 & 0 & 0 & \frac{2}{C}\theta_5 & \frac{2}{C}\theta_6 & 1 \end{bmatrix}}_{A(\theta)} x + \underbrace{\begin{bmatrix} \frac{-2}{C_{dc}}\theta_7 & \frac{-2}{C_{dc}}\theta_8 \\ \frac{1}{2L}\theta_9 & 0 \\ 0 & \theta_9 \\ 0 & 0 \\ 0 & 0 \\ 0 & 0 \end{bmatrix}}_{B(\theta)} u, \quad (4.40)$$

with the parameters:

$$\begin{aligned} \theta_1 &= \frac{p_{pv}}{x_1}, & \theta_6 &= (i_{p,q} - Ni_{h,q}), \\ \theta_2 &= -\left(\frac{N}{C}i_{h,d} + x_6\right) \frac{1}{x_1}, & \theta_7 &= id \frac{v_{dc}}{2}, \\ \theta_3 &= -\left(\frac{N}{C}i_{h,q} + x_6\right) \frac{1}{x_1}, & \theta_8 &= iq \frac{v_{dc}}{2}, \\ \theta_4 &= -\frac{x_6}{x_1}, & \theta_9 &= v_{dc}, \\ \theta_5 &= (i_{p,d} - Ni_{h,d}). \end{aligned} \quad (4.41)$$

Here, states appear in the parameters. The appearance of  $x_1$  in the denominators of some parameters leads to the restriction  $x_1 = v_{dc}^2 \neq 0$ . This is not a limitation, since  $v_{dc} = 0$  will not be reached under normal operating conditions.

The bus currents  $i_{h,d}$  and  $i_{h,q}$  appear directly in the parameters, establishing the coupling to other parts of the power system. Similar to the wind speed of the WECS, the changing solar irradiation is not assumed constant and is considered through  $p_{pv}$  in  $\theta_1$ . Thus, variations from the grid side and from solar irradiation are contained in the model.

## 4.5. Discussion of the LPV Models

As already mentioned, the components and their original DAEs presented in Ch. 3 are only a selection of a variety of possible models of the same component. However,

due to similarities between the existing equations with those selected in this work (see [63]), the presented LPV modeling technique can be applied to other dynamic representations than those introduced in the previous chapter.

The different LPV models for the SG, the WECS, and the PVS have all parameter-dependent state matrices  $A(\theta)$ . Some LPVS have parameter-dependent input matrices  $B(\theta)$  and some have constant input matrices  $B$ . Thus, in the subsequent chapters, the controller synthesis is described for the general case of  $A(\theta)$  and  $B(\theta)$ . During the modeling procedure, other choices for the parameters were considered, but the resulting models were not controllable. For some LPV models, the controllability could only be confirmed during the controller synthesis (described in the next chapter). A systematic technique for the proof of controllability of an LPV model for a large system with several interconnections which are mapped into the parameters of the model, is an open task. Alternatively, a systematic procedure to find parameter ranges with ensured controllability, is a topic for future research.

One remark has to be made concerning the parameters of the LPV-models for the voltage control. In these models, differentiations over time of algebraic variables are used to calculate the parameters. In simulations, the algebraic variables can change discretely from one time-step to the next time-step during a fault. The respective differentiations can be calculated by the division of the difference of the post-fault and the pre-fault value by the time difference.

In contrast to the SG, the mechanical torque  $T_m$  of the WECS and the extracted power of the PVS  $p_{pv}$  must be assumed as varying over time. This variability is encoded in the models by the respective parameters and their ranges and is readily considered in the derived models. The choices for parameters of the three systems establish the coupling to the power system through the parameters. The interactions of grid nodes of the type SG, WECS, and PVS result in a range of parameters. Assume the set of all parameters and their ranges can be conservatively estimated or computed for all subsystems connected to the bus and is known with  $\theta^{[h]} \in [\underline{\theta}^{[h]}, \bar{\theta}^{[h]}]$  for the system  $h^1$ . The operating range of the whole power system can then be represented only by the LPV subsystems and their parameter ranges. The introduction of the parameter sets can be understood as replacement of the grid equations, and it enables the separate (decentralized) synthesis of the controllers for SG, WECS and PVS.

This principle is illustrated for the example of a 9-bus system, which was described in [5], and is shown in Fig. 4.1. The benchmark system comprises three SGs  $G_1$ ,  $G_2$ , and  $G_3$ , three transformers  $T_1$ ,  $T_2$ , and  $T_3$ , and three loads  $A$ ,  $B$ , and  $C$ . Using the modeling procedure from this chapter, the interaction between the subsystems is mapped into the parameters and their ranges. The 9-bus system can then be represented by three separate LPVS, or by one large LPVS, comprising the three subsystems and their parameters.

---

<sup>1</sup>The superscript of a number in square brackets represents the number of the subsystem.

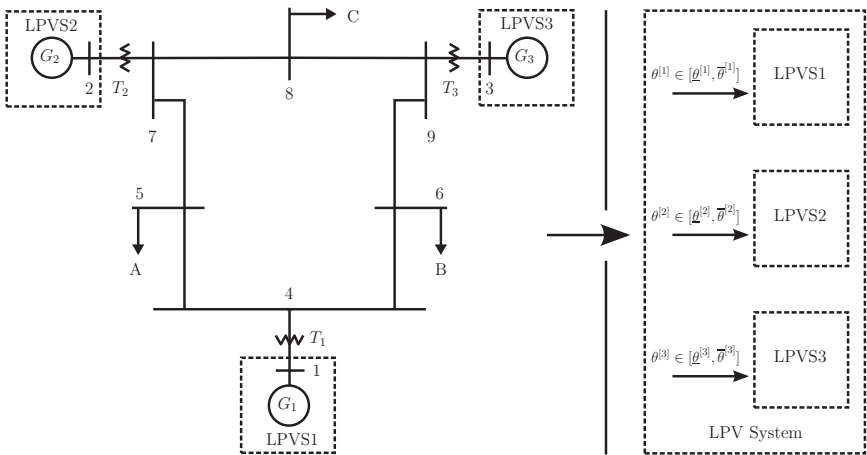


Figure 4.1.: Example of a 9-bus system, leading to three LPVS with corresponding parameter sets for the generators.



# 5. Robust Controller Synthesis for Linear Parameter-Varying Systems

This chapter addresses the task of synthesizing local LPV state feedback controllers for continuous-time LPVS. The control goals are robustly achieved for any parameter vector  $\theta$  within a parameter set  $\theta \in [\underline{\theta}, \bar{\theta}]$  of the respective subsystem described in the previous chapter. The synthesis aims at achieving quadratic stability for polytopic parameter sets, in combination with objectives for the dynamic behavior (through pole placement and  $H_\infty$ -design) and input constraints. Each of the objectives is formulated in terms of linear matrix inequalities (LMIs), and the LPV controllers are synthesized by solving these LMIs. First, a reformulation of the parameter-varying matrices into matrix polytopes is explained, a step required for the synthesis procedure to be described subsequently. After that, the LMIs for the realization of different control objectives, concerning the dynamic behavior of the system, are presented, including their combination in one controller. Next, global stability of the whole system, controlled by the decentralized LPV controllers, is shown and implementation issues of the LPV controllers are discussed. While the controller synthesis techniques for the quadratic stability, the pole placement, and the  $H_\infty$ -design already exist since the 90s, the handling of input constraints of the LPVS with the consideration of the state space constraints by the saturation are new. The proof of stability of the whole LPV controlled system has been presented by the author in [82] and will be discussed here in a more comprehensive way.

## 5.1. Polytopic System-Description

A matrix  $A(\theta)$  is called *affine* if the matrix can be partitioned in matrices  $\tilde{A}_j \in \mathbb{R}^{n_x \times n_x}$ , which depend affinely on the components  $\theta_j$  of the parameter vector  $\theta$ .  $A(\theta)$  can then be rewritten into:

$$A(\theta) = \tilde{A}_0 + \sum_{j=1}^{n_p} \theta_j \cdot \tilde{A}_j. \quad (5.1)$$

Assuming that the parameters change within the known bounds  $\theta_j \in [\underline{\theta}_j, \bar{\theta}_j]$ ,  $A(\theta)$  varies within a convex hull  $C_O \{A_i : i = 1, \dots, n_v\}$  of the vertices  $A_i \in \mathbb{R}^{n_x \times n_x}$ , which

correspond to the parameter bounds [6]. The number of vertices  $n_v$  follows from the possible combinations of interval bounds over the parameters, i.e., for  $n_p$  components of the parameter vector  $\theta$ ,  $n_v = 2^{n_p}$  vertices exist.  $A(\theta)$  can now be represented by its polytope  $\mathcal{A}$ :

$$A(\theta) \in \mathcal{A} := \left\{ \sum_{i=1}^{n_v} \alpha_i \cdot A_i : \sum_{i=1}^{n_v} \alpha_i = 1, \alpha_i \geq 0. \right\} \quad (5.2)$$

with the so called *barycentric coordinates*  $\alpha_i$ ,  $i = [1, \dots, n_v]$ . If the same applies for  $B(\theta)$  in (4.1), the complete LPVS (4.1) can be described as a matrix polytope. In the subsequent sections, calligraphic letters are used for matrix polytopes, and indexed capital letters denote their vertices (e.g., polytope  $\mathcal{A}$  and its vertices  $A_i$ ).

The LPV formulations of the systems presented in the previous chapter are all affine. Thus, they all can be represented as matrix polytopes, if the parameter bounds are known. In the subsequent sections, the polytopic description is used to design LPV controllers in terms of the barycentric coordinates  $\alpha_i$ , which must be retrieved from the parameters  $\theta_j$ ,  $j = [1, \dots, n_p]$ . This can be done by solving a semidefinite optimization problem by equating Eqs. (5.1) and (5.2). For fast dynamical systems, this method might be too time-consuming for online computation. An analytic description of the barycentric coordinates in dependency of  $\theta$  can resolve this problem. Methods for retrieving closed-form expressions for  $\alpha_i$  are presented in [103] or [84] for arbitrary polytopes. These calculations are done offline, with the result that each  $\alpha_i$ ,  $i \in \{1, \dots, n_v\}$  is described by a nonlinear function  $\alpha_i = f_{\alpha_i}(\theta)$  with the parameters  $\theta$  as argument. In this work, the polytopic description of matrices result from the combinations of all  $n_p$  parameters and their ranges. Thus, only axis aligned boxes occur as polytopes. Less conservative polytopic representations were tested but rejected, which is discussed in Ch. 5.8. This simplifies the calculation of  $\alpha_i = f_{\alpha_i}(\theta)$  to the following procedure.

Let the coordinates of a vertex corresponding to one  $\alpha_i$  be defined in terms of the parameter ranges as  $\Theta_i$ . The coordinates for an example for  $n_p = 2$  and  $n_v = 2^{n_p} = 4$  are:

$$\begin{aligned} \alpha_1 : \Theta_1 &= [\underline{\theta}_1, \underline{\theta}_2], & \alpha_2 : \Theta_2 &= [\underline{\theta}_1, \bar{\theta}_2], \\ \alpha_3 : \Theta_3 &= [\bar{\theta}_1, \underline{\theta}_2], & \alpha_4 : \Theta_4 &= [\bar{\theta}_1, \bar{\theta}_2]. \end{aligned} \quad (5.3)$$

Let complementary vertex of  $\Theta_i$  be defined as  $\Theta'_i$ . Staying with the example, the complementary vertex of  $\Theta_1$  is  $\Theta'_1 = [\bar{\theta}_1, \bar{\theta}_2]$ . Then, the functions to describe  $\alpha_i$  can be formulated as follows (e.g.[72]):

$$\alpha_i(\theta) = f_{\alpha_i}(\theta) = \frac{\prod_{j=1}^{n_p} \nu_j}{\prod_{j=1}^{n_p} (\bar{\theta}_j - \underline{\theta}_j)}, \quad (5.4)$$

$$\nu_j = \begin{cases} \theta_j - \Theta'_i(j) & \text{if } \Theta'_i(j) = \underline{\theta}_j \\ \Theta'_i(j) - \theta_j & \text{if } \Theta'_i(j) = \bar{\theta}_j \end{cases} \quad (5.5)$$

Calculations for  $n_p = 3$ , following the technique presented in [103], lead to the same analytic descriptions for  $\alpha_i = f_{\alpha_i}(\theta)$  as with the technique using Eqs. (5.4) and (5.5).

## 5.2. Quadratic Stability

The LMI-based controller synthesis is based on a polytopic description of the closed-loop system. This system is stabilized for all parameter trajectories  $\theta \in [\underline{\theta}, \overline{\theta}]$ , if stability criteria formulated as LMIs can be satisfied for any vertex of the polytope. Boyd et al. use in [10] the more general term *polytopic linear differential inclusions* to describe the *polytopic family of time-varying systems*. With a state feedback control matrix  $K$  the closed-loop system can be written as a polytope  $\mathcal{A}_{cl}$  with the vertices  $A_{cl,i} = A_i + B_i K$  for  $i \in \{1, \dots, n_v\}$ . For the closed-loop system, *quadratic stability* is guaranteed for all  $\theta \in [\underline{\theta}, \overline{\theta}]$ , if a symmetric matrix  $X$  can be found that satisfies [10]:

$$[A_{cl,i}X + XA_{cl,i}^T] < 0, \quad X > 0 \quad (5.6)$$

for any of the  $n_v$  vertices of the polytope  $\mathcal{A}_{cl}$ . The solution of these LMI implies the existence of the Lyapunov function  $V(x) = x^T P x$  with  $P = X^{-1}$  for the specific parameter set  $[\underline{\theta}, \overline{\theta}]$ , and that the system state must be contained in an invariant ellipsoid  $x \in \mathcal{E} = \{x \mid x^T P x \leq 1\}$ .

Instead of using one matrix  $K$  for all vertices with index  $i \in \{1, \dots, n_v\}$ , the following parts parametrize the controller based on  $\theta$  (or  $\alpha$  respectively). Assuming an affine controller structure  $K(\theta)$  and for known parameter limits  $\theta \in [\underline{\theta}, \overline{\theta}]$ , the controller can be expressed as a polytope  $\mathcal{K}$  as well. Several approaches in literature in this context are based on the assumption of a constant matrix  $B$  (e.g. in [19] and [65]). Then, Eq. (5.6) can be used again with  $A_{cl,i} = A_i + B K_i$  (see [6]). In the case that the input matrix is parameter dependent, a filter can be introduced to reformulate the system into one with a constant input matrix as it is done in [19]. In this work, the parameter-dependency of  $B$  is instead handled directly in the controller synthesis. Thus, the input matrix is formulated as  $B(\theta_r)$ , with  $\theta_r$  containing the parameters affecting  $B$ . For better distinction of the parameters affecting the matrices, let  $A$  depend on  $\theta_c$ . For different  $\theta_c$  and  $\theta_r$ , the controller can either be scheduled by  $\theta_c$  or  $\theta_r$ . The objective of the synthesis is here to design a controller which is robust against changes of  $\theta_r$  and which is scheduled by  $\theta_c$ . The closed-loop system results to:

$$A_{cl}(\theta_c, \theta_r) = A(\theta_c) + B(\theta_r)K(\theta_c). \quad (5.7)$$

If all parameter limits are known, i.e.  $\theta_r \in [\underline{\theta}_r, \overline{\theta}_r]$  and  $\theta_c \in [\underline{\theta}_c, \overline{\theta}_c]$ , the matrices over all parameter ranges can be referred to again by matrix polytopes  $\mathcal{A}$ ,  $\mathcal{B}$  and

$\mathcal{K}$ , leading to:

$$\mathcal{A}_{cl} = \sum_{i=1}^{n_v} \alpha_i A_i + \sum_{j=1}^{n_b} \alpha_j B_j \sum_{i=1}^{n_v} \alpha_i K_i \quad (5.8)$$

for the closed-loop. In [12], it is shown that the convex hull of a product of two matrix polytopes can be obtained as the convex hull of the products of the vertices of the two matrix polytopes. The idea behind this reasoning is shown by the example of the previous equation for  $\sum_{j=1}^{n_b} \alpha_j B_j \sum_{i=1}^{n_v} \alpha_i K_i$ . By using the property of the barycentric coordinates with  $\sum_{i=1}^{n_v} \alpha_i = 1, \alpha_i \geq 0$  (same for  $\alpha_j$ ), it follows:

$$\sum_{j=1}^{n_b} \alpha_j \sum_{i=1}^{n_v} \alpha_i = \sum_{j=1}^{n_b} \sum_{i=1}^{n_v} \alpha_j \alpha_i = 1. \quad (5.9)$$

Reorganizing the product of the two polytopes leads to:

$$\sum_{j=1}^{n_b} \alpha_j B_j \sum_{i=1}^{n_v} \alpha_i K_i = \sum_{j=1}^{n_b} \sum_{i=1}^{n_v} (\alpha_j \alpha_i) B_j K_i, \quad (5.10)$$

resulting in a polytopic description according to Eq. (5.2), with the barycentric coordinates  $\alpha_j \alpha_i$  and the vertices  $B_j K_i$ . Thus, the resulting vertices  $A_{cl,p}$  of the polytopic closed-loop matrix can also be formulated as:

$$\begin{aligned} A_{cl,p} &= A_i + B_j \cdot K_i \\ \forall i &= 1, \dots, n_v, j = 1, \dots, n_b \end{aligned} \quad (5.11)$$

for  $p \in \{1, \dots, n_v \cdot n_b\}$ . In [79] and [78], this fact was used to design controllers that are robust against parameter changes in  $\theta_r$ . Using (5.6) (for quadratic stability) and (5.11) and by introducing auxiliary variables  $Y_i = K_i X$ , the LMIs to be satisfied for controller synthesis are [79]:

$$\begin{aligned} A_i X + X A_i^T + B_j Y_i + Y_i^T B_j^T &< 0, X > 0 \\ \forall i &= 1, \dots, n_v, j = 1, \dots, n_b. \end{aligned} \quad (5.12)$$

It is stressed that the parameter vectors  $\theta_r$  and  $\theta_c$  may have common parameters. The consequence is that this common parameters schedule the controller  $K(\theta_c)$  and at the same time the controller is robust against changes of these parameters. However, the robustness remains and the controller is scheduled by the remaining parameters in  $\theta_c$ . In the case that  $\theta_r = \theta_c$ , with the closed-loop vertices  $A_i + B_j \cdot K_i$ , the LMIs (5.12) for controller synthesis must not be built by combining  $B_j, j = i = 1, \dots, n_b = n_v$  with all  $K_i, i = j = 1, \dots, n_v = n_b$ . Instead, either a constant state feedback matrix  $K$  is used or the whole closed-loop system is stabilized only at the vertices with index  $i$ , while the system is described by  $A_i + B_i \cdot K_i$ .

In the following, the LMIs for the presented control objectives are formulated in terms of the vertices  $A_{cl,p}$  of the closed-loop matrix  $A_{cl}(\theta)$ .

### 5.3. Quadratic $\mathfrak{D}$ -Stability

The quadratic stability can be straightforwardly extended by pole placement constraints, leading to the so called *Quadratic  $\mathfrak{D}$ -Stability*. It allows introducing specific dynamic behavior to the closed-loop system. First, a formal description for a pole region is introduced.

**Definition 5.1.** – *LMI-Region [15]: With symmetric matrices  $\alpha_d, \beta_d \in \mathbb{R}^{m \times m}$ , a subset  $\mathfrak{D}$  of the complex plane is defined as (with  $\bar{\mu}$  the conjugate complex of the pole  $\mu$ ):*

$$\mathfrak{D} = \{\mu \in \mathbb{C} : f_D(\mu) = \alpha_d + \mu\beta_d + \bar{\mu}\beta_d^T < 0\}. \quad (5.13)$$

Thus, the choices of the matrices  $\alpha_d$  and  $\beta_d$  define the LMI-regions. Relevant regions and the corresponding matrices will be presented in the subsequent part.

**Lemma 5.1.** – *Quadratic  $\mathfrak{D}$ -Stability [15]: A polytopic (closed-loop) system with a system-matrix  $A_{cl}(\theta)$  as defined in (5.2) is  $\mathfrak{D}$ -stable, i.e. the poles of the matrix polytope are located in the LMI-region  $\mathfrak{D}$ , if there exists a symmetric matrix  $X > 0$  such that:*

$$M(A_{cl,p}, X) = \alpha_d \otimes X + \beta_d \otimes (A_{cl,p}X) + \beta_d^T \otimes (A_{cl,p}X)^T < 0, \quad (5.14)$$

for all vertices of the polytope  $\mathcal{A}_{cl}$ , with  $\otimes$  being the Kronecker product.

The proof of this lemma is presented in [15].  $M(A_{cl,p}, X)$  is obtained by inserting  $(X, A_{cl,p}X, XA_{cl,p}^T)$  in  $f_D(\mu)$  instead of  $(1, \mu, \bar{\mu})$ . In the following, the LMIs for the relevant LMI-regions *half plane* and the *conic sector* are presented, as depicted in Fig. 5.1. With these regions, the velocity and damping of the controlled system can be restricted. The half-plane is realized as an LMI region with  $Re(\mu) < -\alpha_d$ ,  $\alpha_d \in \mathbb{R}^{\geq 0}$  by:

$$2\alpha_d X + A_{cl,p}X + XA_{cl,p}^T < 0, \quad X > 0. \quad (5.15)$$

By moving the poles to the left along the real axis, the closed-loop system dynamics becomes faster. To limit system velocity, the poles can be additionally constrained by  $Re(\mu) > -\alpha_{d,1}$ . Then, the “ $< 0$ ” in (5.15) has to be changed “ $> 0$ ”. The conic sector with the angle  $\varphi_d$ ,  $\varphi_d \in \mathbb{R}$  between the line crossing zero and the real-axis is realized by the following LMI:

$$\begin{bmatrix} \sin(\varphi_d)(A_{cl,p}X + XA_{cl,p}^T) & \cos(\varphi_d)(A_{cl,p}X - XA_{cl,p}^T) \\ -\cos(\varphi_d)(A_{cl,p}X - XA_{cl,p}^T) & \sin(\varphi_d)(A_{cl,p}X + XA_{cl,p}^T) \end{bmatrix} < 0, \quad X_D > 0. \quad (5.16)$$

Similar to the quadratic stability, the vertices  $K_i$  of the controller  $K(\theta)$  are determined based on the closed-loop matrix  $A_{cl,p}$  (e.g.  $A_{cl,p} = A_i + B_j \cdot K_i$  as in Eq. (5.11)). The inequalities are linearized by using the variable  $Y_i = K_i X$ .

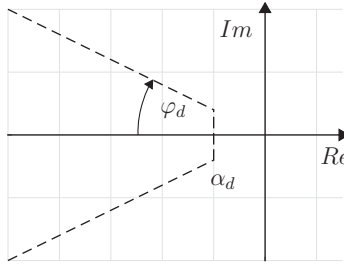


Figure 5.1.: The (left) half plane and conic sector combined to one LMI-region.

## 5.4. LMI Formulations for $H_\infty$ -Design

The  $H_\infty$ -controller design is typically known in the context of robust control. In this work, it is used to improve the dynamic behavior of the closed-loop system, which is detailed in the subsequent part. The  $H_\infty$ -design is presented next. Let the LPV formulation from Eq. (4.1) be extended by outputs  $z \in \mathbb{R}^{n_z}$  for specifying the control performance and by exogenous inputs (e.g. disturbances)  $w \in \mathbb{R}^{n_w}$ , leading to the following description:

$$\begin{aligned}\dot{x}(t) &= A(\theta(t))x(t) + B(\theta(t))u(t) + B_1(\theta(t))w(t), \\ z(t) &= C_1(\theta(t))x(t) + D_{11}(\theta(t))u(t) + D_{12}(\theta(t))w(t).\end{aligned}\tag{5.17}$$

To simplify this description for  $H_\infty$ -design, some assumptions on the LPVS have to be made:

**Assumption 5.1.** *The matrices  $B_1(\theta(t))$  and  $C_1(\theta(t))$  are parameter independent.*

**Assumption 5.2.** *The matrices  $D_{11}(\theta(t))$  and  $D_{12}(\theta(t))$  are set to  $D_{11}(\theta(t)) = 0$  and  $D_{12}(\theta(t)) = 0$ .*

These assumptions are motivated by the LPV models derived in Ch. 4, where the models do not contain any exogenous inputs. However, in Ch. 6, the  $H_\infty$ -constraint for the transfer function from an additive disturbance  $w(t)$  of a state equation for the state  $i$   $\dot{x}_i$  to the output  $z = x_i G_{zw}(s)$  is used for controller design (the state  $x_i$  is chosen depending on the system to be controlled). Thus,  $B_1$  and  $C_1$  are defined to a constant value and  $D_{11}$  and  $D_{12}$  to zero. The constraint pushes the poles of the closed-loop system to the left-hand side, increasing velocity of the controlled system. With these assumptions and the division of the parameter vector in  $\theta_r$  and  $\theta_c$  (Sec. 5.2), the LPVS for state feedback controller design writes as:

$$\begin{aligned}\dot{x}(t) &= A(\theta_c)x(t) + B(\theta_r)u(t) + B_1w(t) \\ z(t) &= C_1x(t).\end{aligned}\tag{5.18}$$

The matrices of the LPV state feedback controlled closed-loop system are then  $B_{cl} = B_1$ ,  $C_{cl} = C_1$ , and  $D_{cl} = 0$ , and the vertices of the closed-loop matrix  $A_{cl}$  are as in Eq. (5.11).

**Lemma 5.2.** – *Quadratic  $H_\infty$  Performance [6]: The closed-loop transfer function  $G_{zw}(s)$  is defined as the transfer function from  $w$  to  $z$ . The  $H_\infty$  closed-loop performance  $\|G_{zw}(s)\|_\infty < \gamma$  can be guaranteed, if a symmetric matrix  $X$  is found which satisfies the following LMI condition:*

$$\begin{bmatrix} A_{cl,p}X + XA_{cl,p}^T & B_{cl} & XC_{cl}^T \\ B_{cl}^T & -\gamma I & D_{cl}^T \\ C_{cl}X & D_{cl} & -\gamma I \end{bmatrix} < 0, \quad X > 0, \quad (5.19)$$

for all vertices of the closed-loop matrix  $A_{cl}$ .

The proof of this lemma is presented in [6]. In order to compute the vertices  $K_i$  of the controller  $K(\theta)$ , the closed-loop matrix  $A_{cl,p}$  (e.g.  $A_{cl,p} = A_i + B_j \cdot K_i$  as in Eq. (5.11)) must be inserted in the inequalities. The linearization of the inequalities is realized by using the variable  $Y_i = K_i X$ . If no specific  $\gamma$  is predefined, the controller synthesis can also be formulated in form of a semidefinite program as:

$$\begin{aligned} \min_{K_i, X} \quad & \gamma \\ \text{s.t. :} \quad & (5.19) \end{aligned} \quad (5.20)$$

## 5.5. LPV Controller Synthesis with Input Saturation

Motivated by the fact that (as for most applications), the control inputs of grid components are subject to physical bounds, an LPV controller which handles input constraints is designed in this section. Existing techniques for input-constrained LPVS are discussed next.

One way of handling input constraints is to use anti-windup techniques, as e.g. in [40], where an additional control loop is added to compensate the saturated input. An alternative is to consider the constraint directly in the synthesis procedure by avoiding saturated inputs, (see in [10] for LTI systems), or by allowing them. The latter design leads to high-gain controllers with good performance. The key step is the integration of a saturation model into the synthesis constraints [94]. Two straightforward results for this step are presented in [19] and [69], in which a tangential hyperbolic function is used to approximate the saturation, or a vector-valued deadzone function, respectively. Both concepts hide the resulting nonlinearity (describing the saturation) in a parameter of the LPVS similarly to the methods presented in the previous chapter. However, the introduced nonlinear functions for the input saturation are approximative. A different option is the direct polytopic modeling of saturations, bearing the advantage of being compatible

to synthesis techniques based in polytopic descriptions: one instant is proposed in [37] for LTI-controllers, and was further developed for LPV controllers in [13]. A drawback is that the controller gain is not constrained in the synthesis, leading possibly to very large values. In [105], a polytopic model of the saturation is provided, while considering the controller gain by encoding the level of saturation. However, the gain is not constrained either, making an anti-windup technique necessary. In [78] and [80], the latter idea is extended by introducing a parameter-dependent input matrix, in which the additional parameter models the level of saturation. The auxiliary parameter is treated as a completely independent one, while depending on the input gain. However, the input gain in turn is not constrained in the underlying LMI-based synthesis technique. This assumption of a consistent match of the parameter limits and the level of saturation is difficult to achieve in practice.

Based on this observation, the idea of an additional parameter for the level of saturation is adapted in this thesis, and the synthesis procedure is extended by proposing LMIs which restrict the system state to regions that comply with the admissible set of inputs.

For the state feedback controller  $K(\theta_c)$ , input saturation can be formulated by  $u = \text{sat}(K(\theta_c)x)$ . Let the superscripted  $l \in \{1, \dots, n_u\}$  index the components of  $u$ , i.e.  $K^l(\theta_c)$  is the  $l$ -th row of the control matrix. The saturation function for the controlled input  $u^l$  with  $-u_{\text{sat}}^l \leq u^l \leq u_{\text{sat}}^l$  for a given  $u_{\text{sat}}^l \in \mathbb{R}^{>0}$  is then:

$$u^l = \begin{cases} u_{\text{sat}}^l & \text{if } K^l(\theta_c)x > u_{\text{sat}}^l \\ K^l(\theta_c)x & \text{if } -u_{\text{sat}}^l \leq K^l(\theta_c)x \leq u_{\text{sat}}^l \\ -u_{\text{sat}}^l & \text{if } K^l(\theta_c)x < -u_{\text{sat}}^l \end{cases}. \quad (5.21)$$

To comply with the polytopic system descriptions, an auxiliary parameter  $\theta_s^l$  is introduced which models the level of saturation of the  $l$ -th input as proposed in [105] and [13]:

$$\theta_s^l = \begin{cases} \frac{u_{\text{sat}}^l}{K^l(\theta_c)x} & \text{if } K^l(\theta_c)x > u_{\text{sat}}^l \\ 1 & \text{if } -u_{\text{sat}}^l \leq K^l(\theta_c)x \leq u_{\text{sat}}^l \\ \frac{-u_{\text{sat}}^l}{K^l(\theta_c)x} & \text{if } K^l(\theta_c)x < -u_{\text{sat}}^l \end{cases} \quad (5.22)$$

leading to the following reformulation of the input saturation:

$$u^l = \text{sat}(K^l(\theta_c)x) = \theta_s^l K^l(\theta_c)x. \quad (5.23)$$

A concise matrix expression for  $u$  with an auxiliary input matrix  $B_s(\theta_s)$ , which is obviously affine in  $\theta_s$ , is:

$$\underbrace{\begin{bmatrix} u^1 \\ u^2 \\ \vdots \\ u^{n_u} \end{bmatrix}}_u = \underbrace{\begin{bmatrix} \theta_s^1 & 0 & \dots & 0 \\ 0 & \theta_s^2 & \dots & 0 \\ \vdots & \vdots & \ddots & \vdots \\ 0 & 0 & \dots & \theta_s^{n_u} \end{bmatrix}}_{B_s(\theta_s)} \underbrace{\begin{bmatrix} K^1(\theta_c) \\ K^2(\theta_c) \\ \vdots \\ K^{n_u}(\theta_c) \end{bmatrix}}_{K(\theta_c)} x. \quad (5.24)$$

For a controlled system with constrained input, the closed-loop matrix (5.7) can now be complemented by (5.24), leading to:

$$\begin{aligned} \dot{x} &= A(\theta)x + B(\theta)u = A(\theta_c)x + B(\theta_r)\text{sat}(K(\theta_c)x) \\ &= \underbrace{A(\theta_c) + B(\theta_r)B_s(\theta_s)K(\theta_c)}_{\mathcal{A}_{cl}(\theta_c, \theta_r, \theta_s)} x. \end{aligned} \quad (5.25)$$

Assume that the limits of  $\theta_s$  are known to be  $\theta_s^l \in [\underline{\theta}_s^l, \bar{\theta}_s^l] = [\underline{\theta}_s^l, 1]$  for all  $l \in \{1, \dots, n_u\}$ , where  $\bar{\theta}_s^l = 1$  corresponds to the unsaturated input. With known parameter ranges, according to Eq. (5.2),  $B_s(\theta_s)$  can be described as a matrix polytope  $\mathcal{B}_s$ . The matrix polytope of the closed-loop system matrix is then:

$$\mathcal{A}_{cl} = \sum_{i=1}^{n_v} \alpha_i A_i + \sum_{j=1}^{n_b} \alpha_j B_j \sum_{k=1}^{n_s} \alpha_k B_{s,k} \sum_{i=1}^{n_v} \alpha_i K_i. \quad (5.26)$$

The vertices of the latter matrix polytope are defined by:

$$A_{cl,p} = A_i + B_j B_{s,k} K_i \quad (5.27)$$

for all combinations of  $i \in \{1, \dots, n_v\}$ ,  $j \in \{1, \dots, n_b\}$ , and  $k \in \{1, \dots, n_s\}$ , i.e.  $p$  is defined on the set  $\{1, \dots, n_v \cdot n_b \cdot n_s\}$ . Again, the controller is scheduled by  $\theta_c$  only.

Motivated by a formulation proposed in [80] for a system similar to (5.26), the following LMIs can be used for synthesizing the matrices  $K_i$ :

$$\begin{aligned} A_i X + X A_i^T + B_j B_{s,k} Y_i + Y_i^T B_{s,k}^T B_j^T &< 0, \quad X > 0 \\ \forall i \in \{1, \dots, n_v\}, j \in \{1, \dots, n_b\}, k \in \{1, \dots, n_s\}, \end{aligned} \quad (5.28)$$

with  $Y_i := K_i X$ . The solution of (5.28) implies that the system state must be contained in an invariant ellipsoid  $x \in \mathcal{E} = \{x \mid x^T X^{-1} x \leq 1\}$ .

The resulting control law is parametrized by  $\theta_c$ , and it is robust against changes of  $\theta_r$  and  $\theta_s$ . However, the parameters in the set  $\theta_s$  are treated as a fully independent parameters without considering that the resulting state space  $x \in \mathcal{E}$  might not comply with the state space corresponding to the input constraint  $\underline{\theta}_s^l \mathcal{K}^l x \geq -u_{sat}^l$  and  $\underline{\theta}_s^l \mathcal{K}^l x \leq u_{sat}^l$ .  $\mathcal{K}^l$  is the  $l$ -th row of the controller matrix polytope. In fact,  $x$  must be bound to a region of the state space, which is consistent to these input constraints. The following result specifies additional LMIs which satisfy these requirements, making sure that the resulting state space  $x \in \mathcal{E}$  comply with the parameter limits  $\theta_s^l \in [\underline{\theta}_s^l, 1]$  of the input saturation, as well. While stability results for the case of LTI-systems with input constraints exist in literature [94], a result for robust control of LPVS with input saturation according to (5.21) and parameter dependent input matrix is new.

**Theorem 5.1.** *Given an LPVS with closed-loop system matrix (5.7) and with inputs constrained according to (5.21). The system is stabilized by  $K(\theta_c) = \sum_{i=1}^{n_v} \alpha_i K_i$*

with vertices  $K_i = Y_i X^{-1}$ ,  $i \in \{1, \dots, n_v\}$  for any  $\theta_c \in [\underline{\theta}_c, \bar{\theta}_c]$ ,  $\theta_r \in [\underline{\theta}_r, \bar{\theta}_r]$ , and  $\theta_s \in [\underline{\theta}_s, 1]$ , if  $X$  and  $Y_i$  exist as solution of the LMIs:

$$A_i X + X A_i^T + B_j B_{s,k} Y_i + Y_i^T B_{s,k}^T B_j^T < 0, \quad X > 0, \quad (5.29)$$

$$\begin{bmatrix} X & (Y_i^l)^T \\ (Y_i^l) & (\frac{u_{sat}^l}{\underline{\theta}_s^l})^2 \end{bmatrix} \geq 0 \quad (5.30)$$

for all  $i \in \{1, \dots, n_v\}$ ,  $j \in \{1, \dots, n_b\}$ ,  $k \in \{1, \dots, n_s\}$ , and  $l$  inputs with  $l \in \{1, \dots, n_u\}$ .

*Proof.* The first LMIs (5.29) imply the existence of a Lyapunov function in the sense of (5.6) and (5.12), i.e., if these LMIs are satisfied quadratic stability is guaranteed with the system states being contained in the invariant ellipsoid  $x \in \mathcal{E} = \{x \mid x^T X^{-1} x \leq 1\}$ .

The input constraints  $\underline{\theta}_s^l \mathcal{K}^l x \geq -u_{sat}^l$  and  $\underline{\theta}_s^l \mathcal{K}^l x \leq u_{sat}^l$ , with  $0 < \underline{\theta}_s^l \leq 1$  according to Eq. (5.22), can be reformulated into:

$$\max_{x \in \mathcal{E}} \|\mathcal{K}^l x\|_2 \leq \frac{u_{sat}^l}{\underline{\theta}_s^l}. \quad (5.31)$$

Now consider an additional polytopic variable  $\mathcal{Y} = \mathcal{K}X$ , with the  $l$ -th row denoted by  $\mathcal{Y}^l$ . Using an alternative representation for the ellipsoid  $\mathcal{E}$  as an image of the unit ball with  $x = X^{\frac{1}{2}} z$ ,  $\|z\|_2 \leq 1$  [10, Ch. 3.7], leads to a transformation of (5.31) to:

$$\max_{x^T X^{-1} x \leq 1} \|\mathcal{Y}^l X^{-1} x\|_2 = \max_{\|z\|_2 \leq 1} \|\mathcal{Y}^l X^{-\frac{1}{2}} z\|_2 \leq \frac{u_{sat}^l}{\underline{\theta}_s^l}. \quad (5.32)$$

Using the largest absolute eigenvalue  $\lambda_{max}$  of the argument of the Euclidean norm together with  $\|z\|_2 = 1$ , Eq. (5.32) is modified to:

$$\sqrt{\lambda_{max}((X^{-\frac{1}{2}})^T (\mathcal{Y}^l)^T \mathcal{Y}^l X^{-\frac{1}{2}})} \leq \frac{u_{sat}^l}{\underline{\theta}_s^l}, \quad (5.33)$$

and further to:

$$(X^{-\frac{1}{2}})^T (\mathcal{Y}^l)^T \mathcal{Y}^l X^{-\frac{1}{2}} \leq \left(\frac{u_{sat}^l}{\underline{\theta}_s^l}\right)^2 \quad (5.34)$$

$$\Leftrightarrow X - (\mathcal{Y}^l)^T \left(\frac{u_{sat}^l}{\underline{\theta}_s^l}\right)^{-2} \mathcal{Y}^l \geq 0. \quad (5.35)$$

The latter nonlinear matrix inequality is transformed by using the Schur complement. Furthermore, using the vertices  $Y_i^l$ ,  $i \in \{1, \dots, n_v\}$  of the polytope  $\mathcal{Y}^l$ , the LMI constraint (5.30) follows.  $\square$

**Remark 5.1.** A controller which avoids input saturation can be designed with the presented technique by choosing  $\underline{\theta}_s = 1$ . The resulting controller typically has a lower performance as its dynamics is much slower compared to one where saturation is permitted.

## 5.6. Multiobjective Design of the LPV Controller

For the synthesis of multiobjective LPV controllers, the LMIs referring to the desired control goals from Ch. 5.2-5.5 have to be combined. If the LMIs for a selected set of control objectives are satisfied for any of the vertices  $A_{cl,p}$  of the polytope  $A_{cl}(\theta)$  with the same matrix  $X > 0$ , the properties established by the constraints of the semidefinite program (SDP) also hold for the complete polytopical space of the parameters  $\theta \in [\underline{\theta}, \bar{\theta}]$  [6]. The obtained matrix inequalities are linearized by using the auxiliary variables  $Y_i := K_i X$ , leading to the following SDP:

$$\begin{aligned} \min_{K_i, X} \quad & \gamma & (5.36) \\ \text{s.t. :} \quad & (5.6), (5.15), (5.16), (5.19), (5.29) \text{ and } (5.30). \end{aligned}$$

The solution consists of  $\gamma$  and the controller matrix  $K_i$ . If the semidefinite optimization problem returns a feasible solution for  $K_i$  and  $X$  for any vertex  $A_{cl,p}$  of the matrix polytope  $A_{cl}(\theta)$ , the LPV controller  $K(\theta_c)$  stabilizes the subsystem for any parameter in  $\theta \in [\underline{\theta}, \bar{\theta}]$ . The number of LMIs for each of the sets as defined by Eqs. (5.6), (5.15), (5.16), (5.19), and (5.29) in the SDP (5.36) is calculated by  $n_v \cdot n_b \cdot n_s$ , where one additional LMI has to be added for  $X > 0$ . Taking the three sets of LMIs for the conic sector, the half plane, and the  $H_\infty$ -design as an example, leads to the total number of LMIs of  $3 \cdot n_v \cdot n_b \cdot n_s + 1$ , defining the size of the SDP. The resulting sizes of the SDPs for the controller synthesis of one LPVS and the computation times are not critical and will be mentioned exemplarily in the next chapter. Due to the modular modeling of the complete system by several LPVS, the overall problem for the controller synthesis grows linearly with the number of the controlled LPVS. It is stressed that the sets of LMIs in (5.15) for the half-plane (with  $\alpha = 0$ ), in (5.16) for the conic sector (with  $\varphi_d = 90^\circ$ ), in (5.19) for the  $H_\infty$ -design (first row and first line of the matrix), as well as in (5.29) for the input constraints contain the LMIs for quadratic stability, as defined by Eq. (5.6). Consequently, the solution of each set of the respective LMIs implies quadratic stability individually.

## 5.7. Global Stability of the LPV controlled System

As established by the previous section, the solution of the corresponding LMIs implies that the local LPV controller stabilizes the respective subsystem with index  $h$  when the parameter vectors adhere to their ranges. Also, there exists a local Lyapunov function  $V^{[h]}(x^{[h]}) = x^{[h]T} P^{[h]} x^{[h]}$  with  $P^{[h]} = X^{[h]-1}$ . As discussed in Sec. 4.5 and shown in Fig. 4.1 by using the same LPVS modeling technique for all subsystems, the complete (uncontrolled) system can be established as one modular

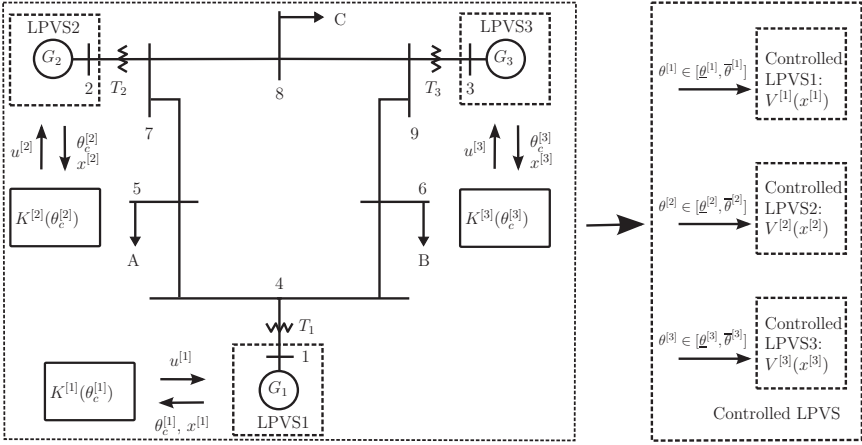


Figure 5.2.: Example of a 9-bus system, leading to three LPVS with corresponding parameter sets for the generators and LPV controllers.

LPVS as:

$$\underbrace{\begin{bmatrix} \dot{x}^{[1]} \\ \dot{x}^{[2]} \\ \vdots \\ \dot{x}^{[q]} \end{bmatrix}}_{\dot{\mathbf{x}}} = \underbrace{\begin{bmatrix} A^{[1]}(\theta^{[1]}) & 0 & \dots & 0 \\ 0 & A^{[2]}(\theta^{[2]}) & \dots & 0 \\ \vdots & \vdots & \ddots & \vdots \\ 0 & 0 & \dots & A^{[q]}(\theta^{[q]}) \end{bmatrix}}_{\mathbf{A}(\theta)} \underbrace{\begin{bmatrix} x^{[1]} \\ x^{[2]} \\ \vdots \\ x^{[q]} \end{bmatrix}}_{\mathbf{x}} \quad (5.37)$$

By using the local Lyapunov functions  $V^{[h]}(x^{[h]})$  obtained from the local syntheses (which is numerically not demanding when carried out in this decentralized fashion), a Lyapunov function for the complete system can be constructed. The stability result for the subsystem can be extended to the complete system, where the system is partitioned into several LPV controlled subsystems as indicated in Fig. 5.2 for the exemplary 9-bus system. Here, the term global stability refers to the stability of all subsystems and for the predefined parameter ranges. This result follows since the same reasoning as derived in [82] holds also for the case that the set of stabilized subsystems include subsystems with input saturation. In order to introduce the extension of the stability result to the complete power system, the following assumption is made:

**Assumption 5.3.** For a system with  $q$  generators and a grid as represented by (3.3), assume that  $\theta^{[h]} \in [\underline{\theta}^{[h]}, \bar{\theta}^{[h]}]$  over-approximates the set of parameters  $[\underline{\theta}_{real}^{[h]}, \bar{\theta}_{real}^{[h]}]$ , which results for generator  $h$  from the effects imposed by all nodes with  $\bar{y}_{hk}^* \neq 0$ . □.

**Theorem 5.2.** *If, for all buses associated with generators  $h \in \{1, \dots, q\}$ , Assumption 5.3 holds and the controller  $K^{[h]}(\theta^{[h]})$  with  $\theta^{[h]} \in [\underline{\theta}^{[h]}, \bar{\theta}^{[h]}]$  is synthesized according to the decentralized solution of Eq. (5.36) for the LPVS, then the power system as described in Ch. 3 is stabilized in terms of quadratic stability, as defined in Ch. 5.2.  $\square$*

*Proof.* The assumption 5.3 implies that  $\theta^{[h]} \in [\underline{\theta}^{[h]}, \bar{\theta}^{[h]}]$  conservatively represents the effects of the power system on the generator  $h$ . The coupling according to Eq. (3.3) is thus replaced by the local robustly parametrized models (see Fig. 5.2). If the problem (5.36) has a solution for any  $h$ , i.e.  $K^{[h]}(\theta^{[h]})$  and  $X^{[h]} > 0$  exist, then theorem 5.2 implies the existence of a local Lyapunov function  $V^{[h]}(x^{[h]})$  for the generator  $h$  and thus Lyapunov stability. A global Lyapunov function for the closed-loop system:

$$\underbrace{\begin{bmatrix} \dot{x}^{[1]} \\ \dot{x}^{[2]} \\ \vdots \\ \dot{x}^{[q]} \end{bmatrix}}_{\dot{\mathbf{x}}} = \underbrace{\begin{bmatrix} A_{cl}^{[1]}(\theta^{[1]}) & 0 & \dots & 0 \\ 0 & A_{cl}^{[2]}(\theta^{[2]}) & \dots & 0 \\ \vdots & \vdots & \ddots & \vdots \\ 0 & 0 & \dots & A_{cl}^{[q]}(\theta^{[q]}) \end{bmatrix}}_{\mathbf{A}_{cl}(\theta)} \underbrace{\begin{bmatrix} x^{[1]} \\ x^{[2]} \\ \vdots \\ x^{[q]} \end{bmatrix}}_{\mathbf{x}} \quad (5.38)$$

is obtained by constructing  $V(\mathbf{x}) = \mathbf{x}^T \mathbf{P} \mathbf{x}$  and  $\mathbf{P} = \mathbf{X}^{-1}$  where:

$$\mathbf{X} = \begin{bmatrix} X^{[1]} & 0 & \dots & 0 \\ 0 & X^{[2]} & \dots & 0 \\ \vdots & \vdots & \ddots & \vdots \\ 0 & 0 & \dots & X^{[q]} \end{bmatrix}. \quad (5.39)$$

$X^{[h]} > 0$  implies  $\mathbf{X} > 0$  and  $V(\mathbf{x}) > 0$ . Then,  $\frac{dV(\mathbf{x})}{dt} = \mathbf{x}^T (\mathbf{A}_{cl}(\theta)^T \mathbf{P} + \mathbf{P} \mathbf{A}_{cl}(\theta)) \mathbf{x} < 0$  follows from the vertex property of the polytopic description of  $\mathbf{A}_{cl}(\theta)$  for any  $\theta \in [\underline{\theta}, \bar{\theta}]$ . Since all LPVS in Ch. 4 are obtained by exact transformations, the complete power system is stabilized<sup>1</sup>.  $\square$

It has to be mentioned that in the considered application of the controllers to power systems, the steady state is usually not zero. However, the stability result is still valid if the state  $x$  is treated as an  $\Delta x$ , which describes the difference between the state and the post-fault steady-state  $x_r$ , assuming that there exists a corresponding value for the parameters.

<sup>1</sup>The proof is considerably simpler as in [32], since the decoupling avoids coupling terms in the Lyapunov functions.

## 5.8. LPV Controller Computation and Implementation

This section deals with the computation of the LPV controllers, i.e. the computation of the parameter limits, and the implementation of the controllers.

The robustness and global stability of the described modeling and controller approach is based on the assumption that the physical links in between the machines are modeled and conservatively mapped into their parameter intervals, i.e. if  $\theta^{[h]} \in [\underline{\theta}^{[h]}, \bar{\theta}^{[h]}]$ . Thus, it is necessary to find the parameter bounds  $[\underline{\theta}^{[h]}, \bar{\theta}^{[h]}]$  for the (local) controller design of subsystem  $h$ . A systematic technique to determine the admissible parameter limits is the so called *Reachability Analysis*, described in [22]. With this technique, starting from a set of initial states, the reachable sets of states are over-approximated successively and conservatively. The same is done for the parameters under the influence of different faults. As the controller influences the ranges, the controller design is performed iteratively. Each iteration, in which controllers for all subsystems can be found, leads to a stable system within the used parameter ranges. The iterations stop until the controller performance is satisfactory and the ranges do not have to be enlarged further. Alternatively, the ranges can be determined by simulation of the considered generators under the influence of different faults, which is done for the simulations in the next chapter. The first guess of the ranges can be based on standard controllers. With known parameter ranges, the synthesis from the previous chapter is carried out offline to find the vertices  $K_i^{[h]}$ ,  $i \in \{1, \dots, n_v^{[h]}\}$  of the local controllers for each generator  $h$ . As mentioned in Sec. 5.1, for the fast controller implementation, the analytic descriptions  $\alpha_i^{[h]} = f_{\alpha_i}^{[h]}(\theta^{[h]})$  for  $i \in \{1, \dots, n_p^{[h]}\}$  have also to be calculated offline. The calculations associated with Eqs. (5.4) and (5.5) can be implemented efficiently using the Matlab symbolic toolbox.

After these two steps, the LPV controller of system  $h$  is applied online as follows:

1. measure or compute the momentary parameters  $\theta_j^{[h]} = f_{\theta_j}^{[h]}(x^{[h]}, z^{[h]}, u^{[h]})$  for  $j \in \{1, \dots, n_p^{[h]}\}$
2. compute the barycentric coordinates  $\alpha_i^{[h]} = f_{\alpha_i}^{[h]}(\theta^{[h]})$  for  $i \in \{1, \dots, n_v^{[h]}\}$
3. compute the momentary state feedback controller  $K^c^{[h]}(\theta_c^{[h]}) = \sum_{i=1}^{n_v^{[h]}} \alpha_i^{[h]} K_i^{[h]}$
4. compute the control input  $u^{[h]} = K^c^{[h]}(\theta_c^{[h]})x^{[h]}$  for any  $h \in \{1, \dots, q\}$

### Conservativeness of the Polytopic Description

The controller is synthesized through the solution of problem (5.36). The underlying LMIs originate from the polytopic description of the LPVS by combining all parameter ranges. The potential conservativeness of the polytopic description of

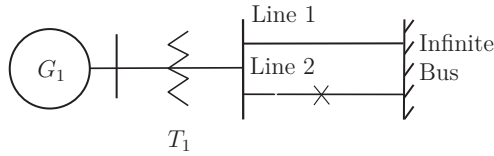
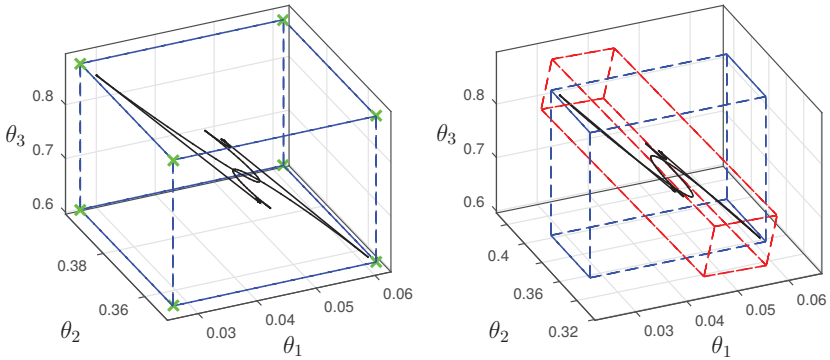


Figure 5.3.: SMIB-System.

the system as an axis aligned box is discussed next. Assuming known parameter bounds, the vertices for the polytopic description are retrieved by combining the upper and lower bounds with each other, as described by the example in Eq. (5.3). Any dependencies between the parameters are not considered. However, these dependencies exist and are evident, e.g. in the parameters  $\theta_1$ ,  $\theta_2$ , and  $\theta_3$  of the SG in the Eqs. (4.9):  $\theta_1 = \frac{(\tau_m - (x_q - x'_d) i_d i_q)}{x_1}$ ,  $\theta_2 = i_q$  and  $\theta_3 = \frac{i_d}{x_1}$  depend on the currents  $i_d$  and  $i_q$ , which in turn are coupled by algebraic equations. Thus, the resulting axis aligned box is conservative and overbounds the occurring values of the parameters.

To illustrate this conservativity, the so called single-machine-infinite-bus system (SMIB) (taken from [41]) is used. As depicted in Fig. 5.3, the SMIB consists of an SG  $G_1$  that is connected through two parallel lines to an infinitely strong bus (constant voltage and a constant phasor). This example was also used in [81] by the author, where the SG is controlled by the described technique, i.e. by solving problem (5.36). The SG is described by the LPVS (4.8) with the above mentioned parameters as in Eqs. (4.9). The simulation scenario is a disconnection of line 2 for several seconds. Without going into detail concerning the power system analysis, it is only to mention that the system is stabilized by the LPV controller.

With the focus on the polytopic description, the box based on the combination of the three parameter bounds is illustrated in blue in Fig. 5.4a. The green crosses represent the 8 vertices used for controller design. Investigating the actual courses of the simulated parameters printed in black, it is obvious that some spaces of the axis aligned box are far from being reached by the real system, implying conservativity. Having this information, the real appearing parameter trajectories can be estimated by a smaller polytope by using the *oriented hyper-rectangular hull* (ORH) technique introduced in [92]. The orientation of the ORH is determined by the *singular value decomposition* (SVD). Then the smallest hyper-rectangular hull is determined that encloses the real occurring parameters. The resulting ORH for the three parameters of the example is illustrated by the red box in Fig. 5.4b. Using the information that the parameter trajectories are within the red and the blue box, a tighter enclosing polytope can be identified. This polytope is determined by the intersection of the axis aligned box and the ORH, leading to the polytope of Fig. 5.5, where the green crosses are the vertices of the new, tighter polytope. The vertices of the intersection can be calculated e.g. by using the multi-parametric toolbox for Matlab [43]. A similar procedure using SVD to find a tighter parameter set mapping is proposed



(a) Polytopic description as an axis aligned box (b) Axis aligned box crossed by the oriented hyper-rectangular hull

Figure 5.4.: Polytopic representation and the real occurring courses of the parameters.

in [46] and complemented by an intersection with the axis aligned box in [45]. The polytope in Fig. 5.5 has 18 vertices, enlarging the SDP for controller synthesis by 10 vertices and thus, by 10 LMIs for each criterion. In the example the criteria for the left and right half-plane with the LMIs (5.15), for the conic sector with the LMIs (5.16) and for  $H_\infty$  criteria with the LMIs (5.19) are used, leading to an increase by  $10 \cdot 4$  LMIs. However, due the offline controller synthesis, the increase of the SDP is not critical. For the online implementation of the resulting controller, the functions of the barycentric coordinates can not be calculated using the Eqs. (5.4) and (5.5) from Ch. 5.1, due to the non-rectangular structure. To evaluate the results with the tight polytope, the calculation of the functions for the barycentric coordinates  $\alpha_i$  described in [103] is used. The result for the controlled system using the new and tight polytope is, however, disappointing. The improvement of the controller performance is marginal. Based on this experience and on the complexity experienced with this method, the simple polytopic description as an axis aligned box is used to validate the LPV modeling and controller synthesis in the next chapter. Nonetheless, the (complex) method can be used in the case where the LMIs based on the axis aligned box can not be solved. The reduced conservativeness of the tight and more realistic polytopic description reduce the parameter space for the SDP. It is to mention that for other applications, using the tighter polytopic description can improve the controller performance significantly [45].

For the interested reader, references to other controller synthesis techniques with reduced conservativity are provided: A parameter dependent Lyapunov matrix  $X(\theta)$  is introduced in [85], leading to a result which “is never more conservative than

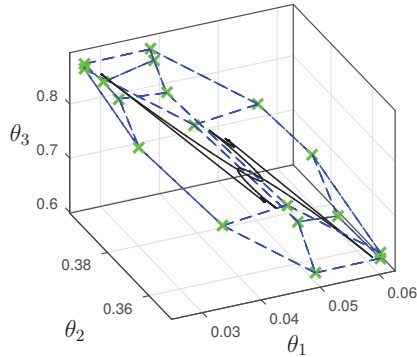


Figure 5.5.: Tight polytopic representation of the real occurring courses of the parameters.

quadratic stabilizability”. Furthermore, the information of the parameter velocity  $\dot{\theta}$  can be exploited for the controller synthesis as in [29].

## 5.9. Conclusions on the LPV-based Controller Synthesis

The proposed synthesis technique establishes a decentralized control structure for the LPVS derived in Ch. 4. For a given set of parameter ranges, an LPV controller is synthesized, which can account for different control objectives, including input constraints. Robustness of this controller is guaranteed and established through the ranges of the parameters. As exemplarily shown in the previous section, techniques exist to handle the conservativeness of the approach. The local synthesis problems for each dynamically modeled component are of moderate size, and the overall design effort grows linearly with the number of the controlled systems. Furthermore, if ranges for the model parameters of any LPVS are determined conservatively, stability of the whole controlled system can be concluded. The implementation of the controller is realized by algebraic equations, allowing an online implementation.



# 6. Simulation Results for Robust LPV Control

In this chapter, the previously derived LPV models and the synthesized LPV controllers are verified based on simulations with the original nonlinear models, as described in Ch. 3. The power systems, their settings and fault scenarios are chosen to demonstrate different aspects of the (local) LPV controller technique and its effects on the controlled power system.

First, in Ch. 6.1, the focus is on the robust control with respect to grid faults and changed wind speed, demonstrated for a grid consisting of SGs and a WECS. This setting is extended by input constraints, followed by the examination of the controller performance in Ch. 6.2. Simulation results for an LPV controlled PVS are shown and discussed in Ch. 6.3. Finally, two settings of a power system composed of SGs and WECS are used to demonstrate transient stability in combination with (local) voltage control.

## Assessment of the reference controllers

The local LPV controllers are compared to reference controllers in the course of this chapter. The introduced reference controllers have controller objectives other than the LPV controllers designed in the subsequent parts. The PSS and the AVR are used for the SG as reference controllers (without integrating behavior), each of the two typically designed separately. The WECS and the PVS both have inner current control loops. With the use of these loops, the active and reactive powers are controlled, as well as other related variables, e.g. the dc-voltage in the case of the PVS. The basis of these two main loops is the decoupling of the  $d$  and  $q$  quantities, in order to have single-input-single-output systems for the use of PI-controllers. Thus, compensation and feed-forward terms are introduced (see figures 3.5, 3.6 and 3.11). In this work, however, controllers for multi-input-multi-output systems are designed, making the need for decoupling obsolete. The systems used for controller synthesis have the same dynamics as the original nonlinear systems (due to analytic transformation for the LPV modeling). The description as LPVS allows direct control of the, e.g., bus voltage, avoiding compensation terms or Taylor linearization around one operating point (see Ch. 4). While different variables are controlled by the reference and the LPV controllers, the common control objective is transient stability: The system must remain stable during and after grid faults or other changes within the grid. It is to mention that the controller parameters of

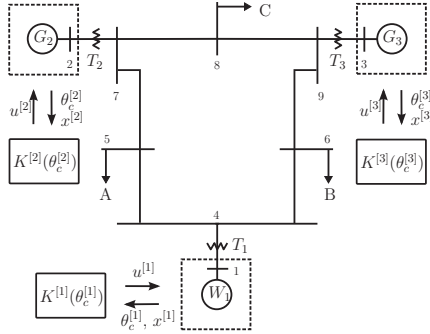


Figure 6.1.: Structure of the modified 9-bus system.

the reference controllers may not be optimally tuned for the used fault scenarios. However, the parameters of the reference controllers for the SG and the PVS are taken from literature where they were used in the context of the same power systems as used here (see [90] and [106], respectively). Only the reference controllers for the WECS from [26] are used in the context of a different power system than it is used in this work. The parameters of the WECS are, however, the same as they were used for the parametrization of the reference controller.

It is stressed that the following simulations scenarios and settings of power systems are only a few of a large set of settings and scenarios tested in the course of this work. The choices were made based on the considered control objectives.

## 6.1. Transient Stability of a Grid with WECSs and SGs

For the first demonstration, the 9-bus system is used, which is taken from [5] and served as an introducing example in Ch. 3. Because the original 9-bus system consists only of the (classic) synchronous generators, the original setting is changed. The first change concerns the injected power of the three generating units of the systems: to achieve equal impact of the three units, the setting is changed such that all three units inject similar shares of power, i.e. the three units connected at the buses with the indices 1, 2 and 3 are initialized with the powers  $p_1 = 0.875$  p.u.,  $p_2 = 1$  p.u., and  $p_3 = 0.9$  p.u. (on a 100 MVA base). The second change concerns the type of units connected to the grid. Instead of the original three synchronous generators, one DFIG-based WECS  $W_1$  is installed instead of the SG at bus 1. The resulting LPV controlled 9-bus system has the structure as depicted in Fig. 6.1. To examine the controller performance, a sequence of events / faults is simulated: First, in order to show that the LPV controlled WECS is able to operate for changed wind

conditions, after one second, the wind speed grows from  $11.4\frac{m}{s}$  to  $12\frac{m}{s}$ . At  $t = 7s$ , a large fault in the form of a voltage drop by approximately 20% (for the LPV controlled system), as described in Ch. 3.5, occurs (with  $g_f = -3$  and  $b_f = -2$ ). This fault is cleared after  $100ms$ . The last fault of the sequence occurs at  $t = 12s$ , where the line admittance between the buses 5 and 7 is doubled for the rest of the simulation, i.e. the entries  $\bar{y}_{57}$ ,  $\bar{y}_{75}$ ,  $\bar{y}_{55}$  and  $\bar{y}_{77}$  of the admittance matrix change.

Without showing the simulation results, the uncontrolled power system becomes unstable, requiring stabilizing controllers. The LPV controller synthesis of the SGs and the WECS is based on the LPV models for transient stability, i.e. on the equations (4.8) and (4.9) for the SG, and (4.23) and (4.24) for the WECS, respectively.

The control objective is the contribution of all energy sources to system damping – this is specified by appropriate pole placement. The LMI-region chosen for the LPV controller synthesis of the SGs is the conic sector with the angles  $\varphi_d = \pm 75^\circ$ , and with  $\varphi_d = \pm 35^\circ$  for the WECS, respectively. These criteria account for sufficient damping, with a relative damping of 26%, and 82%. For power quality and stability reasons, it is essential that oscillations are damped in a reasonable time [18]. For the WECS, LMIs to place the poles in the right half plane with  $Re(\mu) < -1$  are used additionally. The derived LPVS do not contain any extra disturbances. Nevertheless, an  $H_\infty$ -constraint for the transfer function from an additive disturbance of  $\dot{x}_2$  to the output  $x_2$  is used for the three systems. The constraint pushes the poles of the closed-loop system to the left-hand side of the LMI-region. Thus, the controller is synthesized by minimizing the bound  $\gamma$  of the  $H_\infty$ -criterion considering the LMIs (5.15), (5.16), and (5.19) for the vertices of the considered matrix polytopes of the closed-loop systems. For each of the three criteria, the number of the LMIs to solve is  $2^{n_p} = 2^3 = 8$  for the SGs and  $2^{n_p} = 2^5 = 32$  for the WECS. The number of LMIs can be summed up to  $3 \cdot 8 + 1 = 25$  and  $3 \cdot 32 + 1 = 97$ , respectively (the one additional LMI is the LMI  $X > 0$ ). These SDPs are solved in less than 1.5s, what is not critical. The used parameter ranges can be found in the Appendix in Table A.1.

While the mechanical power of the SG can be assumed to be constant for transient stability, the power extracted by the WECS  $P_m$  directly depends on the state  $w_m$ . Thus, the LPV controller of the WECS is designed to control  $w_m$  to a constant value, introducing integrating behavior for  $w_m$ . The resulting controllers are different and depend on the considered generating unit.

The controlled power system is analyzed by the courses of the angular velocities of the two synchronous generators. In Fig. 6.2, the angular velocities of the LPV controlled SGs (right) remain synchronous for the whole simulation sequence, having the largest amplitude for  $\omega_{LPV}$  of  $G_2$  after the voltage drop. Furthermore, the system is well damped and hardly oscillates. In contrast, the system controlled by the reference controllers, indicated by the index *REF* in this chapter (s. Fig. 6.2, left), begins to oscillate after the voltage drop at  $t = 7s$ . It remains stable until the line is switched at  $t = 12s$ , causing the angular velocities to decelerate. This behavior can also be seen in the courses of the injected active powers  $p_{REF}$  in Fig.

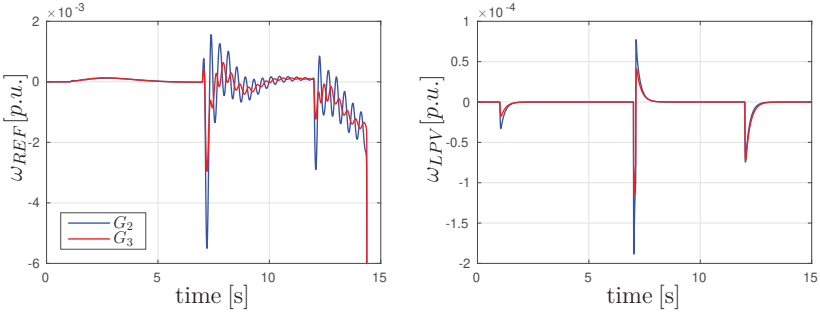


Figure 6.2.: Simulation results for angular velocities of the SGs  $G_2$  and  $G_3$  for the reference and the LPV-controlled system. (Note the difference of the scales of the ordinates.)

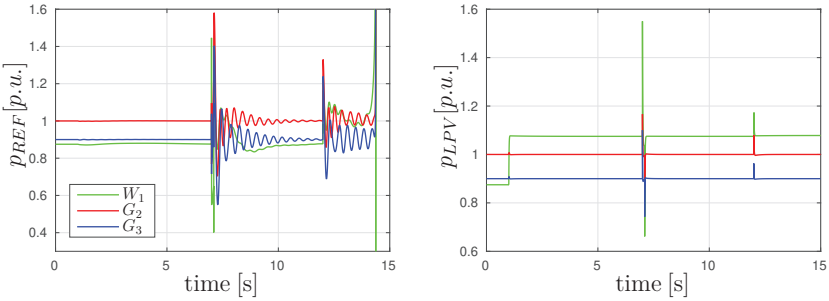


Figure 6.3.: Simulation results of the active powers for the SGs and the WECS for the reference and the LPV-controlled system.

6.3, where the power of the WECS  $W_1$  falls to zero, depicted in green. The LPV and the classically controlled systems remain stable after the wind changes, but their different control objectives become apparent in the courses of  $p_{REF}$  and  $p_{LPV}$  in figures 6.3 and 6.6: The reference controller of the WECS controls the active power to its original value (Fig. 6.3, left), while the LPV controller controls the rotor angular velocity to its original value (Fig. 6.6, left). This may limit comparability of the two controllers but not in terms of system stability and damping: The LPV controlled system remains stable with well damped courses of all variables during the whole simulation. The voltages  $v_{LPV}$  in Fig. 6.4 (right) rise after the wind changes, as they are not controlled in this setting. The effects of the involved AVRs can be seen in the courses  $v_{REF}$  of the SGs, which are controlled close to their original values (left), until the line is switched and the system becomes unstable.

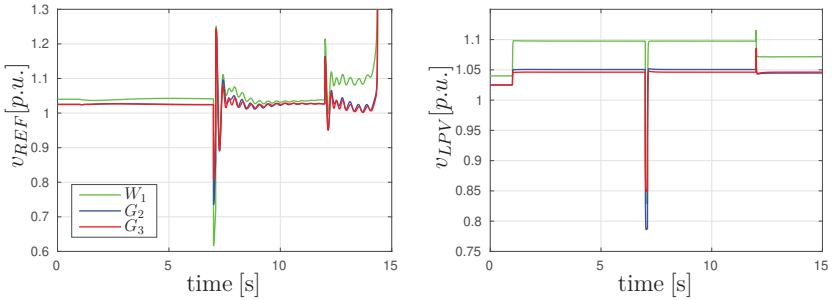


Figure 6.4.: Simulation results for the voltages of the SGs and the WECS for the reference and the LPV-controlled system.

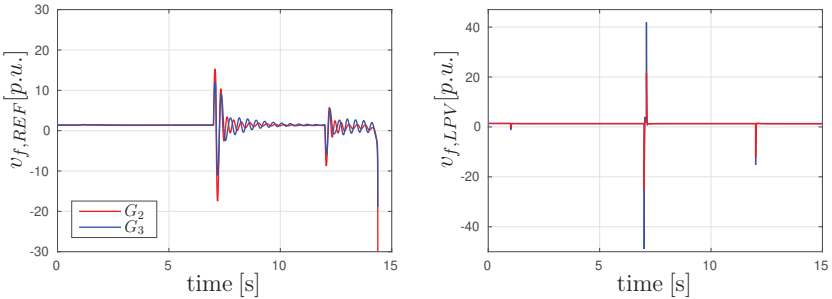


Figure 6.5.: Simulation results for the inputs of the SGs  $G_2$  and  $G_3$  for the reference and the LPV-controlled system.

The maximal voltage drop of  $v_{LPV}$  at  $t = 7s$  is with 0.78 p.u. significantly smaller than for  $v_{REF}$  with ca. 0.61 p.u.. In Fig. 6.5, the control actions of the two controller types are compared showing that the inputs of the classically controlled  $G_1$  and  $G_2$  have amplitudes of less than 15 p.u. and the amplitudes of  $v_{f,LPV}$  are significantly higher with maximum 42 p.u.. The fast dynamics of the LPV controllers are one reason for their good performance. Both controller types exceed the maximum allowed inputs of approximately  $u_{sat} = \pm 10p.u.$ . Consequently, the inputs should be constrained, which will be in the focus of the next section. The inputs of the WECS for both controller types are moderate and are shown only for the LPV controlled system in Fig. 6.6 (right).

For the sake of completeness, the courses of two parameters  $\theta_2$  of  $G_2$  and  $\theta_1$  of  $W_1$  are shown exemplarily in Fig. 6.7. The dashed lines represent the ranges which were used for controller synthesis. Both parameters remain within their ranges (as all

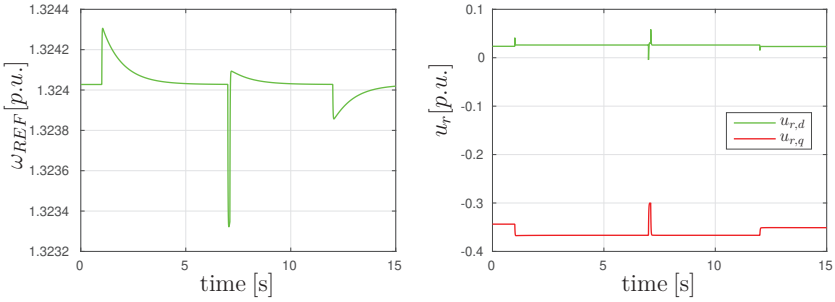


Figure 6.6.: Simulation results for the rotor angular velocity and the inputs of the WECS  $W_1$  for the LPV-controlled system.

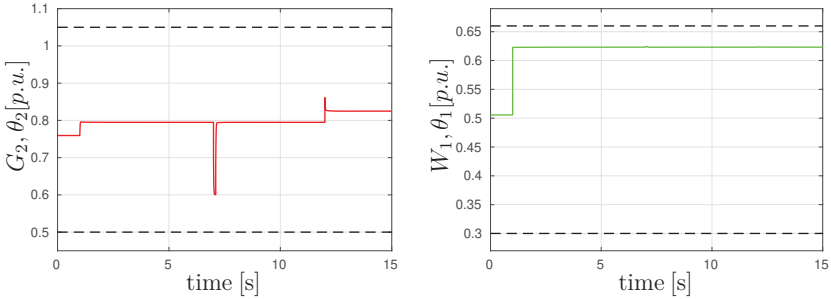


Figure 6.7.: Two exemplary parameter courses of the SG  $G_2$  and the WECS  $W_1$  of the LPV-controlled system.

parameters during the simulation), implying stability of the whole power system. It can also be observed that both parameters react differently on the events during the simulation. While  $\theta_2$  of  $G_2$  changes with every event significantly,  $\theta_1$  of  $W_1$  reacts only on the changes of the wind speed. All in all, the LPV controlled system is robust against changes of the wind and against changes within the grid, introducing good damping by the SG and the WECS.

## 6.2. Transient Stability with Extension to Input Constraints

In the latter simulation studies, the inputs of the SGs have very high values and must be constrained. In this section, the power system setting and the simulation scenario from the previous section are adopted. Only the LPV controllers of the

SGs are complemented by the synthesis with input constraints by solving the SDP consisting of the LMIs (5.29) and (5.30) from theorem 5.1. The auxiliary parameters  $\theta_{s,i}$  for the input constraints of the two SGs are chosen to have the range  $\theta_s \in [0.01 \ 1]$ . The complete set of parameter ranges can be found in the Appendix in Table A.2. As the input variations for the WECS are uncritical for the considered scenarios, the LPV controller is designed for the same LMI-region as in the previous section. As depicted in Fig. 6.8, the LPV controlled system remains stable and the original values of  $\omega_{PLV}$  are reached again in less than one second. The maximum amplitude of the angular velocities is now 0.0002 and is more than doubled compared to the LPV-controlled case without input constraints in Fig. 6.2. However, the remaining courses of the active powers and the bus voltages change only marginally, so that the results are not illustrated here. The controller is still much faster than the system controlled by the reference controllers without any input constraints. The resulting courses of  $v_{f,LPV}$  are depicted in Fig. 6.9 (left). It is obvious that only the input of the generator  $G_2$ , in blue, saturates with the constraint  $u_{sat} = \pm 10$ , implying that the LPV controllers of the SGs are less aggressive than in the previous section. The saturation of the input for  $G_2$  becomes apparent in the course of the respective auxiliary parameter  $\theta_s$  in Fig. 6.9 (right): When the input saturates, the parameter differs from the value 1. The value for  $\theta_s$  of  $G_3$ , depicted in red, is always 1, meaning that this input never saturates during the simulation. As long as  $\theta_s$  remains within the parameter ranges  $\theta_s \in [0.01 \ 1]$ , system stability is guaranteed.

### 6.3. Transient and Voltage Stability by a Photovoltaic System

In order to verify the LPV model and controller for the PVS, a small instance of a grid is introduced, adopted from [106]. As mentioned in Ch. 3, the electromag-

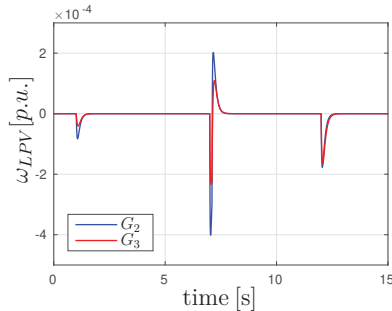


Figure 6.8.: Simulation results for angular velocities of the SGs  $G_2$  and  $G_3$  for the LPV-controlled system with input constraints.

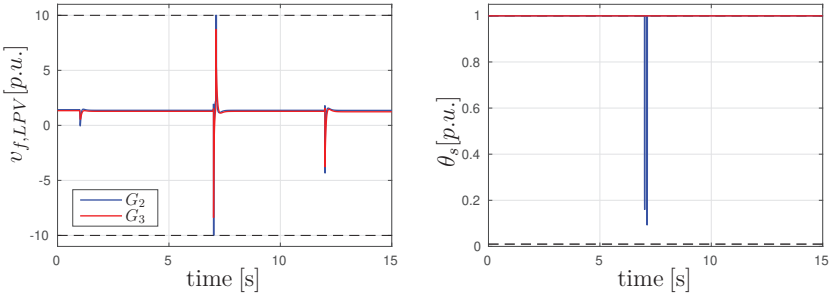


Figure 6.9.: Inputs of the SGs  $G_2$  and  $G_3$  and the respective parameters  $\theta_s$  of the LPV-controlled system with input constraints.

netic dynamics of a grid has to be kept and modeled by differential equations. The used power system is depicted in Fig. 6.10 and consists of a transformer  $T_1$ , two transmission lines with the inductances  $L_1$  and  $L_2$ , and the resistances  $R_1$  and  $R_2$ . The transformer  $T_1$  steps the nominal PVS voltage (480V) up to the nominal distribution network voltage (6.6kV). The transformer is reduced to the voltage ratio  $N = 6.6\text{kV}/480\text{V} = 13.75$  and its leakage inductance and resistance are included in the line inductance  $L_1$  and the resistance  $R_1$ . Furthermore, the load is a resistive-inductive load ( $R_l$  and  $L_l$ ) in parallel to a power factor capacity  $C_l$ . The PVS is modeled as described in Ch. 3, where the bus voltage  $v_1$  is the equivalent of the bus voltage  $v_h$  and the voltage  $v_2$  is the infinite bus (with a constant voltage and phasor, representing an infinitely strong grid). As the grid system is not modeled by the algebraic equations, the system equations are introduced briefly. All equations are derived based on the Kirchhoff's Laws and are dq-transformed. The resulting states are the currents of the two lines  $i_{1,d}$ ,  $i_{1,q}$ ,  $i_{2,d}$ , and  $i_{2,q}$ , and the currents and voltages of the load  $i_{l,d}$ ,  $i_{l,q}$ ,  $v_{l,d}$ , and  $v_{l,q}$ . The dynamics of the described components can

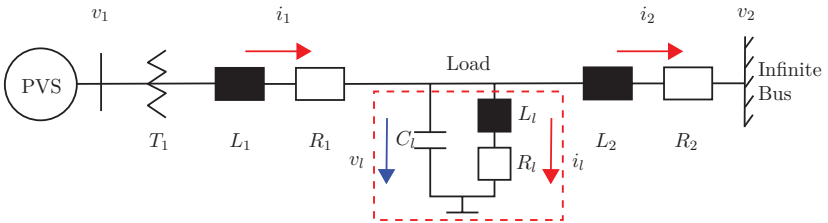


Figure 6.10.: Three-phase PVS coupled to a distribution network through a transformer, shown as single-line schematic diagram [96].

be modeled by the equations:

$$\dot{i}_{1,d} = -\frac{R_1}{L_1}i_{1,d} + \omega i_{1,q} + \frac{N}{L_1}v_{1,d} - \frac{1}{L_1}v_{l,d} , \quad (6.1)$$

$$\dot{i}_{1,q} = -\frac{R_1}{L_1}i_{1,q} - \omega i_{1,d} + \frac{N}{L_1}v_{1,q} - \frac{1}{L_1}v_{l,q} , \quad (6.2)$$

$$\dot{i}_{2,d} = -\frac{R_2}{L_2}i_{2,d} + \omega i_{2,q} + \frac{1}{L_2}v_{1,d} - \frac{1}{L_2}v_{2,d} , \quad (6.3)$$

$$\dot{i}_{2,q} = -\frac{R_2}{L_2}i_{2,q} - \omega i_{2,d} + \frac{1}{L_2}v_{1,q} - \frac{1}{L_2}v_{2,q} . \quad (6.4)$$

$$\dot{i}_{l,d} = -\frac{R_l}{L_l}i_{l,d} + \omega i_{l,q} + \frac{1}{L_l}v_{l,d} , \quad (6.5)$$

$$\dot{i}_{l,q} = -\frac{R_l}{L_l}i_{l,q} - \omega i_{l,d} + \frac{1}{L_l}v_{l,q} , \quad (6.6)$$

$$\dot{v}_{l,d} = \omega v_{l,q} + \frac{1}{C_l}i_{1,d} - \frac{1}{C_l}i_{2,d} - \frac{1}{C_l}i_{l,d} , \quad (6.7)$$

$$\dot{v}_{l,q} = -\omega v_{l,d} + \frac{1}{C_l}i_{1,q} - \frac{1}{C_l}i_{2,q} - \frac{1}{C_l}i_{l,q} . \quad (6.8)$$

The grid frequency is assumed to be constant with  $\omega = 2\pi 60\text{s}^{-1}$ . The infinite bus is defined by  $v_2 = 1$  and  $\varphi_2 = 0$ . The DC interface of the PVS consists of a PV array with 176 PV strings in parallel, and 1500 PV cells per string in series [106]. The initial power injected by the PVS is then  $p_1 = 0.93$  p.u. on a 1.4 MVA power base. The parameters of the system from [106] have to be transformed in p.u.. The respective base units are listed in Table A.3 in the Appendix, and the resulting parameters in p.u. in Table A.4.

To demonstrate the controller performance, the system is subject to a rise of solar irradiation by 10% at  $t = 0.01\text{s}$ , and at  $t = 0.2\text{s}$ , the transmission line 2 is changed permanently, i.e.  $R_2$  and  $L_2$  are multiplied by the factor 10. The whole simulation takes  $0.4\text{s}$ . The system can only be run with controllers, and in subsequent parts the LPV controller is contrasted by the reference controller taken from [106], i.e. the PLL, the current, and the DC-voltage controllers as described in Sec. 3.4.

The LPV controller is designed based on the derived LPV model from Ch. 4.4. The control objectives are the control of the voltage  $v_{dc}$ , in order to influence the power generated by the PV array, and the voltage at the point of connection  $v_1$ . Thus, integrating behavior is introduced by the LPV state feedback controller for these two variables. The poles of the closed loop system are placed within  $-9000 < \text{Re}(\mu) < -200$  and the conic sector is defined by  $\varphi_d = \pm 30^\circ$ , introducing a relative damping of approximately 87%. The  $H_\infty$ -constraint for the transfer functions from additive disturbances of  $\hat{x}_1$  and  $\hat{x}_6$  to the outputs  $x_1$  and  $x_6$  is used to push the poles to the left side within the LMI-region. Thus, the SDP for LPV controller synthesis is defined by the LMIs (5.15) (for the left and right half-plane), (5.16), and (5.19).

The LPVS of the PVS has a relatively large number of parameters: The system matrix has 6 parameters and the input matrix 3, leading to the number of vertices of  $n_v = 2^6 = 64$  and  $n_b = 2^3 = 8$ . Thus, the resulting problem with the 4 criteria, has the number of  $4 \cdot n_v \cdot n_b + 1 = 4 \cdot 64 \cdot 8 + 1 = 2049$  LMIs. The computation time is then approximately 30s. However, due to the fact that the controller is synthesized offline, the computation time is not a problem. The parameter ranges used for the controller synthesis can be found in the Appendix in Table A.5. Parts of the results in this section were published in [96].

Both controllers stabilize the system for the whole simulation scenario. After the solar irradiation rises, the LPV and the reference controller regulate  $v_{dc}$  to its original value as depicted in Fig. 6.11 (left), where the LPV-controlled  $v_{dc}$  shows a greater (but still moderate) amplitude (in blue) but no oscillations. Furthermore, after the change within the grid at  $t = 0.2s$ , the LPV-controlled  $v_{dc}$  does not oscillate and has an overall better performance than the system with the reference controller. What is more important considering the whole power system behavior, is that the resulting injected active power  $p_1$  (right) shows a smaller overshoot and less oscillations for the LPV-controlled case. The voltage  $v_1$  at the bus of connection in Fig. 6.12 (left) shows a large amplitude of around 1.14 for the reference controller. This is an overshoot of approximately 11%, which may violate grid code requirements with typical values of ca.  $\pm 10\%$  around one operating point for the bus voltages at the point of connection of renewables (depending on the country). The LPV-controlled system, in contrast, has only half of that overshoot in  $v_1$ . After the second line is switched, the different control goals become evident in Fig. 6.12 (right): The LPV controller achieves steady-state accuracy for the voltage  $v_1$ , while the reference controller controls the reactive power  $q_1$  of the PVS to the pre-fault value. The oscillations are apparent in the courses of the inputs of the reference controller in Fig. 6.13, as well. The amplitude of  $K_{d,REF}$  is twice as high as that of  $K_{d,LPV}$ , showing the direct connection between  $v_{dc,REF}$  and  $K_{d,REF}$ , which stems from the decoupling of the d- and q-coordinates in the underlying controller design of the reference controller described in Sec. 3.4. Thus, considering the overall results for  $v_1$ ,  $p_1$ , and  $q_1$  after the grid fault, the LPV-controlled system shows better results than the reference controller. Especially the amplitudes of the two grid variables  $v_1$  and  $p_1$  are lower and the courses are better damped than for the system controlled by the reference controllers, showing a more grid-friendly behavior.

For the sake of completeness, the courses of  $\theta_1$  and  $\theta_4$ , as defined in Eqs. (4.41) are shown exemplary in Fig. 6.14. The robustness against the rise of the solar irradiation is encoded in  $\theta_1$  and it can be observed that the parameter ranges (dashed lines) are not violated. The course of  $\theta_4$  shows reactions to all events during the simulation, where all limits are met, implying robustness against grid changes.

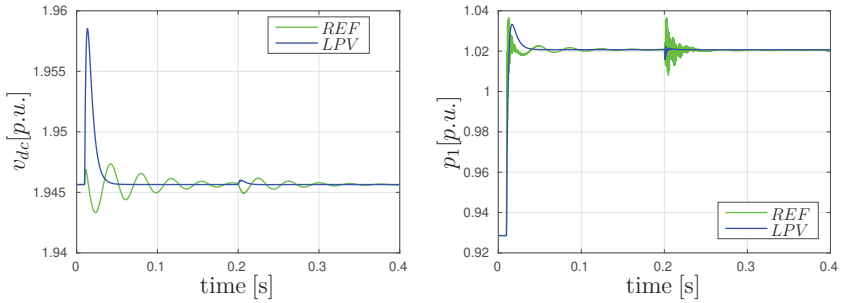


Figure 6.11.: Simulation results for dc-voltage and the active powers of the PVS for the reference and the LPV-controlled system.

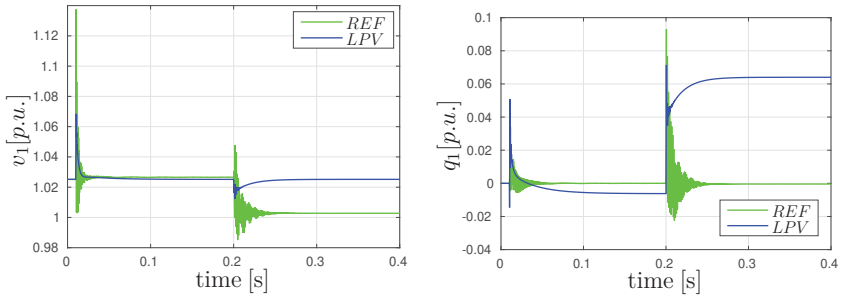


Figure 6.12.: Simulation results for bus voltage and the reactive powers of the PVS for the reference and the LPV-controlled system.

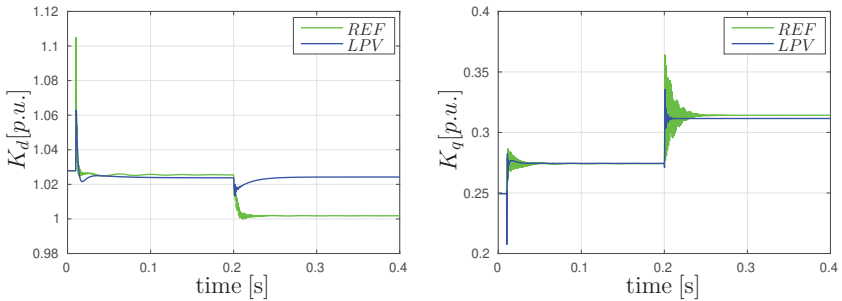


Figure 6.13.: Simulation results for system inputs of the PVS for the reference and the LPV-controlled system.

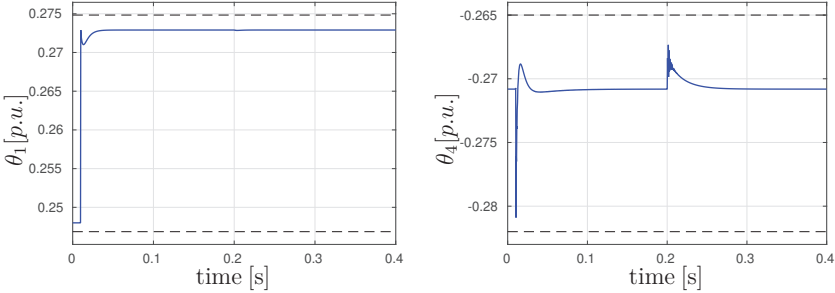


Figure 6.14.: Simulation results for the parameters  $\theta_1$  and  $\theta_4$  of the PVS for the LPV-controlled system.

## 6.4. Voltage and Transient Stability by WECSs and SGs

The LPV controller objectives are now extended to the control of the voltage at the bus of connection, described by  $v_h$  in Ch. 3. The focus is on the impact of the voltage controller on the whole grid. Input constraints are not necessary for the considered scenario. To simulate the controllers for the SG and the WECS, two variants of the 9-bus system are used: In the first variant,  $G_1$  and  $G_2$  are SGs and  $G_3$  is replaced by the WECS  $W_3$ . In the second variant of the benchmark system, all three generators are SGs. While the control of  $G_3$  and  $W_3$ , respectively, addresses voltage control of  $v_3$  at bus 3 and transient stability, the control of  $G_1$  and  $G_2$  aims at control of transient stability, only. The rotor angle velocity  $\omega_m$  of the WECS remains a controlled variable with integrating behavior for  $\omega_m$ . Parts of the results of this section were published in [83].

### Voltage Control by the WECS

The simulation scenario is as follows: starting from steady-state, the wind speed is changed from  $v_w = 11.4 \frac{m}{s}$  to  $v_w = 12 \frac{m}{s}$  at  $t = 1$  s, and the line admittance between the buses 5 and 7 is doubled at  $t = 10$  s, simulating a small gust and a permanent change of the grid, respectively.

Similar to the results in Sec. 6.1, this system needs a controller to remain stable for the considered scenario. Again, the LPV controller is compared to the reference controllers for the SGs and the WECS. To achieve good relative damping of the system (more than 26%) and fast dynamics for the close-loop system, the LPV controllers are designed such that the poles of the closed loop systems are placed in the LMI regions  $-100 < Re(\mu^{[1]}) < 0$  and  $\varphi_d^{[1]} = 75^\circ$  for  $G_1$ ,  $-150 < Re(\mu^{[2]}) < 0$  and  $\varphi_d^{[2]} = 75^\circ$  for  $G_2$ , and  $-7 < Re(\mu^{[3]}) < -1.5$  and  $\varphi_d^{[3]} = 15^\circ$  for  $W_3$ . The

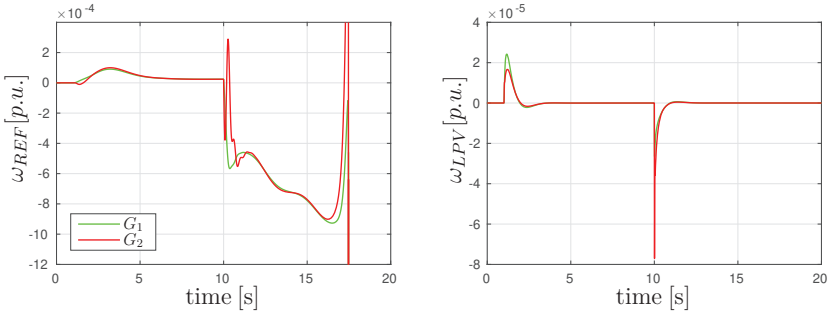


Figure 6.15.: Simulation results for angular velocities of the SGs  $G_2$  and  $G_3$  for the reference and the LPV-controlled system.

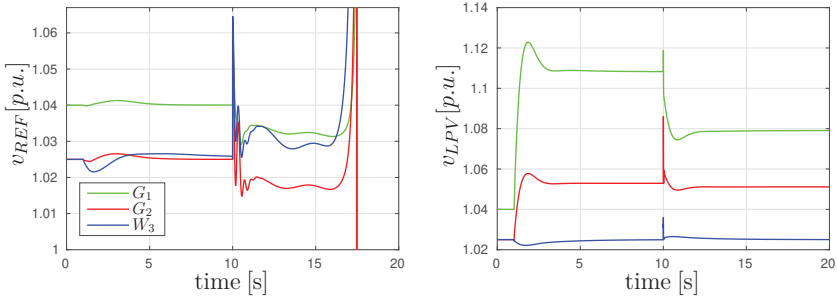


Figure 6.16.: Simulation results for the voltages of the SGs and the WECS for the reference and the LPV-controlled system.

$H_\infty$ -constraints for the SG and the WECS are implemented with the same transfer functions as in Ch. 6.1. The used parameter ranges are provided in the Appendix in Table A.6.

As it is shown in Fig. 6.15, both controllers manage to stabilize the system after the wind is changed and the SGs remain synchronous, while the amplitudes of  $\omega$  of the LPV-controlled system are five times lower. At the same time, the bus voltage of  $W_3$  recovers, showing steady-state accuracy for both controllers for the changed wind, depicted in Fig. 6.16. When the operating point is changed at  $t = 10$  s, the SGs with the reference controllers do not remain synchronous any more and the system becomes unstable. The voltage of  $W_3$  rises until the simulation stops. For the LPV-controlled case, the system remains stable and the bus voltage of  $W_3$  regains its steady state. Thus, the LPV-controlled system remains stable during the whole simulation. Without showing the results, the steady-state accuracy of the LPV

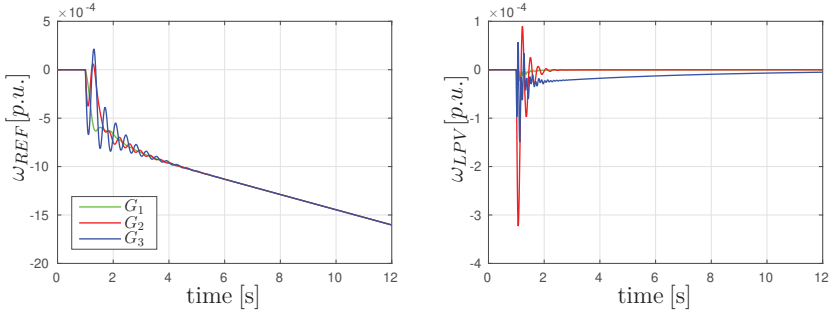


Figure 6.17.: Simulation results for angular velocities of the SGs  $G_1$ ,  $G_2$  and  $G_3$  for the reference and the LPV-controlled system.

controller for  $\omega_m$  is kept. Overall, the system reacts robustly to changes of the wind and the grid, while quickly damping down the electromechanical oscillations and controlling  $v_3$  of  $W_3$ . It can also be observed that the dynamics in response to the grid-changes are much faster than the dynamics caused by the wind.

One comment is made on the voltages of  $G_1$  and  $G_2$  in Fig. 6.16: In the LPV-controlled system, these SGs have no voltage controllers, and thus their values deviate from their original values after the wind is changed. The voltage control of the bus voltage of an SG by an LPV controller will be discussed next.

### Voltage Control by the SG

The following scenario is used to show transient stability and voltage control for the SG  $G_3$ : At  $t = 1$  s, the line admittance between the buses 5 and 7 is doubled and remains in this condition, changing the grid permanently. The LPV controllers are designed such that the poles of the closed loop systems are placed in the LMI regions  $-20 < \text{Re}(\mu^{[1]}) < 0$  and  $\varphi_d^{[1]} = 65^\circ$  for  $G_1$ ,  $-7 < \text{Re}(\mu^{[2]}) < 0$  and  $\varphi_d^{[2]} = 65^\circ$  for  $G_2$ , and  $-8 < \text{Re}(\mu^{[3]}) < -2$  and  $\varphi_d^{[3]} = 55^\circ$  for  $G_3$ . Consequently, a relative damping of more than 42% is introduced for all closed-loop systems. The transfer functions for the  $H_\infty$ -constraints for the SG are chosen as in Ch. 6.1, and the used parameter ranges can be found in the Appendix in Table A.7.

This time the SGs remain synchronous with the LPV and the reference controllers. The simulation results for the LPV-controlled system in Fig. 6.17 (right) show that the values of  $\omega_{LPV}$  are recovered and that the oscillations vanish within 1s. The bus voltage  $v_{LPV}$  of  $G_3$  recovers its initial value, see Fig. 6.18 (right). In contrast,  $\omega_{REF}$  is not controlled to steady-state. In the standard control strategy of an SG, the original rotational velocity is recovered by droop control, which is not modeled in this work. The maximum amplitude of  $\omega_{LPV}$  is half of the amplitude obtained with the reference controller. Even though the values for  $\omega_{REF}$  change their speeds,

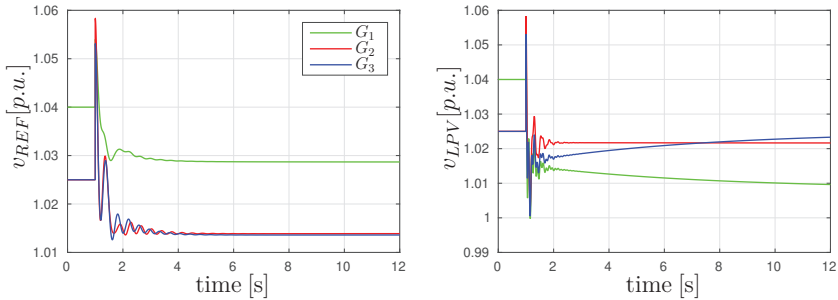


Figure 6.18.: Simulation results for the voltages of the SGs  $G_1$ ,  $G_2$  and  $G_3$  for the reference and the LPV-controlled system.

the SGs remain synchronous. However, the voltage of the three SGs move into steady-state in Fig. 6.18, but without regaining the pre-fault values of any voltage. All in all, the LPV-controlled system recovers the steady-states for  $\omega_{LPV}$  and good damping is introduced, together with robustness against changes within the grid and steady-state accurate control of the voltage of  $G_3$ .

## 6.5. Discussion on the LPV-controlled System

In this chapter, the proposed decentralized control structure for power systems is established and validated. The DAE-model of the power system is partitioned into subsystem, each modeled as an LPVS. The coupling between the systems is mapped into the parameters of the LPVS and their ranges, allowing to synthesize the LPV controllers for the generating units separately. The local synthesis problems are of moderate size, and in addition the overall design effort grows moderately with the size of the power system. It is demonstrated that the presented LPV controllers i) stabilize the grid after grid faults and introduce good damping of oscillations and ii) are robust against permanent grid changes. In the case of the WECS and the PVS, it is also shown that normal operation, i.e. changes of wind speed and solar irradiation, can be handled as well. Robustness against the considered fluctuations of the operating conditions is ensured by the choice of large parameter ranges.

It is also shown that steady-state accuracy for the control of the bus voltage of one module can be realized by the LPV controller. In the previous section, only one of the three generating units is simulated with an LPV controller for the voltage control. It is also possible to include two units with voltage control into the 9-bus system. However, it is not feasible to control all units with the introduced LPV controller for the voltage with a steady-state error of zero (it is stressed that the AVR of the used reference controller has no integrating behavior and thus accepts

a steady-state error for the bus voltages of the SGs, s. Fig. 6.18, left). As it can be observed in Fig. 6.18, the bus voltage of  $G_3$  is controlled to its original value by the LPV controller for the considered scenario. At the same time, the voltage of  $G_1$  sinks by the same amount. The underlying idea is that the sum of all reactive powers in one power system must be in balance, affecting the voltages. However, it is not necessary to control all voltages exactly and it is satisfactory to keep the voltages around their original values. These and other parameters are typically specified in grid codes and for the voltages, in most grid codes, a band of e.g.  $\pm 10\%$  around the nominal value is sufficient for the WECS or the PVS at the point of connection [95]. Furthermore, the local LPV controllers can only control the voltage at their bus of connection. Control of one distant bus voltage (e.g. at the bus of a large load with a predefined voltage) within the grid can not be realized by the introduced decentralized technique.

Thus, a centralized controller which can control some bus voltages to predefined values and, at the same time, the other voltages within a certain level is one possible solution. Introducing a source for reactive power (e.g. in form of FACTS) can, of course, also solve the problem of unbalanced reactive powers, but is omitted due to the objective of this work to use the existent generating units, only. In the next chapter, a centralized controller for the voltage control of a grid is introduced, while the underlying units are controlled by LPV controllers. These LPV controllers ensure stability after faults and get their reference values by the centralized controller, ensuring stable operation of a grid in terms of transient and voltage stability.

**Part III.**

**Grid-Wide Coordinating  
Control**



## 7. Model Predictive Control for the LPV-Controlled System

In the previous part, *Synthesis of Local Robust Controllers*, a control approach was presented, in which the system was decomposed and their dynamically modeled components were controlled by the LPV technique. The coupling was realized through the parameter ranges leading to an LPV representation of the complete system. Robustness against grid fault and exogenous effects was shown and proof of stability of the whole grid was presented, based on the assumption that the parameter ranges are not violated. Bus voltage control for some generating units could also be realized by this strategy. However, it was not possible to control the bus voltages of all generation units with a steady-state error of zero at the same time consistently. One explanation is that the capability of the grid to restore all voltages at the same time is insufficient for the demonstrated grid faults, due to the lack of reactive power. In fact, the effect of insufficient reactive power supply within a grid is one of the most common causes for voltage instability [31]. Typically, it is not required to control all voltages to predefined values with a steady-state error of zero, but to keep them within limits as defined by the grid code [95]. Grid codes define boundaries for relevant variables within which the WECS and the PVS have to stay connected to the grid. This allows deviations from the pre-faults values, but within required ranges to ensure grid stability. However, to meet consumer demands, for some buses a more accurate voltage control may be required. In particular, the control of the voltage at a distant bus can in general not be realized by the local LPV controller. In classical grid operation, centralized controller approaches exist to achieve the balance of powers, e.g. the so-called *Automatic Generation Controllers* for the frequency (LTI controller of the type PI), by which the injected active powers are changed such that a balance is reached [63]. A centralized approach may also solve the problem of voltage control for all desired buses within one grid. These (global) effects are typically connected to dynamics with larger time constants than the effects relevant for transient stability.

In this chapter, a controller strategy is developed, in which the robust local LPV controllers are coordinated by a centralized controller, while ensuring stability of the whole system. The controller type of choice is a model predictive controller (MPC). The underlying controlled system is described by DAEs. While the local LPV controllers are used for stabilizing the system after grid faults (for fast transients), the global MPC controls variables on a coarser timescale. The objective to control certain variables with high accuracy, while keeping other variables only within pre-

defined ranges, can be realized by the MPC. At the same time, physical limits of the system are considered. The control input is computed by solving an optimization problem, minimizing a cost function which depends on the inputs and the predicted controlled variables. The optimization is repeated at each (discrete) time-step with system data measured for the current point of time. One important requirement for the coordinating controller is its online applicability. The MPC approach has been used for decades in industry, and fast and effective solvers have been developed such that it can be used for complicated and large systems such as power systems [48]. Several results exist in which the MPC is used to control power systems.

## 7.1. Literature Review of MPC

In order to categorize the large variety of existing results for literature review, several aspects should be considered. From the point of view of application to power systems, one possible categorization is motivated by approaches in which an MPC coordinates several underlying dynamically modeled and (locally) controlled components. These components, together with the grid equations, are typically modeled by DAEs. This leads to the second classification of the literature review which is motivated by the underlying model comprising DAEs. A few results for the model predictive control of DAEs exist. Regarding the Part II of this work, in which local LPV controllers for the dynamically modeled components are designed, the third category for the literature review is motivated by the description of the local system as LPVS. Thus, results introducing MPC for LPVS are relevant, i.e. MPC approaches for (polytopic) LPVS.

### MPC for LPVS

As discussed in chapter 4, a requirement for the polytopic description of the LPV subsystems used in this work is the knowledge of parameter ranges. A common property of the existing MPC approaches for such LPVS is their robust design against changes of the (unknown) parameters within these ranges. For example, the cost function in [9] is minimized over the complete parameter ranges. In [109] and [54], similar optimization problems are reformulated in terms of an LMI problem, in which at each step a state feedback controller is computed. While being robust against unknown changes of the parameters, the min-max problem is computationally expensive and the resulting controllers conservative. For the large systems considered in this work, the applicability and computability of the mentioned approaches is questionable. In this work, the beneficial property of the LPVS is the existence of algebraic equations describing the parameters. Together with the analytic equations for the LPV controllers, a prediction for the closed-loop LPVS can be used for the MPC framework. Thus, MPC controllers for differential algebraic systems appear to be more relevant in the context of this work. The review also

covers MPC approaches for power systems, which are typically modeled by DAEs.

### **MPC for DAE-Systems**

In [27], a nonlinear model predictive controller (NMPC) approach for index-one DAE systems is presented. The term nonlinear indicates that the prediction is calculated by using an original nonlinear model of the system. The control objective is formulated in terms of the states, only. To avoid infinite horizons, two similar concepts are presented for the proof of stability: the quasi-infinite horizon and the dual-mode NMPC. Both approaches avoid infinite horizons by using a terminal region, leading to stability of the system and tractability of the optimization problem. This is done by introducing a state feedback controller which stabilizes the system within this region. In the case of NMPC with quasi-infinite horizon, this region is included in the optimization problem in form of a constraint. NMPC with a dual-mode approach switches to a terminal state feedback controller when the terminal region is reached. In both cases, the terminal state feedback controller is found based on a linearization of the system around one operating point, leading to a small terminal region. Constraints for the algebraic variables or their control are not included in the approaches and are named for future research by the authors. This is a large drawback considering the control objectives for power systems, in which relevant variables are modeled as algebraic variables (e.g. the voltage). A quasi-infinite horizon approach is adopted in [91] and extended to smoothness condition for the input. This is motivated by the nature of algebraic equations: a discrete change of the input may cause an impulse in the courses of the states. The impulses are avoided by using linear equality constraints for the inputs in the optimization problem. Control of algebraic variables is not presented, as well.

### **MPC in the Context of Power Systems**

Other results for MPC of systems formulated by index-one DAEs are motivated by the application to (global or supervisory) control of power systems. As mentioned before, typical control objectives for global controllers are voltage and frequency stability, typically achieved by reactive power and active power balance, respectively. In [68], and further detailed in [67], MPC is used as a supervisory controller for a power system. Only SGs are integrated in the considered system and the DAEs are similar to those in Ch. 3. Thus, the underlying equations are of the type of index-one DAEs, and the objective is to control the algebraically modeled voltage. The centralized MPC computes the reference values for the underlying standard controllers PSS, AVR, and the governor of the SG. The prediction model is a discrete-time linearized model. Other types of components than SG, with faster dynamics such as WECS, are not considered, due to the use of only one large sampling time for the discretization. Furthermore, stability of the MPC approach is not shown in that paper and remains an open question. Similarly, an MPC approach

for the control of the voltages is introduced in [3] and [4]. The considered power system comprises AVR-controlled SGs, only. Stability of the controller approaches is not discussed. In contrast to the previous results, the MPC approach presented in [31] considers stability. The cost function comprises a terminal region defined in terms of algebraic variables, called safety set by the authors. The assumption behind this procedure is that the system remains stable if a specific region defined by algebraic variables is reached, e.g. a band of  $\pm 5\%$  of the controlled bus voltages around their desired steady-state values. The authors call it a “pseudo-stability” condition, because the stability of the system within the safety set is not proven and a method to determine the safety set is not provided.

Alternatively to using one centralized approach, the power system can be decomposed into smaller subsystems, as done in [49] within a distributed MPC approach. The underlying power system is modeled by DAEs and only AVR-controlled SGs are considered as energy sources. The coupling between subsystems is realized by voltage phasors of the coupling buses. The MPC for each subsystem only needs the data of the respective (local) system, with the advantage of reduced optimization problems, but without discussing the stability of the approach. In [101] and in [55], distributed MPC approaches are used for frequency control of a power system. Similarly to the previous approach, the system is decomposed into subsystems. Proof of stability of the approach is declared as open task for future research, while in [101] stability is introduced by including terminal costs in the optimization problem. For both results, the underlying power system is modeled very simplified by using lumped SG models, i.e. detailed DAE-systems for system description are not used. Furthermore, control objectives are defined in terms of states, only. Thus, the application to more complicated systems with diverse energy sources, and the possibility to control algebraically modeled variables is questionable. A coordinating control of two different energy sources - the SG and the WECS - is realized in [100]. To control the grid frequency, the inertia of the SG as well as the inertia of the WECS are used and coordinated by an MPC. The WECS and the SG are modeled by their mechanical parts only, and the interconnections of the components are realized through power flows. The authors compare a centralized and a distributed MPC approach with each other. Stability is guaranteed by using terminal costs in the cost function of the MPC. Both approaches show good performance, and the frequency recovers fast. However, only slow (mechanical) dynamics are modeled. As only states are controlled by this method, the extension to the control of algebraic variables is not discussed.

Except of the last result, each of the reviewed publications consider only the SG for the voltage and frequency control, respectively. Furthermore, all coordinating controllers assume existing controllers on the lower level, which are synthesized and treated completely independently from the controller on the higher level. Except of [91], possible impulses (within the original system) caused by the MPC are not considered. The major drawback is, however, the lack of proof of stability of the approaches that control algebraic variables.

## Contribution

In this chapter, an MPC approach is presented that coordinates the dynamically modeled components and their LPV controllers with the objective to control predefined algebraic variables. The decentralized LPV controller approach derived in the previous chapters is utilized in order to proof stability of the MPC. The impulses caused by the controller actions are handled by the use of an adaptive sampling time: One small sampling time is used to account for the fast dynamics of the system in the first period after the controller action. The main control objectives are realized by using (long term) predictions based on a large sampling time. With this controller structure, algebraic variables and states can be controlled and constraints for any variable can be realized. The computation times of the optimization problem of the MPC, which will be discussed in Ch. 8, allow an online implementation. Due to the general formulations for the controlled system, the controller approach is applicable to many dynamically modeled systems and to power systems with diverse components with different dynamics.

The controller structure which will be derived in detail in the subsequent parts is schematically shown in Fig. 7.1 and is outlined next. While the use of the MPC is motivated by the global control of the voltage, other algebraic variables  $z$  and states  $x$  can be controlled, too. Thus, the controlled variable is generally defined by the system output  $y \subseteq \{x_1, \dots, x_{n_x}, z_1, \dots, z_{n_z}\}$ . In order to control  $y$  to the reference values  $\mathbf{r}_k$ , the optimal control input  $u_k^*$  (input of the system) is calculated by solving an optimization problem at each (discrete) time step. In this chapter, the superscript  $k$  indicates a discrete-time variable at time  $k$  and bold variables represent a vector, comprising predictions of the respective variable for a horizon  $H$  starting at time  $k$ . The cost function to be minimized contains the control objective and depends on the predicted values of the controlled variable  $\mathbf{y}_k$ , which in turn depend on the respective control inputs  $\mathbf{u}_k$ . For an online implementation of the approach for a large nonlinear system like a power system, the continuous-time nonlinear system (including the LPV controllers) is linearized and discretized around the actual operating point. The prediction is based on this model, which also adapts to exogenous inputs  $w^1$ , e.g. changed system parameters such as (known / planned) line switches or changed wind speed. The optimal control input  $u_k^*$  at time  $k$  is applied to the system, and at the next discrete time-step the whole procedure is repeated. As already mentioned, the control objectives for  $y$  are realized on a large timescale with several seconds to minutes, while impulses caused by controller actions are handled with a small sampling time. This allows the implementation of constraints on variables on a higher resolution. The prediction of the MPC with adapted sampling time is detailed in Ch. 7.4. In this work, the control inputs of the system for the MPC will be the reference values for the subordinated LPVS and their LPV controllers. With the application to power systems, these inputs

---

<sup>1</sup> $w$  will not be explicitly mentioned in the equations in the subsequent parts and is considered as part of the functions describing the DAEs.

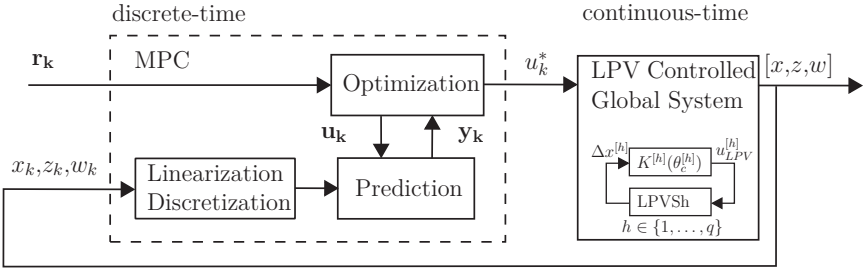


Figure 7.1.: Structure of the two layer control, with the matrix of predicted control inputs  $\mathbf{u}_k$ , the matrix of predicted controlled variables  $\mathbf{y}_k$ , and the matrix of the desired reference values  $\mathbf{r}_k$ . The vectors of the states, the algebraic variables, the exogenous inputs, and the optimal control inputs at time  $k$  are defined by  $x_k, z_k, w_k$ , and  $u_k^*$ .

may also be the mechanical torques of the SGs, or the injected active and reactive powers at a bus, if power sources are available (e.g. FACTS).

The chapter is structured as follows. First, the derivation of the LPV-controlled system through linearization and discretization is described. After that, the optimization problem for the MPC is formulated, including a proof of stability. For the efficient implementation of the optimization problem, the cost function is formulated as a quadratic function in matrix notation. Lastly, with the objective to handle the different timescales of power systems, together with constraints for different variables, the MPC technique is extended by a second sampling time. To simplify the understanding, the control variable  $u$ , in this chapter, is used for the MPC output only. The output of the LPV controller is indexed with  $LPV$  to  $u_{LPV}$ . Simulation results for an instance of a power system will be presented in Ch. 8 for the control of the bus voltages.

## 7.2. Prediction Model

For the model-based prediction, a model of the LPV-controlled power system is required. The classical first-order DAEs as described in Ch. 3:

$$\dot{x}(t) = f(x(t), z(t), u(t)), \quad (7.1)$$

$$0 = g(x(t), z(t), u(t)), \quad (7.2)$$

$$y(t) = h(x(t), z(t), u(t)), \quad (7.3)$$

have to be complemented by the equations of the LPV-controllers of any subsystem  $h \in \{1, \dots, q\}$ . The analytic description of the controllers was discussed in Ch. 5.8. The algebraic equations of the parameters  $\theta^{[h]}$ , the resulting barycentric coordinates

$\alpha^{[h]}$ , the state feedback matrices  $K^{[h]}(\theta^{[h]})$ , and the inputs  $u_{LPV}^{[h]}$  can now be reused from this chapter. The algebraic equations  $0 = g(x(t), z(t), u(t))$  are then extended by the following algebraic equations:

$$0 = -\theta_j^{[h]} + f_{\theta_j}^{[h]}(x^{[h]}, z^{[h]}, u^{[h]}) \quad \text{for } j \in \{1, \dots, n_p^{[h]}\}, \quad (7.4)$$

$$0 = -\alpha_i^{[h]} + f_{\alpha_i}^{[h]}(\theta^{[h]}) \quad \text{for } i \in \{1, \dots, n_v^{[h]}\}, \quad (7.5)$$

$$0 = -K^{[h]}(\theta_c^{[h]}) + \sum_{i=1}^{n_v^{[h]}} \alpha_i^{[h]} K_i^{[h]}, \quad (7.6)$$

$$0 = -u_{LPV}^{[h]} + K^{[h]}(\theta_c^{[h]}) \Delta x^{[h]}. \quad (7.7)$$

The expression  $\Delta x^{[h]}$  is defined by  $\Delta x^{[h]} = x^{[h]} - x_r^{[h]}$ , with the steady-state  $x_r$  of  $x$ . As already mention in Ch. 5, this formulation is motivated by the fact that the states of the LPV-controlled systems mostly do not have zero as their equilibrium.

If an input saturation is present as described in Ch. 5.5, then the saturation of the input has to be represented by a continuous function, allowing a differentiation of the function. Thus, an estimation of the hybrid function of the saturation of the input as in Eq. (5.21) and of the corresponding parameter as in Eq. (5.22) is required. In [19], the use of the hyperbolic tangent function is proposed for the estimation of the saturation. The saturated input for the system  $h$  is formulated as:

$$u_{LPV,sat}^{[h]} = u_{sat}^{[h]} \tanh(u_{LPV}^{[h]}/u_{sat}^{[h]}), \quad (7.8)$$

and is added to the algebraic equations of the system. For a system with several inputs, each input is handled similarly. An exemplary course is depicted in Fig. 7.2, in which the real course of a saturated input  $u_{LPV,real}$  is compared to the estimated course  $u_{LPV,sat}$ . It can be observed that at a value close to  $u_{sat}$ , the tanh-function underestimates the real value of the input by more than 20%, and the function almost saturates only at  $2 \cdot u_{sat}$ . Due to the fast dynamics of the closed-loop LPVS, the input of the unsaturated LPV controllers  $u_{LPV}$  rises very fast after faults. Thus, the approximation by an hyperbolic tangent as in Eq. (7.8) is well suited for the centralized controller.

## Linearization

The LPV-controlled power system described by the equations (7.1)-(7.8) is nonlinear and consists of numerous variables and states. In particular, the number of the algebraic variables is additionally increased by the variables describing the LPV controllers from the nonlinear Eqs. (7.4)-(7.8). Thus, an optimization of a cost function based on the prediction using exactly these equations would not be suitable for the application to power systems, leading to large durations for optimization. Using a linearization of these equations mitigates this problem. The resulting linear system description describes the system behavior well, allowing the use of this

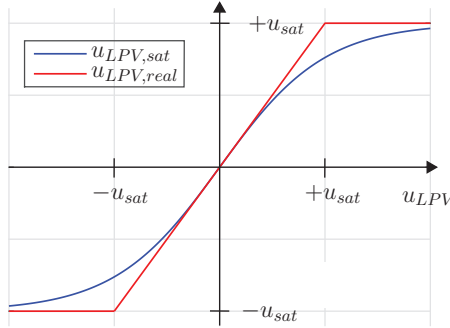


Figure 7.2.: tanh

model for the MPC, as demonstrated in the next chapter. The reason for this is that the linearized model is updated at each time step of the MPC, adapting to changed operating conditions on the coarser timescale, (while the embedded LPV controllers operate with exact models on a refined timescale). Furthermore, the faults or changes of system parameters appear locally and not all at the same time, mitigating the influence on the complete system. The linearization at the time  $k$  around  $[x_k, z_k, u_k]$  leads to the continuous-time linear system description:

$$\dot{x}(t) = A_c x(t) + B_c u(t) + F_c \quad (7.9)$$

$$y(t) = C_c x(t) + D_c u(t) + G_c \quad (7.10)$$

The algebraic variables are inserted into the description of the states, and the system matrices for the state-space model are calculated by <sup>2</sup>[91, 27]:

$$A_c = \frac{\partial f}{\partial x} + \frac{\partial f}{\partial z} \left( -\frac{\partial g}{\partial z} \right)^{-1} \frac{\partial g}{\partial x}, \quad (7.11)$$

$$B_c = \frac{\partial f}{\partial u} + \frac{\partial f}{\partial z} \left( -\frac{\partial g}{\partial z} \right)^{-1} \frac{\partial g}{\partial u}, \quad (7.12)$$

$$F_c = \left( f(x_k, z_k, u_k) - \frac{\partial f}{\partial x} x_k - \frac{\partial f}{\partial u} u_k - \frac{\partial f}{\partial z} z_k \right) + \frac{\partial f}{\partial z} \left( -\frac{\partial g}{\partial z} \right)^{-1} \left( g(x_k, z_k, u_k) - \frac{\partial g}{\partial x} x_k - \frac{\partial g}{\partial u} u_k - \frac{\partial g}{\partial z} z_k \right). \quad (7.13)$$

The algebraic variables do not appear in Eqs. (7.9) and (7.10) explicitly. However, the output vector can consist of states and algebraic variables with  $y \subseteq$

---

<sup>2</sup>The index  $c$  is used to indicate a continuous-time representation of an LTI system and appears only in this section.

$\{x_1, \dots, x_{n_x}, z_1, \dots, z_{n_z}\}$ . For an index-one DAE, the function  $\frac{\partial g}{\partial z}$  is invertible [75]. The respective matrices are defined by the following equations:

$$C_c = \frac{\partial h}{\partial x} + \frac{\partial h}{\partial z} \left( -\frac{\partial g}{\partial z} \right)^{-1} \frac{\partial g}{\partial x}, \quad (7.14)$$

$$D_c = \frac{\partial h}{\partial u} + \frac{\partial h}{\partial z} \left( -\frac{\partial g}{\partial z} \right)^{-1} \frac{\partial g}{\partial u}, \quad (7.15)$$

$$G_c = \left( h(x_k, z_k, u_k) - \frac{\partial h}{\partial x} x_k - \frac{\partial h}{\partial u} u_k - \frac{\partial h}{\partial z} z_k \right) + \frac{\partial h}{\partial z} \left( -\frac{\partial g}{\partial z} \right)^{-1} \left( g(x_k, z_k, u_k) - \frac{\partial g}{\partial x} x_k - \frac{\partial g}{\partial u} u_k - \frac{\partial g}{\partial z} z_k \right). \quad (7.16)$$

The algebraic variables in  $y$  are encoded in matrix  $G_c$ . In this work, the partial derivatives in Eqs. (7.11)-(7.16) are calculated analytically and offline, using the MATLAB symbolic toolbox. Apart from  $x$ ,  $z$ , and  $u$ , selected physical parameters of the system can be used as symbolic variables in the functions describing the derivatives. In this thesis, these physical parameters are elements of the admittance matrix and the wind speed. During the online operation of the MPC, the actual values are inserted into the analytic functions and the matrices  $A_c$ ,  $C_c$ ,  $F_c$ ,  $C_c$ ,  $D_c$ , and  $G_c$  are calculated online numerically. This method allows an online implementation of the linearization procedure. Alternatively, the linear system matrices can be expressed symbolically directly and time is saved as more calculations are carried out offline. However, this works for small systems only, because the symbolic calculation of the inverse  $\left(\frac{\partial g}{\partial z}\right)^{-1}$  is computationally demanding. In fact, the solution for the inverse  $\left(\frac{\partial g}{\partial z}\right)^{-1}$  for the 9-bus system with a symbolically described admittance matrix of the dimension  $9 \times 9$  could not be found.

## Discretization

The use of a continuous-time MPC is not an option in the context of large power systems, due to potentially high computation times for the optimization problem. Thus, the MPC technique in this work requires a linear discrete-time model of the form:

$$x(k+1|k) = Ax(k|k) + Bu(k|k) + F, \quad (7.17)$$

$$y(k|k) = Cx(k|k) + Du(k|k) + G, \quad (7.18)$$

where a value  $x(k+1|k)$  denotes the value of  $x$  for the time  $k+1$  predicted at time  $k$ . The system matrices of the discretized system with the sampling time  $T_d$  are

calculated by [68]:

$$A = e^{A_c T_d}, \quad (7.19)$$

$$B = \int_0^{T_d} e^{A_c \tau} d\tau B_c, \quad (7.20)$$

$$F = \int_0^{T_d} e^{A_c \tau} d\tau F_c. \quad (7.21)$$

The calculation of the matrix exponential function and the integral can be accomplished by standard MATLAB functions. For the discrete-time model of the output  $y$ , the matrices remain the same as those of the continuous system and are  $C = C_c$ ,  $D = D_c$ , and  $G = G_c$ .

### Prediction Model in Matrix-Notation

The vector  $\mathbf{y}_k = [y(k|k), y(k+1|k), \dots, y(k+H|k)]^T$  of predictions of the controlled variable for the prediction horizon  $H$  is derived by inserting the respective state descriptions into the equations for the output  $y$ . Starting with the actual (measured or known) state  $x(k|k)$  at time  $k$ , the state prediction for  $k+1$  based on (7.17) is inserted into (7.18) to obtain:

$$\begin{aligned} y(k|k) &= Cx(k|k) + Du(k|k) + G, \\ y(k+1|k) &= Cx(k+1|k) + Du(k+1|k) + G \\ &= C(Ax(k|k) + Bu(k|k) + F) + Du(k+1|k) + G \\ &= CAx(k|k) + CBu(k|k) + u(k+1|k) + CIF + G \end{aligned} \quad (7.22)$$

Repeating this for the times  $k+2$  to  $k+H$  leads to the following matrix notation:

$$\underbrace{\begin{bmatrix} y_{k|k} \\ y_{k+1|k} \\ y_{k+2|k} \\ \vdots \\ y_{k+H|k} \end{bmatrix}}_{\mathbf{y}_k} = \underbrace{\begin{bmatrix} C \\ CA \\ CA^2 \\ \vdots \\ CA^{(H-1)} \end{bmatrix}}_{=: \mathbf{C}} x_k + \underbrace{\begin{bmatrix} D & 0 & 0 & \dots & 0 \\ CB & D & 0 & \dots & 0 \\ CAB & CB & D & \dots & 0 \\ \vdots & \vdots & \vdots & \ddots & \vdots \\ CA^{H-2}B & CA^{H-3}B & CA^{H-4}B & \dots & D \end{bmatrix}}_{=: \mathbf{D}} \underbrace{\begin{bmatrix} u_{k|k} \\ u_{k+1|k} \\ u_{k+2|k} \\ \vdots \\ u_{k+H|k} \end{bmatrix}}_{\mathbf{u}_k} + \underbrace{\begin{bmatrix} G \\ CIF+G \\ (CA+CI)F+G \\ \vdots \\ (CA^{H-2}+\dots+CA+CI)F+G \end{bmatrix}}_{=: \mathbf{G}}. \quad (7.23)$$

where  $x_k = x(k|k)$  is the vector of states at time  $k$ . The vector  $x_k$  is also used as the linearization point. The control input vector  $\mathbf{u}_k$  is calculated in the MPC by solving an optimization problem, which is described in the next section.

## 7.3. MPC for the LPV-Controlled System

In this section, an MPC scheme for the LPV-controlled system is presented. The result concerning the stability of the complete LPV-controlled system is reused,

leading to the first assumption to prepare the result in the subsequent part:

**Assumption 7.1.** *All subsystems of the grid can be described as one LPVS each. The parameter ranges of all LPVS are known, and the system can be stabilized by the set of local LPV controllers as described in Ch. 5 with guaranteed global stability according to Theorem 5.2.*

Moreover, the predictions of the MPC are based on a discrete-time linear system, making the next assumption necessary:

**Assumption 7.2.** *The choice of the parameter ranges  $\theta \in [\underline{\theta}, \bar{\theta}]$ , with  $\theta = [\theta_c, \theta_r, \theta_s]$  as defined in Ch. 5, accounts for the linearization error of the linear system model. Furthermore, the sampling time  $T_d$  of the subsequent discretization is chosen such that the courses of the parameters in continuous-time  $\theta(t)$  are contained in the ranges of the discretized variables. Thus, it is assumed that:*

$$\begin{aligned} \text{for any } k \in \mathbb{N}, l \in \{0, \dots, H\} : & \left( \theta(t_{k+l|k}) \in [\underline{\theta}, \bar{\theta}], \theta(t_{k+l+1|k}) \in [\underline{\theta}, \bar{\theta}], T_d \in \mathbb{R}^{>0} \right) \\ & \Rightarrow \left( \theta(k+l|k) \in [\underline{\theta}, \bar{\theta}], \theta(k+l+1|k) \in [\underline{\theta}, \bar{\theta}] \right) \end{aligned} \quad (7.24)$$

As already mentioned in the introduction of this chapter, the objective of the MPC is the control of variables contained in  $y$ , leading to the following cost function for the optimization problem to be formulated later:

$$\begin{aligned} J(k) = & \sum_{l=0}^H \Delta y^T(k+l|k) \cdot Q_l \cdot \Delta y(k+l|k) \\ & + \Delta u^T(k+l|k) \cdot R_l \cdot \Delta u(k+l|k) \end{aligned} \quad (7.25)$$

in which  $\Delta y(k+l|k) = y(k+l|k) - r(k+l|k)$  is the difference between the controlled variable  $y(k+l|k) = Cx(k+l|k) + Du(k+l|k) + G$  and the reference value  $r(k+l|k)$ , and  $\Delta u(k+l|k) = u(k+l|k) - u_{ref}$  is the difference of the current control input and the reference control input of the system ( $u_{ref}$  typically has the value of the control input at the pre-fault condition).  $Q_l \in \mathbb{R}^{n_y \times n_y}$  and  $R_l \in \mathbb{R}^{n_u \times n_u}$  are the weighting matrices for the controlled variable and the control input of the controlled system for the prediction at the time  $l$ . Both matrices are chosen such that  $Q_l > 0$  and  $R_l > 0$ . The controlled variables can be weighted by  $Q_l$  individually, depending on the importance of how close to the reference value the respective value has to be controlled. In the context of power systems, it is often physically not possible to control all of these variables to predefined values with a steady-state error of zero. However, to comply with requirements of a grid, pre-defined ranges of these variables have to be met, while some selected variables have to be controlled more accurately. The compulsory ranges  $y_{min}$  and  $y_{max}$  for the controlled variables (according to the requirements for the grid), and  $u_{min}$  and  $u_{max}$  for the control inputs, are included in the following theorem, specifying also the optimization problem for the MPC.

**Theorem 7.1.** Let  $y_{min}$ ,  $y_{max}$ ,  $u_{min}$ , and  $u_{max}$  denote the constraints for the controlled variable and the control input. Furthermore, let  $y_p$  introduce the predicted variables which are not part of the controlled variables with  $y_p = [\theta_c, \theta_r, u_{LPV}]$ . Suppose that the Assumptions 7.1-7.2 hold and that the optimization problem:

$$\min_{u(k|k), \dots, u(k+H|k)} J(k) \quad (7.26)$$

$$\text{subject to } \underline{\theta}_c \leq \theta_c(k+l|k) \leq \bar{\theta}_c \quad (7.27)$$

$$\underline{\theta}_r \leq \theta_r(k+l|k) \leq \bar{\theta}_r \quad (7.28)$$

$$\underline{u}_{LPV} \leq u_{LPV}(k+l|k) \leq \bar{u}_{LPV} \quad (7.29)$$

$$y_{min} \leq y(k+l|k) \leq y_{max} \quad (7.30)$$

$$u_{min} \leq u(k+l-1|k) \leq u_{max} \quad (7.31)$$

$$y(k+l|k) = Cx(k+l|k) + Du(k+l|k) + G \quad (7.32)$$

$$y_p(k+l|k) = C_p x(k+l|k) + D_p u(k+l|k) + G_p \quad (7.33)$$

with the cost function as in Eq. (7.25) has a feasible solution in any  $k \in \{0, 1, \dots\}$ . Then, the application of the first element of the solution of the optimization problem  $u^*(k|k)$  to the controlled system according to (7.25)-(7.33) stabilizes the system in terms of Lyapunov.

*Proof.* First, it is shown that the cost function is not increasing. The following result is based on the interpretation of the cost function as a Lyapunov function and is standard in model predictive control, see e.g. [56]. Assuming that the solution of the optimization problem exists and is found at each time step, let  $\mathbf{u}_{opt,k} = \{u(k|k), u(k+1|k), \dots, u(k+H|k)\}$  be the optimal control input at time  $k$  with the optimal cost function value  $J_{opt}(k)$ . Using the optimal control input at time  $k$ , the cost function at time  $k+1$  is:

$$J(k+1) = J_{opt}(k) - \Delta y^T(k|k) \cdot Q_0 \cdot \Delta y(k|k) - \Delta u^T(k|k) \cdot R_0 \cdot \Delta u(k|k) \quad (7.34)$$

However, at time  $k+1$  a new optimization problem is solved. The optimal cost function at time  $k+1$  is then  $J_{opt}(k+1)$  and with  $Q_0 > 0$  and  $R_0 > 0$ , it follows that:

$$\begin{aligned} J_{opt}(k+1) &\leq J(k+1) \\ &= J_{opt}(k) - \Delta y^T(k|k) \cdot Q_0 \cdot \Delta y(k|k) - \Delta u^T(k|k) \cdot R_0 \cdot \Delta u(k|k) \\ &\leq J_{opt}(k) \end{aligned} \quad (7.35)$$

Consequently, the cost function is not increasing and approaches a finite value. If no further requirements for the horizon  $H$  are specified, this result is only valid for a stable (open-loop) plant (if the system is not stabilized within the horizon  $H$ , the plant is unbounded and the costs would become infinite)[56].

However, the LPV-controlled system<sup>3</sup> is stable as long as the parameter ranges  $[\underline{\theta}, \bar{\theta}]$  are not violated, which is recalled next. This stability result is covered by Assumption 7.1 and was presented in Ch. 5.7. The stability was achieved by using the Lyapunov function  $V(\mathbf{x}) = \mathbf{x}^T \mathbf{P} \mathbf{x}$  and  $\mathbf{P} = \mathbf{X}^{-1}$  with:

$$\mathbf{X} = \begin{bmatrix} X^{[1]} & 0 & \dots & 0 \\ 0 & X^{[2]} & \dots & 0 \\ \vdots & \vdots & \ddots & \vdots \\ 0 & 0 & \dots & X^{[q]} \end{bmatrix}. \quad (7.36)$$

for the complete grid, in which  $X^{[h]} > 0$  is the matrix of the Lyapunov function for subsystem  $h$ , originating from the LPV controller synthesis. With this global Lyapunov function it could be shown that the LPV-controlled system:

$$\underbrace{\begin{bmatrix} \dot{x}^{[1]} \\ \dot{x}^{[2]} \\ \vdots \\ \dot{x}^{[q]} \end{bmatrix}}_{\dot{\mathbf{x}}} = \underbrace{\begin{bmatrix} A_{cl}^{[1]}(\theta^{[1]}) & 0 & \dots & 0 \\ 0 & A_{cl}^{[2]}(\theta^{[2]}) & \dots & 0 \\ \vdots & \vdots & \ddots & \vdots \\ 0 & 0 & \dots & A_{cl}^{[q]}(\theta^{[q]}) \end{bmatrix}}_{\mathbf{A}_{cl}(\theta)} \underbrace{\begin{bmatrix} x^{[1]} \\ x^{[2]} \\ \vdots \\ x^{[q]} \end{bmatrix}}_{\mathbf{x}} \quad (7.37)$$

is stabilized for any  $\theta \in [\underline{\theta}, \bar{\theta}]$ . The linearization and discretization error between the model used for the predictions of the MPC and the original nonlinear continuous-time model is covered by the parameter ranges  $[\underline{\theta}, \bar{\theta}]$  with  $\theta = [\theta_c, \theta_r, \theta_s]$ , as stated by Assumption 7.2. Thus, the stability of the original nonlinear open-loop system is ensured by satisfying these ranges which is realized by the constraints (7.27)-(7.29) and discussed next.

In the case of the parameters  $\theta_c$  and  $\theta_r$ , the constraints for their ranges are enforced straightforwardly by Eqs. (7.27) and (7.28). The constraint for  $\theta_s$  is encoded implicitly in Eq. (7.29). This is motivated by its definition as in Eq. (5.22): it is obvious that this parameter has a hybrid description and can not be described by an algebraic equation (in contrast to the parameters  $\theta_c$  and  $\theta_r$ ). This equation is required for the prediction of the parameter. It is recalled that the reformulation of the saturation for the  $l$ -th system input of the LPV controller from Ch. 5.5 as in Eq. (5.23) is  $u^l = \text{sat}(K^l(\theta_c)x) = \theta_s^l K^l(\theta_c)x$ . Thus, the unsaturated system input is defined by  $u_{LPV} = K(\theta_c)x$ . The constraint for the  $\theta_s$  can now be reformulated in terms of the LPV controller output  $u_{LPV}$  by using  $u_{LPV} = \frac{u_{sat}}{\theta_s}$ , leading to the limits  $\underline{u}_{LPV} = \frac{-u_{sat}}{\underline{\theta}_s}$  and  $\bar{u}_{LPV} = \frac{u_{sat}}{\underline{\theta}_s}$ . These limits are introduced in the constraint (7.29).  $\underline{\theta}_s$  is used for the calculation of both limits of  $u_{LPV}$  because  $\bar{\theta}_s$  is  $\bar{\theta}_s = 1$ , and this represents the unsaturated input.  $\square$

<sup>3</sup>From the perspective of the MPC, the LPV-controlled system is the open-loop system to be controlled.

In [27], the stability of the MPC with a quasi-infinite horizon for an index-one DAE system is introduced by a terminal region, for which the stability is ensured by a state feedback controller. Here, the LPV controller plays the role of the terminal controller. The parameter ranges have to be kept for the complete horizon of the MPC. The optimal input is applied to the system. At the next sampling instance, the prediction is updated and the problem is solved again.

The predictions of  $y_p = [\theta_c, \theta_r, u_{LPV}]$  are required for the realization of the constraints for the parameters  $\theta_c$ ,  $\theta_r$ , and  $u_{LPV}$  (Eqs. (7.27)-(7.29)). These predictions are calculated in the same fashion as is done for the controlled variables  $y$ , described in the previous section. Similarly, constraints for other variables can be realized, as is often required in grid codes of power systems. This is a major advantage of the MPC scheme.

One remark has to be made on the linearization error (covered by assumption 7.2). Practically, the error is taken into account by a conservative choice of the parameter ranges. One possible method for over-approximation of the linearization error is the use of the Lagrange remainder, see e.g. [7].

### Online Realization of the MPC

Considering the complete system, the LPV controllers are designed offline and are operated online by using the algebraic equations (7.4)-(7.7), which are implemented in the prediction of the MPC. For the MPC, as already mentioned, the partial derivatives of Eqs. (7.11)-(7.16) are calculated symbolically offline, to reduce the calculation time. Furthermore, in order to be able to use an efficient solver for the quadratic program, the cost function in Eq. (7.25) can be described in matrix notation by using the prediction matrices in (7.23). The resulting costs are:

$$J(k) = 2 \left( x_k^T \mathbf{C}^T \mathbf{Q} \mathbf{D} + \mathbf{G}^T \mathbf{Q} \mathbf{D} - \mathbf{r}_k^T \mathbf{Q} \mathbf{D} - \mathbf{u}_{ref}^T \mathbf{R} \right) \mathbf{u}_k + \mathbf{u}_k^T \left( \mathbf{D}^T \mathbf{Q} \mathbf{D} + \mathbf{R} \right) \mathbf{u}_k. \quad (7.38)$$

The diagonals of the weighting matrices  $\mathbf{Q}$  and  $\mathbf{R}$  consist of the weighting matrices  $Q_l$  and  $R_l$  with  $l \in \{0, \dots, H\}$ . The matrices  $\mathbf{C}$ ,  $\mathbf{D}$ , and  $\mathbf{G}$  are the prediction matrices defined by Eq. (7.23), and  $\mathbf{u}_{ref}$  is a column vector consisting of a sequence of  $(H + 1)$  times  $u_{ref}$ .  $\mathbf{r}_k$  is the vector of reference values for the complete prediction horizon. The matrix representation for the predictions of  $y_p$  is calculated in exactly the same fashion as for the controlled variables in  $y$ , repeating the complete procedures defined by Eqs. (7.11)-(7.16) (linearization), (7.19)-(7.21) (discretization), and (7.23) (prediction in matrix-notation). Based on the prediction in matrix notation, additional constraints can be implemented into the optimization problem.

The algorithm for online implementation of the MPC at each time step  $k$  is as follows:

- the (continuous-time) model of the power system is linearized around the current values  $x_k$ ,  $z_k$ ,  $u_k$ , and the exogenous inputs  $w_k$  (e.g. the admittance

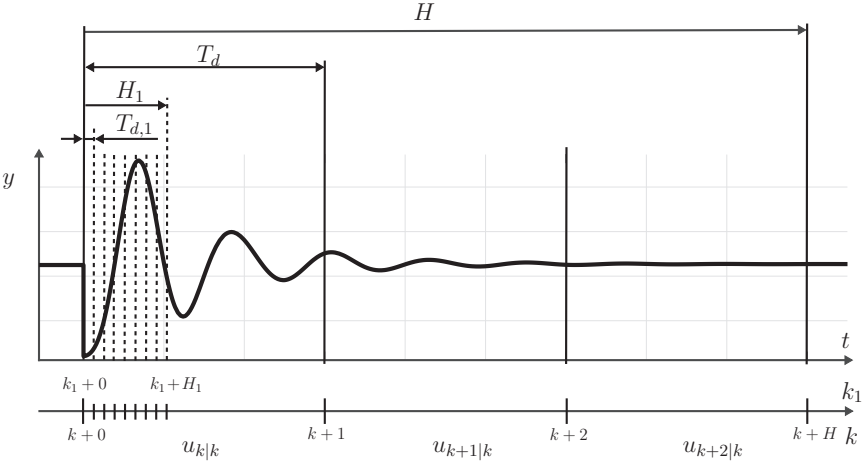
matrix  $\bar{Y}$  or the wind speed  $v_w$ ), using the symbolic description of the partial derivatives and Eqs. (7.11)-(7.16),

- the linear discrete-time model of the power system is determined according to (7.19)-(7.21),
- the prediction matrices  $\mathbf{C}$ ,  $\mathbf{D}$ , and  $\mathbf{G}$  for the controlled variables are calculated from (7.23) (and for the variables to be constrained:  $\mathbf{C}_p$ ,  $\mathbf{D}_p$ , and  $\mathbf{G}_p$ ),
- the sequence of optimal inputs  $\mathbf{u}_k^*$  is computed by solving the optimization problem (7.26),
- the input  $u_k^* = u^*(k|k)$  is applied to the system.

The objective of the MPC is the grid-wide coordinating control of the controlled variables  $y$ . Typical long term objectives are the control of the voltage or the frequency, aiming at maintaining long term grid stability, while controlling the selected variables close to predefined values. Sampling times and horizons of several seconds or minutes should be chosen, depending on the size of the controlled system and the control objective (e.g. primary control, secondary control, or tertiary control). However, following Assumption 7.2,  $T_d$  must be chosen such that the dynamics of the parameters is represented by the discrete-time model. This dynamics is fast. Considering the simulation results from Ch. 6, only the first swing within the first milliseconds typically causes the largest changes of the parameters. Thus,  $T_d$  must be chosen very small. The prediction with a very small sampling time for a horizon of several seconds renders the optimization problem intractable for an online implementation. Thus, in the next section, an MPC scheme with adapted sampling times is introduced: one sampling time accounts for the first swing after controller actions, and the second one for the long term prediction and the controller actions.

## 7.4. MPC with Adapted Sampling Times

For the considered control objective, a horizon of several seconds to minutes is needed. To keep the computations sufficiently small, the horizon implies a large sampling time  $T_d$ , for which the Assumption 7.2 does not hold. Using a very small sampling time for a control horizon of several seconds or minutes is not an option due to a rising complexity of the optimization. Thus, adapted sampling times with the corresponding horizon are introduced, leading to the use of two different sampling times and horizons. An illustration is shown in Fig.7.3: a swing appears after the time  $k$  and is considered in the prediction of  $y$  by the use of  $T_{d,1}$  and  $H_1$ . As mentioned before, this swing typically appears after abrupt changes of algebraic variables of the grid or the controller actions of the MPC. The time span defined by these variables should be smaller than the sampling time for the controller action with  $T_{d1} \cdot H_1 < T_d$ . This avoids overlapping predictions of  $y$  for the two horizons


 Figure 7.3.: Prediction of  $y$  with adapted sampling times and horizons.

$H$  and  $H_1$ . Because the predictions for the times  $k_1$  are used for the realization of constraints only, the control inputs are held constant for the complete horizon  $H_1$ . Thus, the optimization problem for the MPC is extended by the auxiliary constraints for the control inputs:

$$u(k_1|k_1) = u(k_1 + 1|k_1) = \dots = u(k_1 + H_1|k_1) \stackrel{!}{=} u(k|k). \quad (7.39)$$

To avoid that the costs for predictions over the horizon  $H_1$  do become too dominant, lower weights for the first  $H_1$  values of the prediction are chosen in the cost function. A balanced choice of the weights may improve the controller performance in two ways: due to the weighting of the first swing, the control input is computed such that the amplitudes of the first swing do not become arbitrary high. On the other hand, the first swing should not be represented too dominantly in the cost function, leading to good controller performance in the long term. Thus, the individual diagonal entries  $Q_{l,i}$ ,  $i \in \{1, \dots, n_y\}$  and  $R_{l,j}$ ,  $j \in \{1, \dots, n_u\}$  of the weighting matrices  $Q_l$  and  $R_l$  of the cost function should be chosen such that:

$$\begin{aligned} Q_{1,i} = Q_{2,i} = \dots = Q_{H_1,i} < Q_{H_1+1,i} = Q_{H_1+2,i} = \dots = Q_{H_1+H,i}, \\ R_{1,j} = R_{2,j} = \dots = R_{H_1,j} < R_{H_1+1,j} = R_{H_1+2,j} = \dots = R_{H_1+H,j}. \end{aligned} \quad (7.40)$$

One option is to choose the weighting for the variables associated with the small time constant  $T_{d,1}$  as one  $H_1$ -th of the weighting associated with the large time constant  $T_d$ .

With the additional constraints for the control inputs as in (7.39) and the choice of the weighting as in (7.40), in general, the online realization of the MPC with

adapted sampling times remains the same as in the previous section. The cost function in matrix notation (7.38) can be reused. The required prediction in matrix notation for selected  $H_1$  and  $H$  is:

$$\underbrace{\begin{bmatrix} y_{k_1|k} \\ y_{k_1+1|k} \\ \vdots \\ y_{k_1+H_1|k} \\ y_{k|k} \\ y_{k+1|k} \\ \vdots \\ y_{k+H|k} \end{bmatrix}}_{\mathbf{y}'_k} = \underbrace{\begin{bmatrix} \mathbf{C}_1 \\ \mathbf{C} \end{bmatrix}}_{=:\mathbf{C}'} x_k + \underbrace{\begin{bmatrix} \mathbf{D}_1 & \mathbf{0} \\ \mathbf{0} & \mathbf{D} \end{bmatrix}}_{=:\mathbf{D}'} \underbrace{\begin{bmatrix} u_{k|k} \\ u_{k|k} \\ \vdots \\ u_{k|k} \\ u_{k+1|k} \\ \vdots \\ u_{k+H|k} \end{bmatrix}}_{\mathbf{u}'_k} + \underbrace{\begin{bmatrix} \mathbf{G}_1 \\ \mathbf{G} \end{bmatrix}}_{=:\mathbf{G}'}. \quad (7.41)$$

It is to mention that the controlled variables  $y_{k_1|k}$  and  $y_{k|k}$  are equal and, hence, the respective values appear twice in the cost function. This is not a problem as the weighting of  $y_{k_1|k}$  is significantly smaller than that of  $y_{k|k}$ .

## 7.5. Discussion of the Grid-Wide Coordinating Controller

The presented MPC technique is tailored to the distributed LPV controller approach and preserves the stability of the controlled system, if the ranges of the parameters are not violated. The control objective can be formulated in terms of algebraic variables and states, in contrast to many reviewed results. It allows handling of variables that are important for power system operation such as the voltage. Physical variables which are dependent on the balance of power (e.g. the voltage), can be controlled optimally, while satisfying constraints required for grid operation and defined by the grid codes. Systems with dynamics of different timescales can be accounted for, due to the use of adapted sampling times. By using a small sampling time, amplitudes of oscillations caused by controller actions can be constrained directly. One important advantage is that constraints can also be implemented for variables that are not part of the cost function. The robustness of the overall approach is ensured through the fast LPV controllers, which are integrated in the MPC scheme. By using analytic (offline) linearizations of the system model, the computation time is reduced, allowing a real time implementation. The reference values of the LPV controllers can be used as control inputs of the MPC. It is also possible to use other sources of active and reactive powers, if they are available.

The scalability in terms of the computation times and a simulative demonstration of the MPC approach will be presented and discussed in the next chapter.



## 8. Simulation Results for the MPC

The MPC approach for LPV-controlled systems is demonstrated for the 9-bus system with the same setting as it was used in Ch. 6.2. Here, in addition to keeping the system stable by the LPV controllers, the control objective is extended to the control of four bus voltages. The faults and exogenous effects remain the same as in Ch. 6.2, while their timing is slightly changed to improve observability of the effects with a sampling time of the controller of  $T_d = 2s$ . The sequence is as follows: after one second, the wind speed grows from  $11.4\frac{m}{s}$  to  $12\frac{m}{s}$ . The voltage drops by approximately 20% at  $t = 9.1s$  until the fault is cleared after  $100ms$ . The last fault of the sequence occurs at  $t = 11.2s$ , permanently doubling the line admittance between the buses 5 and 7. It is stressed that the first and the third event are assumed to be measured and thus are “known” to the MPC, i.e. they can be in the prediction. The second event lasts only  $100ms$  and can not be considered by the MPC with  $T_d = 2s$ . This fault is robustly controlled by the LPV controllers only. In the case of the other two events, the LPV controllers stabilize the system and damp the oscillations, but do not control the voltage.

The controlled variables of the MPC are consequently the 9 bus voltages  $y = [v_1, v_2, \dots, v_9]^T$ . The reference values  $r_k$  for the MPC are the pre-fault values of the voltages. As it is not possible to control all voltages exactly to their reference values, the voltages  $v_1$  and  $v_4$  at the buses 1 and 4 are chosen to be controlled close to their reference values. The other 7 voltages must be kept within a  $\pm 10\%$  band around their pre-fault values, which is a value close to typical values used for most grid codes [95]. The control of  $v_4$  is prioritized to show that voltages for which a power source is not in close proximity can be controlled by the MPC, too. The weights of the cost function used in the optimization problem (7.26) are chosen to 200 for  $v_1$  and  $v_4$ , and to 1 for the remaining voltages.

One typical countermeasure for control of the voltages (and the frequency) of a power system is the use of the so-called load shedding, where some loads are temporarily disconnected from the grid. This step is a severe change and is not considered in this work, in order to achieve the control goals by using the controlled subsystems, only. Thus, the control inputs of the MPC are chosen such that they only affect the dynamically modeled systems, i.e. the two SGs and the WECS. Two simulations are described in this chapter, with two different choices of control inputs of the MPC.

In the first simulation, the MPC uses 6 control inputs. As mentioned in the previous chapter, the LPV-controlled subsystems do not have steady-states at zero and, consequently, the inputs for the LPV controllers are not the states, but the

differences between the initial steady-states (being the reference values for the LPV controllers) and actual states. Thus, the input for the LPV controller  $u_{LPV}$  of a subsystem  $h$  is calculated by  $u_{LPV} = K^{[h]}(\theta_c^{[h]})\Delta x^{[h]}$  with  $\Delta x^{[h]} = x^{[h]} - x_{ref}^{[h]}$ . In this work, parts of the reference values  $x_{ref}^{[h]}$  for the LPV state feedback are used as control inputs of the MPC, i.e. for the SG, the variables  $\delta_{ref}^{[h]}$  and  $e'_{q,ref}{}^{[h]}$ , and for the WECS, the reference values  $\omega_{m,ref}^{[h]}$  and  $\psi_{d,ref}^{[h]}$  are to be determined by the MPC. It is to mention that only for the reference value  $\omega_m^{[h]}$  steady-state accuracy can be reached, because  $\omega_m^{[h]}$  is the only state with integrating behavior introduced by the LPV controller.

For the second stimulation, the vector of control inputs is extended to the two mechanical torques  $\tau_m^{[h]}$  of the SGs. In standard control of power systems, the mechanical torques are used for frequency control and are changed in order to restore the frequency. In this work, the frequency is regulated by the LPV controllers. The second simulation is carried out to analyze the effects of the torques on the control of the voltage. Typically, the torques are determined by the dynamics of the respective turbine. This dynamics is not considered in detail, but is estimated by restricting the rate of change by a ramp, as discussed in a subsequent section.

The MPC is implemented such that for both simulations the optimization problem comprises 8 control inputs, but with different weighting. For the first simulation the changes of the torques are weighted by 1000, leading to no changes at all, and by 1 for the second simulation. The two control inputs  $e'_{q,ref}{}^{[h]}$  (for  $h \in [2, 3]$ ) are weighted by 0.01 to allow a significant change of these variables. The remaining 4 control inputs are weighted by 1. The resulting system is shown in Fig. 8.1, in which the MPC and the respective signals are marked in blue.

The remaining variables to specify the MPC parametrization are the sampling times  $T_d$  and  $T_{d1}$ , as well as the horizons  $H$  and  $H_1$ . As already mentioned in the beginning of this chapter, the controller sampling time for the MPC is chosen to  $T_d = 2s$ . This sampling time can be seen as a design parameter, and is dependent on the relevant system dynamics and the available computation time for the optimization problem, i.e. it should be larger than the computation time (this point will be discussed in a subsequent section). Simulations showed that a horizon of  $H = 5$  with a  $T_d = 2s$  is sufficient to achieve an overall good controller performance. A small  $T_d$  leads to frequent control actions to correct the voltage.  $T_{d1}$  accounts for fast effects after faults or control actions of the MPC itself. Motivated by the results from Ch. 6,  $H_1$  is chosen to 15 and  $T_{d1}$  is chosen to 0.01s to cover the first swing with a sufficient accuracy (smaller sampling times were tested, but did not lead to improvements of the controller performance).

Next, the two simulation results for the introduced scenario are presented for 6 and for 8 control inputs of the MPC. After that, the effect of the length of the horizons on the computation time is evaluated. Lastly, the use of the MPC for the control of power systems is discussed.

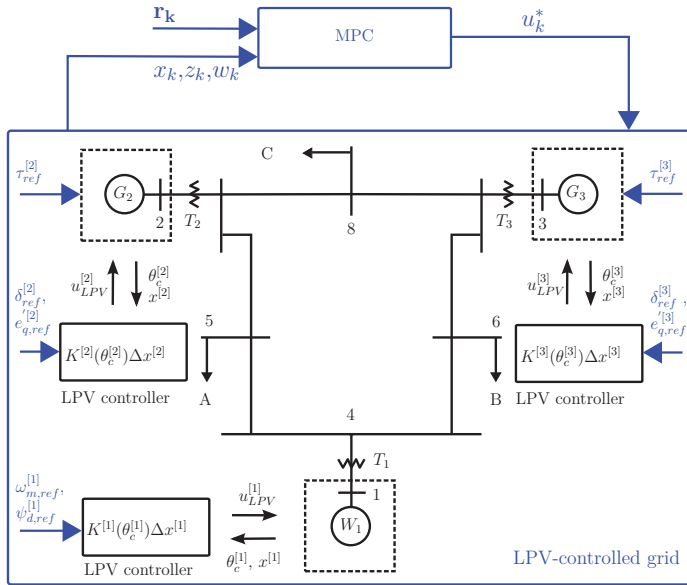


Figure 8.1.: Structure of the 9-bus system with two layer control. The reference for the controlled variables is defined as  $r_k = \{v_{1,ref}, \dots, v_{9,ref}\}$  and the control inputs as  $u = \{\omega_{m,ref}^{[1]}, \psi_{d,ref}^{[1]}, \delta_{ref}^{[2]}, e_{q,ref}^{[2]}, \delta_{ref}^{[3]}, e_{q,ref}^{[3]}, [\tau_m^{[2]}, \tau_m^{[3]}\}$ .

## 8.1. Voltage Control by MPC

The MPC approach is applied to the LPV-controlled 9-bus system with the objective to control the voltage. Referencing the results from Ch. 6.2, the input constraints of the SGs are kept and are part of the synthesis of the LPV controllers. The results without the use of the MPC are depicted in Fig. 8.2 and are the same as the results presented in Ch. 6.2. The LPV controllers stabilize the system and the oscillations are very well damped. However, the steady-states of the voltages are changed, i.e. their values deviate from the pre-fault values. First, the MPC is applied to the system with exactly the same setting for the LPV controllers as in Ch. 6.2, and with the respective parameter ranges as given in the Appendix in Table A.2. Good control performance can be achieved (which will be discussed later) but the parameter ranges of parameter  $\theta_2$  of the WECS  $W_1$  are violated, which can be observed in Fig. 8.3 (left): the ranges are plotted as dashed black lines and their violation is marked with a red circle. The MPC has constraints on the parameter ranges of the LPV-controlled system. However, the parameter range is violated for the second event. This event takes place between two discrete time steps of the

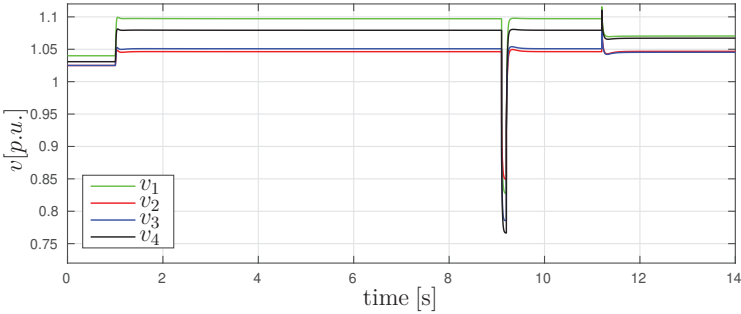


Figure 8.2.: Simulation results for bus voltages of the LPV-controlled 9-bus system.

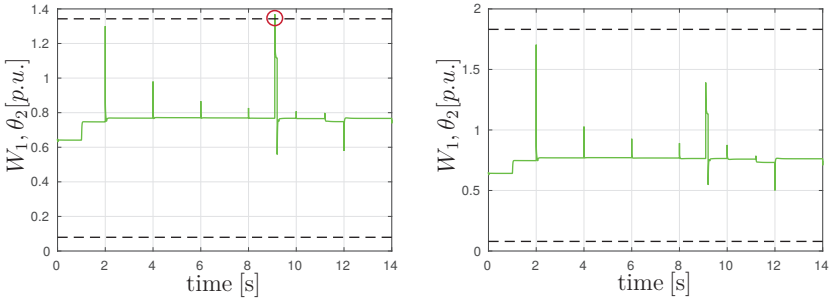


Figure 8.3.: Simulation results for the parameters  $\theta_1$  of  $W_1$  with violated (left) and modified (right) parameter ranges.

MPC and can not be seen by the MPC. Thus, this fault is controlled by the LPV controllers completely. However, before the fault occurs, the MPC changed the operating condition of the system. As the used parameter ranges were determined without the consideration of the MPC controller actions, the parameter range of this one parameter is not chosen conservatively enough. Adjusting the parameter range to  $\theta_2 \in [0.0793, 1.8311]$  solves the problem, see Fig. 8.3 (right) (requiring a new LPV controller synthesis). The impulses in the course of the parameter are caused by the controller actions of the MPC. The remaining parameters never violate their ranges and the stability condition is kept.

The resulting controller performance for the voltages is depicted in Fig. 8.4. The controller actions of the MPC can be observed by changed courses of the voltages every two seconds. The wind increases at  $t = 1s$ , in the middle of the sampling time of  $T_d = 2s$ , and it takes on more second until the MPC responds to this changed operating condition. As already mentioned, the second event (voltage drop) is not

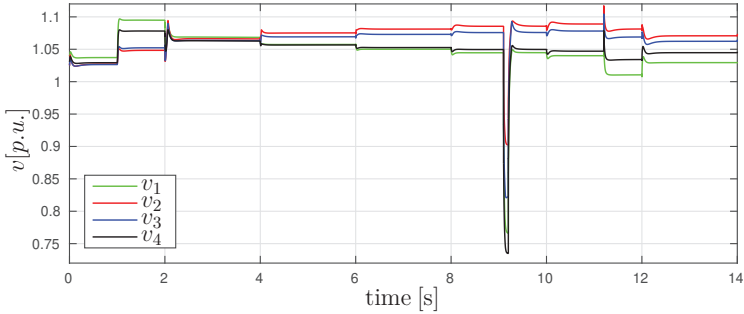


Figure 8.4.: Simulation results for the voltages controlled by MPC.

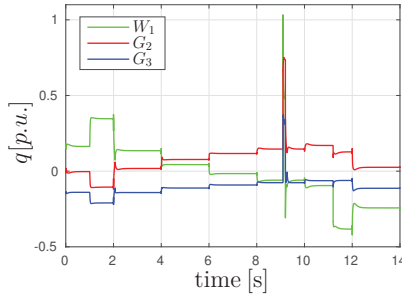


Figure 8.5.: Simulation results for the reactive powers for the 9-bus system controlled by MPC.

perceived by the MPC. The system is stabilized by the LPV controllers only. At  $t = 10\text{s}$ ,  $v_1$  and  $v_4$  are controlled close to their pre-fault values, while the other two voltages rise, keeping balanced reactive and active powers. The three energy sources inject only a limited amount of reactive (and active) powers, as can be observed in Fig. 8.5: While the reactive power at bus 1 is reduced, the other two powers of  $G_2$  and  $G_3$  rise at the same time. The reactive power at bus 4 is zero, due to a missing load at bus 4. However, the voltage  $v_4$ , which is distant to the three power sources, is controlled well by the MPC.

In this setting, the input constrained LPV controllers for the SGs  $G_2$  and  $G_3$  are used. As it was already mentioned in the previous chapter, the constraints for the corresponding parameters  $\theta_s^{[h]} \in [0.01, 1]$  are realized through the constraints on  $u_{LPV}^{[h]}$  (the input of the LPV controller before the saturation through  $\theta_s^{[h]}$ ). The courses of  $u_{LPV}^{[h]}$  for the two SGs are depicted in Fig. 8.6 (left). While the impulses

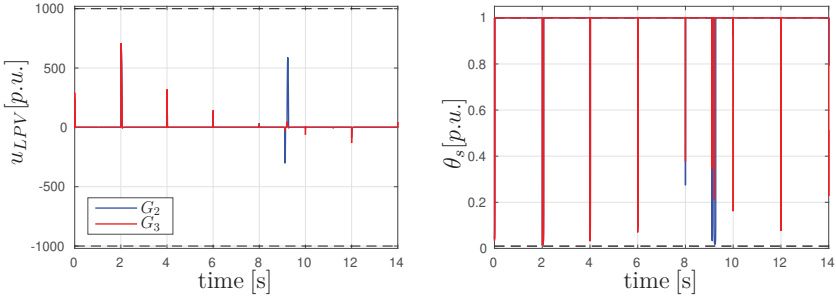


Figure 8.6.: Simulation results for the inputs of the (unconstrained) LPV controllers  $u_{LPV}$  (left) and the respective parameters  $\theta_s$  (right) of the two SGs.

every two seconds are caused by the MPC, the impulse between  $t = 9.1$  s and  $t = 9.2$  s is caused by the LPV controllers and the fault only. The dashed black lines show the constraints for  $u_{LPV}^{[h]}$ , which are between  $-1000$  and  $+1000$ . This value is calculated based on the input constraint  $u_{sat} = 10$ , and the chosen parameter limits for the auxiliary parameter for the realization of the constraints in the LPV controller synthesis with  $\theta_s^{[h]} \in [0.01, 1]$ . The range for  $u_{LPV}$  is calculated by using  $\underline{u}_{LPV} = \frac{-u_{sat}}{\underline{\theta}_s} = \frac{-10}{0.01} = -1000$  and  $\bar{u}_{LPV} = \frac{u_{sat}}{\underline{\theta}_s} = \frac{10}{0.01} = 1000$  (see Ch. 7.3). In the resulting courses of  $\theta_s^{[h]}$  it can be observed that the condition  $\theta_s^{[h]} \in [0.01, 1]$  is satisfied.

Next, some of the control inputs of the MPC are examined. The courses of the two control inputs  $\omega_{m,ref}$  and  $\psi_{q,ref}$  are shown in Fig. 8.7. The blue dashed lines represent the reference values which are computed and dictated by the MPC, and the green lines refer to time values of the respective variables of the WECS  $W_1$ . Typically, the control inputs computed by the MPC change in a discrete manner as it can be observed for  $\psi_{q,ref}$  in Fig. 8.7. For  $\omega_{m,ref}$ , the change is realized by a ramp due to the problem that the DAE solver could not find a solution for discrete changes of the reference values for  $\omega_m$ . The step for  $\omega_m$  enforced by the MPC is too large for the solver. The ramp is implemented such that the desired reference value is reached within  $T_d$ . As depicted in Fig. 8.7 (left), the true value for  $\omega_m$  follows the reference values due to the integrating behavior for this variable, introduced by the LPV controller. In the courses of  $\psi_q$ , a small error between  $\psi_q$  and  $\psi_{q,ref}$  remains.

In contrast, a relatively large error remains between the reference values for the LPV controllers of the SGs computed by the MPC and the respective true signals. Exemplary results are shown in Fig. 8.8: the LPV state feedback controller cannot control  $e'_q$  to  $e'_{q,ref}$  with a steady-state error of zero, due to the missing integrator for this state. This behavior, however, does not represent a problem and is considered automatically in the model of the power system used by the MPC, which comprises

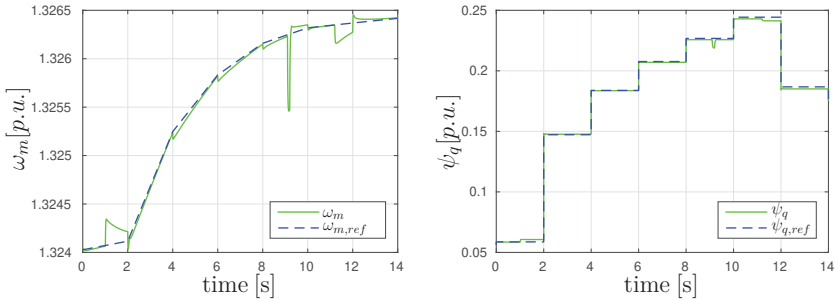


Figure 8.7.: Simulation results for the control inputs of MPC  $\omega_{m,ref}$  (left) and  $\psi_{q,ref}$  (right), and the respective states of the WECS  $W_1$ .

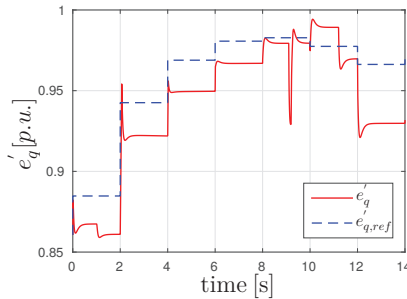


Figure 8.8.: Simulation results for the control input of MPC  $e'_{q,ref}$  and the respective state of the SG  $G_2$ .

the full set of equations for the LPV controllers. It can be summarized that the MPC controlled system meets the requirements stated for the control of the voltages, i.e. that all constraints are kept, while the voltages  $v_1$  and  $v_4$  are controlled close to their pre-fault values. In the next section, the simulations are repeated with the use of two more control inputs for the MPC.

## 8.2. Voltage Control by MPC with an Extended Number of Inputs

The mechanical torques of the two SGs are used as control inputs of the MPC by setting their weights to 1 in the cost function of the optimization problem. As already mentioned, the change of the torque is connected to dynamics of turbines. Thus, the torques can not be changed discretely. Alternatively, a ramp for the

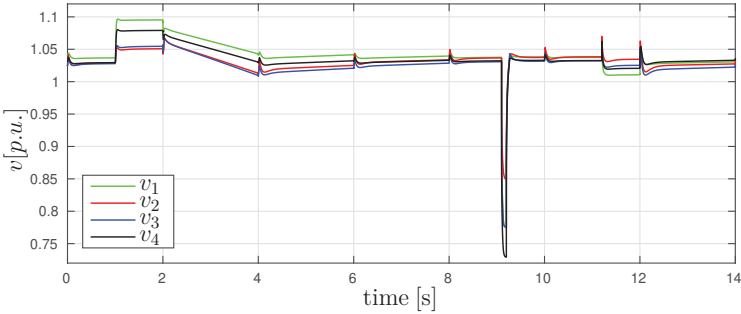


Figure 8.9.: Simulation results for the voltages controlled by MPC using 8 control inputs.

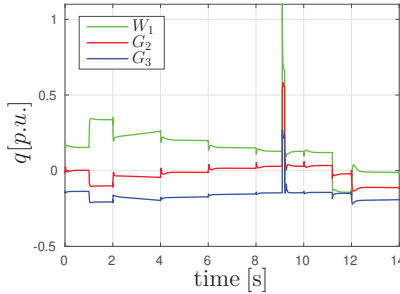


Figure 8.10.: Simulation results for the reactive powers for the controlled 9-bus system, with the MPC using 8 control inputs.

torques is used such that the value computed by the MPC is reached within  $T_d = 2s$ . This is a simplification, but the ramps with less than  $1p.u$  per second are within the scope of what can be realized by steam turbines (see [41]).

The results for the voltage control can be observed in Fig. 8.9. The voltages  $v_1$  and  $v_4$  (weighted with 200 in the cost function) are controlled faster to their pre-fault values than in the case with 6 control inputs (compare with Fig. 8.4). Furthermore, due to the ramps of the two additional control inputs, their changes are smoother compared to the results of the previous section. The most important observation is that the other two voltages  $v_2$  and  $v_3$  (weighted with 1 in the cost function) are controlled close to their pre-fault values, as well. The behavior of the respective reactive powers has also changed. In Fig. 8.10, it can be observed that the reactive powers injected by  $G_2$  and  $G_3$  change only slightly during the whole simulation, and the original value for  $W_1$  is almost recovered after 10s. This behavior is

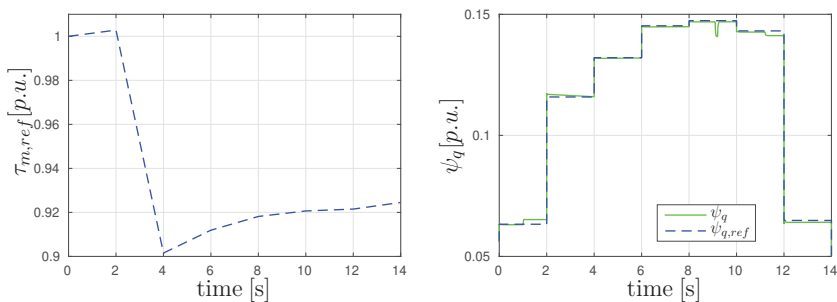


Figure 8.11.: Simulation results for the control inputs of MPC  $\tau_{m,ref}$  (left) and  $\psi_{q,ref}$  (right) and the respective state  $\psi_q$  of the WECS  $W_1$ .

different compared to the results of the previous section and can be explained by the injected torques. An exemplary result for the torque of  $G_2$  is shown in Fig. 8.11 (left): the mechanical torque is decreased by the MPC (and similarly for the  $G_3$ ). Typically, reactive powers are adjusted to control the voltage and active powers to control the frequency, and the mechanical torques affect the active powers. The observed behavior, namely, that the control of the voltage is improved by adapting mechanical torques, is, however, not a contradiction because a relation between the four variables exists [2]. This relation is sufficiently strong to control the voltage as well. At the end of the simulation, the frequency and the voltages are at their desired values. The use of the torques as control inputs of the MPC leads to less controller actions of the control inputs, which is exemplary shown for the control input  $\psi_{q,ref}$  in Fig. 8.11 (right). The course shows a maximum value of circa 0.14, which is significantly lower than the one for  $\psi_{q,ref}$  in the previous section (ca. 0.24). The use of the torques as control inputs of the MPC significantly improves the controller performance.

### 8.3. Size of the Optimization problem and Computation Time

Next, the time for solution of the optimization problem is discussed. One important requirement for the MPC is its real-time applicability. In order to give an insight into the computation times, some exemplary computation times for different settings of the optimization problem are presented.

First, the number of variables of the 9-bus system is discussed. The system at hand has 10 states, 24 algebraic variables of the components, and 36 algebraic variables of the grid. With the total amount of 11 parameters ( $\theta_c$ ), the number of auxiliary algebraic variables motivated by the LPV controllers is 69, making a

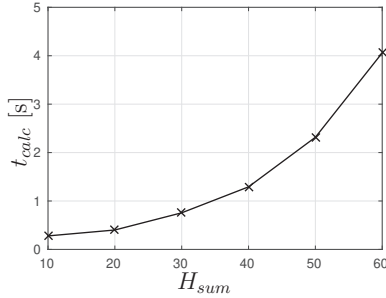


Figure 8.12.: Computation time for the optimization in dependence on the horizon of the prediction.

large part of all variables. The LPV controller also motivates the most constraints necessary for stability of the MPC. 22 inequality constraints ensure that the parameter ranges are not left and 4 inequality constraints are added to limit the two inputs  $u_{LPV}$  for the LPV controllers of the SGs. 18 inequality constraints are introduced to limit the deviations of the 9 bus voltages to  $\pm 10\%$  of their original values. These constraints are valid for the complete prediction horizon  $H_{sum} = H + H_1$ .  $H_1$  equality constraints are needed for each of the 8 control inputs so that they are constant for the horizon  $H_1$ . The number of variables (algebraic and states) sums up to 139 (for the horizon  $H_{sum}$ ), the number of inequality constraints is 44 (for the horizon  $H_{sum}$ ), and the number of equality constraints is 8 (for the horizon  $H_1$ ). The horizons determine the length of the vectors that represent the predictions of these variables and the constraints. Simulations showed that a sampling time of  $T_{d1} = 0.01s$ , a horizon of  $H_1 = 15$ , a sampling time of  $T_d = 2s$ , and a horizon of  $H = 5$  are sufficient to achieve an overall good controller performance. This setting was used for the previous two simulation studies and the time needed to solve the optimization problem (7.26) is in average 0.383s. This allows an online realization of the MPC, which controls the system every 2s.

To examine the computation time for the optimization in dependence of the horizon, simulations with the aforementioned setting were carried out. The results are presented in Fig. 8.12, where  $H_{sum} = H + H_1$ , and  $H$  has a share of 25% to 40% of  $H_{sum}$ . This last relation defines the equality constraints. The time needed for the optimization is  $t_{calc}$  and appears to depend exponentially on  $H_{sum}$ . In consequence, the two horizons must not be chosen too large. With a horizon of  $H_{sum} = 20$  the MPC achieves good performance while having a sufficiently small computation time.

The computation times with different numbers of variables is investigated by using the significantly smaller SMIB-system introduced in Ch. 5. As only the MPC-controlled SMIB-system and the MPC-controlled 9-bus system are used for compar-

ison, this comparison can only be seen as an example. The SMIB has 3 states, 11 algebraic variables for the SG and the grid, and 13 algebraic variables for the LPV controller. The setting for the MPC is as follows: The system is controlled with only one sampling time  $T_d = 1s$  and with a horizon of  $H = 20$ . The control input for the MPC is  $e_{q,ref}^{[h]}$ . The average computation time for the optimization problem is  $t_{calc} = 0.047$ . This computation time with an overall number of 27 variables is compared with the computation time needed for the optimization for the MPC of the 9-bus system with 139 variables and the same overall horizon. For better comparison, no constraints are implemented for both systems. The computation time for the MPC for the 9-bus system is  $t_{calc} = 0.214s$  in average. With 5 times more variables, a ca. 4.5 times higher computation time is obtained for the 9-bus system compared to the SMIB-system. This result indicates that the horizon affects the computation time for the solution of the optimization problem stronger than the number of variables involved in the optimization problem. However, the latter effect should be further investigated in future research.

## 8.4. Conclusion

The MPC is used to complement the LPV-controlled system by the control of the bus voltages. The prediction model of the power system to be controlled comprises the grid equations, the dynamically modeled components and the LPV controllers. By formulating the optimization problem for the MPC with the inclusion of the constraints for all parameters, the stability of the grid established by the LPV controllers is preserved. One major advantage of the MPC is that voltages of buses to which no dynamic and controlled systems are connected can be controlled as well. Furthermore, limits for pre-defined variables are kept by the MPC. This simplifies control which complies with grid codes. The computation times for the optimization problem of the MPC for the used examples are much less than the used sampling time of 2s. Thus, the MPC can be implemented online. By using a larger sampling time  $T_d$  and with the sufficient choice of the prediction horizon, the application to much larger grids seems possible.

All in all, it could be demonstrated that by coordinating all involved power sources, the grid can be controlled such that multiple objectives are met, i.e. the voltage and transient stability can be controlled at the same time by one unifying approach. Moreover, robustness against severe grid faults and fluctuating operating conditions is ensured. The fluctuations can be motivated by the changes of line impedances, but also by changing wind speed. The occurrence of changing operating conditions has grown and will further grow with the expanding use of renewable energy sources.



**Part IV.**

**Conclusion**



# 9. Conclusions and Future Research

## 9.1. Conclusions

The actual transition of power grids from centralized to decentralized power generation by fluctuating renewable energy sources produces many challenges for the stable operation of power systems. One approach to address the challenges is presented in this work by employing principles of system decomposition and hierarchy. The multi-level control approach accounts for the fast transients, (e.g. after severe grid faults,) while the upper layer proposes an integrating framework to coordinate the local control loops based on the LPVS on a coarser timescale.

To achieve this, polytopic and exact LPVS representations of the three types of components the SG, the DFIG-based WECS, and the PVS are derived. The modeling is one of the main contributions of this work, allowing the use of a unified control framework for all three types of generating units. By using this framework, robustness against grid changes and changes caused by the renewable power sources is achieved by the definition of the parameter ranges. Although, different LPVS representations were derived in the course of this work, a systematic technique for the derivation of LPVS representations could not be found. Each system had to be derived individually, based on the physical variables to be controlled. The controllability requirement, in connection with the required knowledge of the parameter ranges, is a difficulty for the formulation of a systematic technique. However, the ideas of hiding nonlinearities in parameters, of mapping the interconnections between the subsystems into parameter ranges, and the introduction of auxiliary variables to prevent zero row and columns, can be reused for the derivation of LPVS representations of other types of components, than of those considered in this thesis.

The number of parameters of the derived LPVS varies between 3 and 9 (for the PVS). This, however, is not a problem as the local controllers are designed offline by solving SDPs, while algebraic descriptions are used for the online implementation of the controllers. Even for the PVS, involving the largest number of parameters, the problem can still be solved within 30 s. By using modularization, the overall problem for the LPVS controller synthesis grows linearly with the number of components to be controlled. With the resulting LPVS controllers, different controller objectives can be conjunctively addressed. The involved LMI-based technique allows the definition of the desired closed-loop dynamics, i.e. velocity and damping of oscillations, while handling input constraints. This is a major benefit of the technique as most of the systems have physical limitations for the control input which need to

be considered. One requirement for the controller synthesis is the knowledge of the parameters. This motivates the need for the systematic calculation of the ranges and was addressed by the reachability analysis in [22] (as mentioned in Ch. 5.8). Due to the fact that the synthesis is carried out offline, the possibly time intensive computations of the reachability analysis are not critical. Alternatively, the ranges can be derived based on simulations. However, the use of the LPVS technique for all component allows a conclusion on grid-wide stability. This is a completely new approach compared to the isolated controller synthesis of each component and represents a major advantage.

The higher level controller coordinates the lower level controllers. Due to the use of the power system model within the MPC approach, physical limits of the grid can be exploited to achieve optimal control (in terms of the control objectives). The optimization of the centralized MPC is based on predictions for numerous variables. The resulting computation times of the optimization for large systems were not sufficiently evaluated in this work. This point should be further analyzed. A solution for growing optimization times for large system is proposed in the next section. However, the approach allows using predictions for all algebraic variables and, thus, allowing to impose constraints on them. In the simulation example, a  $\pm 10\%$  range around the nominal values of the bus voltages could be implemented by the MPC. This is a common requirement for grid-connected WECS and PVS [95]. The possibility of straightforward implementation of requirements formulated in grid codes is a major advantage of the approach. In this work, the MPC is used in the context of power systems. However, the approach presented in Ch. 7 can be used for systems, in which the modules are controlled by the presented LPV controllers. Stability is still ensured by the use of the parameter constraints. Furthermore, the MPC can also work for arbitrary systems modeled by DAEs. Similarly to the calculation of the parameters, the knowledge of many variables is necessary for the predictions for the MPC. This point can be attenuated by the growing use of phasor measurement units, improving power system monitoring [17]. These metering devices can measure voltages, currents, and frequencies at a rate of 30 or 60 samples per second [2].

One of the major challenges of power systems is the handling of different dynamics on different timescales. This challenge is addressed by the fast controllers on the lower level and the centralized MPC operating on a slower timescale. However, the MPC still accounts for the fast dynamics by using an adapted sampling time. This allows the use of the approach for power systems, while still ensuring stability of the complete grid. By coordinating the closed-loop systems on the lower level, a true integrating multi-level controller approach is presented, addressing the challenges introduced by the transition of power systems.

---

## 9.2. Future Research

Several aspects presented in this work may be further developed. These are aspects motivated by the models of power systems, or they concern the controller design.

- In this work, grids were simulated which either comprise SG and WECS, or PVS. This separation was motivated by the very fast dynamics of the PVS (compared to the SG and the WECS). It should be examined how the different dynamics of the controlled components affect the realization of the control objectives transient stability and voltage stability.
- Moreover, the execution of the MPC requires the knowledge of the involved variables for the calculation of the predictions. This point could be further evaluated, motivating research on observers in the case that some variables can not be measured (by phasor measurement units) or calculated from measurable variables.
- For some LPVS, the controllability of the derived model depends on the parameter ranges and was only confirmed during the controller synthesis. A systematic technique for finding parameter ranges which ensure controllability of an LPVS (without controller synthesis) is an open question for future research. This point can be further developed by considering LPVS which are interconnected to other LPVS by their parameter ranges. Furthermore, the controller synthesis for the local LPVS controllers should be extended to handling of constraints for the algebraic variables and by considering non-symmetric constraints for the inputs.
- As shown in Ch. 8.1, the used parameter ranges of the LPVS can be changed by the controller action of the MPC, requiring a recalculation of the ranges and the LPVS controllers. This can be avoided by an a-priori conservative choice of the parameter ranges. The reachability analysis, mentioned in Ch. 5, can be used and extended to the consideration of all possible controller actions of the MPC. Furthermore, the estimation of the linearization error could be integrated into the MPC, as well, to render the assumption 7.2 superfluous.
- Finally, in order to reduce computation time for the MPC for large systems (but to still allow low sampling times of a few seconds), the presented multi-level MPC with adapted sampling times could be realized as a distributed MPC. By decomposing the whole system into smaller subsystems comprising a few LPV controlled components, the optimization problem for each MPC would be reduced in size.



# Appendix A. Simulation Parameters

## A.1. Parameters of the Simulations in Chapter 6

Table A.1.: Parameter ranges of  $W_1$ ,  $G_2$ , and  $G_3$  for the controller synthesis in Ch. 6.1.

$\theta$		$W_1$		$G_2$		$G_3$	
		$\underline{\theta}$	$\bar{\theta}$	$\underline{\theta}$	$\bar{\theta}$	$\underline{\theta}$	$\bar{\theta}$
$\theta_c$	$\theta_1$	0.3000	0.6600	0.0320	0.1100	0.1000	0.6000
	$\theta_2$	0.0793	1.3428	0.5000	1.0500	0.4000	0.9000
	$\theta_3$	-17.0644	17.0644	0.4500	2	0.3400	1.5000
	$\theta_4$	-0.1100	0.0500	-	-	-	-
	$\theta_5$	0.1000	0.5000	-	-	-	-

Table A.2.: Parameter ranges of  $W_1$ ,  $G_2$ , and  $G_3$  for the controller synthesis in Ch. 6.2.

$\theta$		$W_1$		$G_2$		$G_3$	
		$\underline{\theta}$	$\bar{\theta}$	$\underline{\theta}$	$\bar{\theta}$	$\underline{\theta}$	$\bar{\theta}$
$\theta_c$	$\theta_1$	0.3000	0.6600	0.5000	1	0.1000	0.6000
	$\theta_2$	0.0793	1.3428	0.5000	1.0500	0.4000	0.9000
	$\theta_3$	-17.0644	17.0644	0.4500	1.6500	0.3400	1.5000
	$\theta_4$	-0.1100	0.0500	-	-	-	-
	$\theta_5$	0.1000	0.5000	-	-	-	-
$\theta_s$	$\theta_6$	-	-	0.0100	1	0.0100	1

Table A.3.: Power and voltage base units, used for the calculation in p.u. for the values in Table A.4.

Quantity	$S^{base}$	$V_{DC}^{base}$	$V_{AC,low}^{base}$	$V_{AC,high}^{base}$
Value	1.4MVA	480V	480V	6.6KV

Table A.4.: Distribution network, dynamic load and PVS parameters from [106] converted in *p.u.*, as used in Ch. 6.3 (see Table A.3 for the used base units).

Line Parameter	Value	PV Plant Parameter	Value
$L_1$ incl. $L_{T_1}$	$2.82e - 4$	$L$	$4.05e - 4$
$R_1$ incl. $R_{T_1}$	0.02	$R$	0.012
$L_2$	$1.69e - 5$	$C$	$7.41e - 5$
$R_2$	$2.81e - 5$	$C_{dc}$	0.0033
Load Parameter	Value	$I_{ph}$	0.4846
$L_l$	0.002	$I_s$	$7.24e - 9$
$R_l$	2.38	$\beta_{pv}$	6.45
$C_l$	$1.05e - 4$		

Table A.5.: Parameter ranges of the PVS for the controller synthesis in Ch. 6.3.

$\theta$	$\underline{\theta}$	$\bar{\theta}$	
$\theta_c$	$\theta_1$	0.2468	0.2749
	$\theta_2$	-3600	-3250
	$\theta_3$	-430	-150
	$\theta_4$	-0.2820	-0.2650
	$\theta_5$	-0.0093	0.0039
	$\theta_6$	0.0148	0.0519
$\theta_r$	$\theta_7$	0.0198	0.0225
	$\theta_8$	0.0014	0.0033
	$\theta_9$	1.9444	1.9615

Table A.6.: Parameter ranges of  $G_1$ ,  $G_2$ , and  $W_3$  for the controller synthesis in Ch. 6.4.

$\theta$	$G_1$		$G_2$		$W_3$		
	$\underline{\theta}$	$\bar{\theta}$	$\underline{\theta}$	$\bar{\theta}$	$\underline{\theta}$	$\bar{\theta}$	
$\theta_c$	$\theta_1$	9.9288	31.2048	0.0128	2.8160	0.0630	0.0880
	$\theta_2$	0.5400	0.9300	0.2500	2	0.0800	-0.0730
	$\theta_3$	2.2000	14	-1.200	6	-1	1.7000
	$\theta_4$	-	-	-	-	-0.1600	-0.1200

Table A.7.: Parameter ranges of  $G_1$ ,  $G_2$ , and  $G_3$  for the controller synthesis in Ch. 6.4.

$\theta$		$G_1$		$G_2$		$G_3$	
		$\underline{\theta}$	$\bar{\theta}$	$\underline{\theta}$	$\bar{\theta}$	$\underline{\theta}$	$\bar{\theta}$
$\theta_c$	$\theta_1$	0.2200	12	0.0380	1	0.3792	0.5298
	$\theta_2$	0.8000	0.9200	0.7200	1.0350	-0.4816	-0.4394
	$\theta_3$	-3.2000	4	0.7200	1	-1	1.7000
	$\theta_4$	-	-	-	-	-0.9424	-0.7068
$\theta_r$	$\theta_5$	-	-	-	-	0.5831	0.6421



# List of Symbols

## Acronyms

AVR	Automatic Voltage Regulator
DAE	Differential-Algebraic Equations
DFIG	Doubly-Fed Induction Generator
DFL	Direct Feedback Linearization
GSC	Grid Side Converter
LMI	Linear Matrix Inequality
LPVS	Linear Parameter-Varying System
LQR	Linear-Quadratic Regulator
MPC	Model Predictive Controller
MPP	Maximum Power Point
MPPT	Maximum Power Point Tracking
NMPC	Nonlinear Model Predictive Controller
ORH	Oriented Hyper-Rectangular Hull
PFL	Partial Feedback Linearization
PLL	Phase-Locked-Loop
PSS	Power System Stabilizer
PVS	Photovoltaic System
RSC	Rotor Side Converter
SDP	Semidefinite Program
SG	Synchronous Generator

SMIB	Single Machine Infinite Bus System
SVD	Single Value Decomposition
VSC	Voltage Source Converter
WECS	Wind Energy Conversion System

### General

$(\cdot)^T$	transpose of a matrix
$(\cdot)^{[h]}$	value of subsystem $h$
$(\cdot)^l$	value of input $l$
$H, H_1$	prediction horizons
$H_{sum}$	sum of the prediction horizons with $H_{sum} = H + H_1$
$T_d, T_{d,1}$	sampling times
$t_{calc}$	time for the calculation of the optimization for the MPC
$\ \cdot\ _2$	Euclidean norm of a matrix
$\ \cdot\ _\infty$	infinity norm of a matrix
$\Delta x$	difference vector of the actual value for $x$ and its equilibrium value $x_{ref}$ : $\Delta x^{[h]} = x^{[h]} - x_{ref}^{[h]}$
$\gamma$	upper bound on the infinity norm of $G_{zw}(s)$
$\otimes$	Kronecker product
$sat(\cdot)$	saturated value
$u_{LPV,real}$	real saturated input controlled by the LPV controller
$u_{LPV,sat}$	saturated value of the input controlled by the LPV controller as approximated by the hyperbolic tangent function
$u_{LPV}$	unsaturated input controlled by the LPV controller

### Grid Wide Variables

$\bar{s}_h$	complex power of bus $h$
$\bar{V}$	matrix representing the bus voltages on the diagonal

$\bar{v}^*$	vector of the conjugate complex bus voltages
$\bar{Y}$	admittance matrix
$\bar{y}_{hk}$	negative value of the sum of admittances connecting the buses $h$ and $k$
$\varphi_h$	phasor of the voltage of bus $h$
$b_f$	shunt conductance to simulate a fault
$g_f$	shunt susceptance to simulate a fault
$G_i$	synchronous generator $i$
$p_h$	active power of bus $h$
$q_h$	reactive power of bus $h$
$s_f$	factor for the change of a faulted impedance
$t_c$	clearing time of a fault
$t_f$	time of fault occurrence
$T_i$	transformer $i$
$v_h$	voltage of bus $h$
$W_i$	WECS $i$

### Variables of the PVS

$\rho_1, \rho_2, \rho_3, \gamma_p$	control parameters of the DC-voltage controller of the PVS
$\vartheta$	$p$ - $n$ junction temperature
$\xi_1, \xi_2, \text{ and } \xi_3$	controller parameters of the PLL
$C_{dc}$	DC-side capacitor
$e_d, e_q$	AC-side terminal voltages of the VSC
$i_{h,d}, i_{h,q}$	currents of transmission line connecting the PVS to the bus $h$
$i_{p,d}, i_{p,q}$	AC-side currents
$I_{ph}$	temperature adjusted short-circuit current of one PV string
$i_{pv}$	current of the overall PV-array

$I_s$	reverse saturation current caused by the $p$ - $n$ junction
$k_p, k_i$	control parameters of the current controllers of the PVS
$K_d, K_q$	control inputs of the PVS
$L, C$	AC-phase reactor and shunt capacitor
$N$	transformer ratio
$n_{pv,p}, n_{pv,s}$	PV-cells per string in parallel/series
$p_{dc}$	DC real power output of the VSC
$p_{pv}$	power generated by the PV array
$S$	solar irradiation
$v_{dc}$	DC-link voltage
$v_{h,d}, v_{h,q}$	dq-transforms of the bus voltage $v_h$

### Variables of the SG

$\delta$	rotor angle
$\omega$	angular velocity
$\Omega_b, \omega_b$	base synchronous / reference frequency
$\tau_e$	electrical torque
$\tau_m$	mechanical torque
$D$	damping coefficient
$e'_q$	transient voltage
$H$	inertia constant
$i_d, i_q$	machine currents
$K_A, T_A$	controller gain and time constant of the excitation system of the SG
$K_w, T_w$	gain and time constant of the washout filter of the PSS
$r_a$	armature resistance
$T'_{dO}$	d-axis open circuit transient time constant

$T_1, T_2, T_3, T_4$	time constants of the PSS
$v_d, v_q$	machine voltages
$v_f$	field voltage
$x'_d$	d-axis transient reactance
$x_d, x_q$	synchronous reactances

## Vectors, Matrices, and Sets

$u_{ref}$	reference value for the control input
$\underline{\theta}, \bar{\theta}$	vector of lower and upper bounds of a parameter vector
$f_{\theta_j}(x, z, u)$	analytic function to describe $\theta_j$ in terms of $x, z,$ and $u$
$[x_k, z_k, u_k]$	operating point of the state, the algebraic variable, and the control input used for linearization
$\alpha$	vector of barycentric coordinates with the components $\alpha_i, i \in \{1, \dots, n_v\}$
$\alpha_d, \beta_d$	matrices to define a complex plane
$\lambda_{max}$	largest absolute eigenvalue
$\mathbf{C}', \mathbf{D}',$ and $\mathbf{G}'$	overall prediction matrices with adapted sampling times
$\mathbf{C}_1, \mathbf{D}_1,$ and $\mathbf{G}_1$	prediction matrices (with sampling time $T_{d,1}$ )
$\mathbf{C}_p, \mathbf{D}_p,$ and $\mathbf{G}_p$	prediction matrices for variables $y_p$ which are not part of the controlled variables $y$ (with sampling time $T_d$ )
$\mathbf{C}, \mathbf{D},$ and $\mathbf{G}$	prediction matrices (with sampling time $T_d$ )
$\mathbf{Q}$	weighting matrix for the output for the complete prediction horizon
$\mathbf{R}$	weighting matrix for the input for the complete prediction horizon
$\mathbf{u}'_k$	prediction matrix for the control inputs with adapted sampling times
$\mathbf{u}_k, \mathbf{u}_k^*$	prediction matrix for the control inputs and a vector with their optimal values, as calculated by the MPC

$\mathbf{y}'_{\mathbf{k}}$	prediction matrix for the controlled variables with adapted sampling times
$\mathbf{y}_{\mathbf{k}}$	prediction matrix for the controlled variables
$\mathcal{A}$	polytopic representation of $A(\theta)$ for $\theta \in [\underline{\theta}, \bar{\theta}]$
$\mathcal{A}_{cl}$	polytopic representation of $A_{cl}(\theta)$ for $\theta \in [\underline{\theta}, \bar{\theta}]$
$\mathcal{B}$	polytopic representation of $B(\theta)$ for $\theta \in [\underline{\theta}, \bar{\theta}]$
$\mathcal{B}_s$	polytopic representation of $B_s(\theta_s)$ for $\theta \in [\underline{\theta}, \bar{\theta}]$
$\mathcal{E}$	invariant ellipsoid with $\mathcal{E} = \{x \mid x^T P x \leq 1\}$
$\mathcal{K}$	polytopic representation of $K(\theta)$ for $\theta \in [\underline{\theta}, \bar{\theta}]$
$\mathcal{Y}$	linearizing polytopic variable with $\mathcal{K}X$
$\mu$	pole of a system
$\theta$	parameter vector of an LPVS with components $\theta_j, j \in \{1, \dots, n_p\}$
$\theta_c$	parameter vector to parametrize the LPV state-feedback controller $K(\theta_c)$
$\Theta_i$	coordinates of a vertex corresponding to one $\alpha_i$ in terms of the parameter ranges
$\theta_r$	parameter vector to parametrize the input matrix $B(\theta_r)$
$\theta_s$	auxiliary parameter vector to describe the level of saturation of the inputs
$\varphi_d$	the angle between the real-axis and the line crossing zero (to define the conic sector)
$\tilde{A}_j$	matrix of the affine description for $A(\theta), j \in \{1, \dots, n_p\}$
$A, B, F, C, D,$ and $G$	matrices defining linear dynamics (discrete-time)
$A(\theta), B(\theta), C(\theta),$ and $D(\theta)$	matrices defining the dynamics of a LPVS
$A_c, B_c, F_c, C_c, D_c,$ and $G_c$	matrices defining linear dynamics (continuous-time)
$A_i$	vertex of the polytope $\mathcal{A}, i \in \{1, \dots, n_v\}$
$A_{cl,i}, A_{cl,p}$	vertex of the polytope $\mathcal{A}_{cl}$
$A_{cl}(\theta)$	state-matrix of a closed-loop LPVS

$B_j$	vertex of the polytope $\mathcal{B}$ , $j \in \{1, \dots, n_b\}$
$B_s(\theta_s)$	auxiliary input matrix
$B_{s,k}$	vertex of the polytope $\mathcal{B}_s$ , $k \in \{1, \dots, n_s\}$
$f_{\alpha_i}(\theta)$	analytic function to describe the barycentric coordinate $\alpha_i$ in terms of $\theta$
$K$	state-feedback controller matrix
$K(\theta), K(\theta_c)$	LPV state-feedback controller
$K_i$	vertex of the polytope $\mathcal{K}$ , $i \in \{1, \dots, n_v\}$
$P$	matrix of the Lyapunov function $V(x) = x^T P x$
$Q_l$	weighting matrix for the output of the controlled system for the prediction for time $l$
$R_l$	weighting matrix for the input of the controlled system for the prediction for time $l$
$u$	input vector of a dynamic system, $u \in \mathbb{R}^{n_u}$
$u_{min}, u_{max}$	constraints for the control inputs (calculated by the MPC)
$X$	inverse of $P$ : $P = X^{-1}$
$x$	state vector of a dynamic system, $x \in \mathbb{R}^{n_x}$
$y$	output vector of a dynamic system, $y \in \mathbb{R}^{n_y}$
$Y_i$	vertex of the polytope $\mathcal{Y}$ , $Y_i = K_i X$
$y_p$	predicted variables which are not part of the controlled variables $y$
$y_{min}, y_{max}$	constraints for the controlled variables (controlled by the MPC)
$z$	vector of algebraic variables of a dynamic system, $z \in \mathbb{R}^{n_z}$

### Variables of the DFIG-based WECS

$\omega_m$	rotor angular velocity
$\omega_s$	stator angular velocity
$\omega_{sh}$	shaft speed

## List of Symbols

---

$\psi_{r,d}, \psi_{r,q}$	rotor fluxes
$H_m$	sum of turbine and rotor inertia
$i_{r,q}, i_{r,d}$	rotor currents
$i_{s,d}, i_{s,q}$	stator currents
$K_{P,i}, K_{I,i}$	controller gains of the active and reactive power controllers of the WECS
$P_B$	base power
$r_r, r_s$	rotor / stator resistances
$s$	slip
$T_m, T_{el}$	mechanical / electrical torque
$v_{r,d}, v_{r,q}$	rotor voltages
$v_{s,d}, v_{s,q}$	stator voltages
$x_\mu$	magnetizing reactance
$x_r, x_s$	rotor / stator reactances
$x_{s,\mu}, x_{r,\mu}$	$x_{s,\mu} = x_s + x_\mu, x_{r,\mu} = x_r + x_\mu$

# References

- [1] M. Abbes and J. Belhadj, “New control method of a robust NPC converter for renewable energy sources grid connection,” *Electric Power Systems Research*, vol. 88, pp. 52–63, 2012.
- [2] J. Aho, M. Amin, A. M. Annaswamy, G. Arnold, A. Buckspan, A. Cadena, D. Callaway, E. Camacho, M. Caramanis, A. Chakraborty *et al.*, “Smart grid research: Control systems-IEEE vision for smart grid controls: 2030 and beyond,” 2013.
- [3] R. Amgai, J. Shi, and S. Abdelwahed, “Lookahead control based framework for power system applications,” in *North American Power Symposium (NAPS), 2012*. IEEE, 2012, pp. 1–6.
- [4] R. Amgai, J. Shi, and S. Abdelwahed, “An integrated lookahead control-based adaptive supervisory framework for autonomic power system applications,” *Int. Journal of Electrical Power & Energy Systems*, vol. 63, pp. 824–835, 2014.
- [5] P. M. Anderson and A. A. Fouad, *Power system control and stability*. Wiley-Interscience, 2003.
- [6] P. Apkarian, P. Gahinet, and G. Becker, “Self-scheduled  $H_\infty$  control of linear parameter-varying systems: a design example,” *Automatica*, vol. 31, no. 9, pp. 1251–1261, 1995.
- [7] L. Asselborn, D. Gross, and O. Stursberg, “Control of uncertain nonlinear systems using ellipsoidal reachability calculus,” in *9th IFAC Symp. on Nonlinear Control Systems*, 2013.
- [8] B. Bamieh and L. Giarré, “Identification of linear parameter varying models,” *Int. Journal of Robust and Nonlinear Control*, vol. 12, no. 9, pp. 841–853, 2002.
- [9] T. Besselmann, J. Lofberg, and M. Morari, “Explicit MPC for LPV systems: Stability and optimality,” *Tr. on Automatic Control*, vol. 57, no. 9, pp. 2322–2332, 2012.
- [10] S. P. Boyd, L. El Ghaoui, E. Feron, and V. Balakrishnan, *Linear matrix inequalities in system and control theory*. SIAM, 1994, vol. 15.

- [11] C. Briat, *Linear parameter-varying and time-delay systems*. Springer, 2014, vol. 3.
- [12] F. Bünger, “A note on the boundary shape of matrix polytope products.” *Reliable Computing*, vol. 20, pp. 73–88, 2014.
- [13] Y.-Y. Cao, Z. Lin, and Y. Shamash, “Set invariance analysis and gain-scheduling control for LPV systems subject to actuator saturation,” *Systems & Control Letters*, vol. 46, no. 2, pp. 137–151, 2002.
- [14] R. Cardenas, R. Pena, S. Alepuz, and G. Asher, “Overview of control systems for the operation of DFIGs in wind energy applications,” *IEEE Tr. on Industrial Electronics*, vol. 60, no. 7, pp. 2776–2798, 2013.
- [15] M. Chilali and P. Gahinet, “ $H_\infty$  design with pole placement constraints: an LMI approach,” *IEEE Tr. on Automatic Control*, vol. 41, no. 3, pp. 358–367, 1996.
- [16] M. A. Chowdhury, M. A. Mahmud, W. Shen, and H. R. Pota, “Nonlinear controller design for series-compensated DFIG-based wind farms to mitigate subsynchronous control interaction,” *Tr. on Energy Conversion*, vol. 32, no. 2, pp. 707–719, 2017.
- [17] J. De La Ree, V. Centeno, J. S. Thorp, and A. G. Phadke, “Synchronized phasor measurement applications in power systems,” *IEEE Tr. on Smart Grid*, vol. 1, no. 1, pp. 20–27, 2010.
- [18] R. V. de Oliveira, R. A. Ramos, and N. G. Bretas, “An algorithm for comp. automatic tuning of power system stabilizers,” *Control Eng. Practice*, vol. 18, no. 1, pp. 45–54, 2010.
- [19] A.-L. Do, O. Sename, and L. Dugard, “An LPV control approach for semi-active suspension control with actuator constraints,” in *American Control Conf. (ACC)*. IEEE, 2010, pp. 4653–4658.
- [20] J. L. Domínguez-García, O. Gomis-Bellmunt, F. D. Bianchi, and A. Sumper, “Power oscillation damping supported by wind power: a review,” *Renewable and Sustainable Energy Reviews*, vol. 16, no. 7, pp. 4994–5006, 2012.
- [21] A. Edris, “Proposed terms and definitions for flexible AC transmission system (FACTS),” *IEEE Tr. on Power Delivery*, vol. 12, no. 4, 1997.
- [22] A. El-Guindy, B. Schürmann, M. Althoff, K. Schaab, , and O. Stursberg, “Formal LPV control for transient stability of power systems,” in *IEEE PES General Meeting*, 2017.

- 
- [23] M. Eremia and M. Shahidehpour, *Handbook of electrical power system dynamics: modeling, stability, and control*. John Wiley & Sons, 2013, vol. 92.
- [24] L. Fan, “Review of robust feedback control applic. in power systems,” in *IEEE Power Systems Conf.*, 2009, pp. 1–7.
- [25] L. Fan, H. Yin, and Z. Miao, “On active/reactive power modulation of DFIG-based wind generation for interarea oscillation damping,” *Tr. on Energy Conversion*, vol. 26, no. 2, pp. 513–521, 2011.
- [26] L. M. Fernández, F. Jurado, and J. R. Saenz, “Aggregated dynamic model for wind farms with doubly fed induction generator wind turbines,” *Renewable energy*, vol. 33, no. 1, pp. 129–140, 2008.
- [27] R. Findeisen and F. Allgöwer, *Nonlinear Model Predictive Control for Index—one DAE Systems*. Basel: Birkhäuser Basel, 2000, pp. 145–161.
- [28] G. Fusco and M. Russo, “Nonlinear control design for excitation controller and power system stabilizer,” *Control Eng. Practice*, vol. 19, no. 3, pp. 243–251, 2011.
- [29] P. Gahinet, P. Apkarian, and M. Chilali, “Affine parameter-dependent lyapunov functions and real parametric uncertainty,” *Tr. on Automatic control*, vol. 41, no. 3, pp. 436–442, 1996.
- [30] D. Gautam, V. Vittal, and T. Harbour, “Impact of increased penetration of DFIG-based wind turbine generators on transient and small signal stability of power systems,” *Tr. on Power Systems*, vol. 24, no. 3, pp. 1426–1434, 2009.
- [31] B. Gong and I. Hiskens, “A stable finite horizon model predictive control for power system voltage collapse prevention,” in *IEEE Conf. on Decision and Control and European Control Conf. (CDC-ECC)*. IEEE, 2011, pp. 7105–7110.
- [32] M. Gordon and D. Hill, “Global transient stability and voltage regulation for multimachine power systems,” in *Conversion and Delivery of Electrical Energy in the 21st Century*, 2008, pp. 1–8.
- [33] R. He, K.-Z. Liu, and S. Mei, “LPV modelling and gain-scheduled control approach for the transient stabilization of power systems,” in *4th IEEE Conf. on Ind. Electronics and Applications*, may 2009, pp. 29–34.
- [34] R. He, K.-Z. Liu, S. Mei, and X. Gui, “A gain-scheduled state feedback control method for transient stability control of a single-machine infinite-bus power system,” in *IEEE Chinese Control Conf.*, 2006, pp. 2147–2152.

- [35] C. Hoffmann and H. Werner, “A survey of linear parameter-varying control applications validated by experiments or high-fidelity simulations,” *Tr. on Control Systems Technology*, vol. 23, no. 2, pp. 416–433, 2015.
- [36] M. Hossain, H. R. Pota, M. A. Mahmud, and M. Aldeen, “Robust control for power sharing in microgrids with low-inertia wind and pv generators,” *Tr. on Sustainable Energy*, vol. 6, no. 3, pp. 1067–1077, 2015.
- [37] T. Hu and Z. Lin, *Control systems with actuator saturation: analysis and design*. Springer Science & Business Media, 2001.
- [38] F. M. Hughes, O. Anaya-Lara, N. Jenkins, and G. Strbac, “Control of DFIG-based wind generation for power network support,” *IEEE Tr. on Power Systems*, vol. 20, no. 4, pp. 1958–1966, 2005.
- [39] F. M. Hughes, O. Anaya-Lara, N. Jenkins, and G. Strbac, “A power system stabilizer for DFIG-based wind generation,” *IEEE Tr. on Power Systems*, vol. 21, no. 2, pp. 763–772, 2006.
- [40] F. A. Inthamoussou, F. D. Bianchi, H. De Battista, and R. J. Mantz, “LPV wind turbine control with anti-windup features covering the complete wind speed range,” *IEEE Tr. on Energy Conversion*, vol. 29, no. 1, pp. 259–266, 2014.
- [41] P. Kundur, *Power System Stability and Control*. McGraw-Hill, 1994.
- [42] P. Kundur, J. Paserba, V. Ajjarapu, G. Andersson, A. Bose, C. Canizares, N. Hatziargyriou, D. Hill, A. Stankovic, C. Taylor, T. Van Cutsem, and V. Vittal, “Definition and classification of power system stability,” *IEEE Tr. on Power Systems*, vol. 19, no. 2, pp. 1387–1401, 2004.
- [43] M. Kvasnica, P. Grieder, M. Baotić, and M. Morari, “Multi-parametric toolbox (MPT),” in *Int. Workshop on Hybrid Systems: Computation and Control*. Springer, 2004, pp. 448–462.
- [44] A. Kwiatkowski, M.-T. Boll, and H. Werner, “Automated generation and assessment of affine LPV models,” in *45th IEEE Conf. on Decision and Control*, 2006, pp. 6690–6695.
- [45] A. Kwiatkowski, S. Trimpe, and H. Werner, “Less conservative polytopic LPV models for charge control by combining parameter set mapping and set intersection,” in *46th IEEE Conf. on Decision and Control*. IEEE, 2007, pp. 3363–3368.
- [46] A. Kwiatkowski and H. Werner, “PCA-based parameter set mappings for LPV models with fewer parameters and less overbounding,” *Tr. on Control Systems Technology*, vol. 16, no. 4, pp. 781–788, 2008.

- 
- [47] D. Lalili, A. Mellit, N. Lourci, B. Medjahed, and C. Boubakir, "State feedback control and variable step size MPPT algorithm of three-level grid-connected photovoltaic inverter," *Solar Energy*, vol. 98, pp. 561–571, 2013.
- [48] J. H. Lee, "Model predictive control: Review of the three decades of development," *International Journal of Control, Automation and Systems*, vol. 9, no. 3, pp. 415–424, 2011.
- [49] P. Li, B. Zhang, L. Cheng, Z. Bo, and A. Klimek, "Study on the coordinated voltage control with the distributed model prediction," in *Power and Energy Society General Meeting*. IEEE, 2010, pp. 1–6.
- [50] M. Liserre, R. Cardenas, M. Molinas, and J. Rodriguez, "Overview of multi-mw wind turbines and wind parks," *IEEE Tr. on Industrial Electronics*, vol. 58, no. 4, pp. 1081–1095, 2011.
- [51] H. Liu, Z. Hu, and Y. Song, "Lyapunov-based decentralized excitation control for global asymptotic stability and voltage regulation of multi-machine power systems," *IEEE Tr. on Power Systems*, vol. 27, no. 4, pp. 2262–2270, 2012.
- [52] Q. Liu, V. Vittal, and N. Elia, "Expansion of system operating range by an interpolated LPV FACTS controller using multiple Lyapunov functions," *IEEE Tr. on Power Systems*, vol. 21, no. 3, pp. 1311–1320, 2006.
- [53] Q. Liu, V. Vittal, and N. Elia, "LPV supplementary damping controller design for a thyristor controlled series capacitor device," *IEEE Tr. on Power Systems*, vol. 21, no. 3, pp. 1242–1249, 2006.
- [54] Y. Lu and Y. Arkun, "Quasi-min-max MPC algorithms for LPV systems," *Automatica*, vol. 36, no. 4, pp. 527–540, 2000.
- [55] M. Ma, H. Chen, X. Liu, and F. Allgöwer, "Distributed model predictive load frequency control of multi-area interconnected power system," *Int. Journal of Electrical Power & Energy Systems*, vol. 62, pp. 289–298, 2014.
- [56] J. M. Maciejowski, *Predictive control: with constraints*. Pearson Education, 2002.
- [57] A. Mahesh and K. S. Sandhu, "Hybrid wind/photovoltaic energy system developments: Critical review and findings," *Renewable and Sustainable Energy Reviews*, vol. 52, pp. 1135–1147, 2015.
- [58] M. Mahmud, M. Hossain, H. Pota, and A. M. Oo, "Robust partial feedback linearizing excitation controller design for multimachine power systems," *Tr. on Power Systems*, vol. 32, no. 1, pp. 3–16, 2017.

- [59] M. Mahmud, H. Pota, M. Aldeen, and M. Hossain, "Partial feedback linearizing excitation controller for multimachine power systems to improve transient stability," *Tr. on Power Systems*, vol. 29, no. 2, pp. 561–571, 2014.
- [60] M. Mahmud, H. Pota, and M. Hossain, "Dynamic stability of three-phase grid-connected photovoltaic system using zero dynamic design approach," *Journal of Photovoltaics*, vol. 2, no. 4, pp. 564–571, 2012.
- [61] M. Mahmud, H. Pota, M. Hossain, and N. Roy, "Robust partial feedback linearizing stabilization scheme for three-phase grid-connected photovoltaic systems," *Journal of photovoltaics*, vol. 4, no. 1, pp. 423–431, 2014.
- [62] Z. Miao, L. Fan, D. Osborn, and S. Yuvarajan, "Control of DFIG-based wind generation to improve interarea oscillation damping," *IEEE Tr. on Energy Conversion*, vol. 24, no. 2, pp. 415–422, 2009.
- [63] F. Milano, *Power System Modelling and Scripting*, ser. Power Systems. Springer, 2010.
- [64] Y. Mishra, S. Mishra, M. Tripathy, N. Senroy, and Z. Dong, "Improving stability of a DFIG-based wind power system with tuned damping controller," *IEEE Tr. on Energy Conversion*, vol. 24, no. 3, pp. 650–660, 2009.
- [65] J. Mohammadpour and C. Scherer, *Control of Linear Parameter Varying Systems with Applications*, J. Mohammadpour and C. Scherer, Eds. Springer, 2012.
- [66] E. B. Muhando, T. Senjyu, A. Uehara, and T. Funabashi, "Gain-scheduled control for WECS via LMI techniques and parametrically dependent feedback part ii: Controller design and implementation," *IEEE Tr. on Industrial Electronics*, vol. 58, no. 1, pp. 57–65, 2011.
- [67] R. Negenborn, "Multi-agent model predictive control with applications to power networks," Dissertation, Delft Univ. of Technology, 2007.
- [68] R. Negenborn, A. Becuti, T. Demiray, S. Leirens, G. Damm, B. De Schutter, and M. Morari, "Supervisory hybrid model predictive control for voltage stability of power networks," in *American Control Conf.*, 2007, pp. 5444–5449.
- [69] M. Q. Nguyen, J. M. G. da Silva, O. Sename, and L. Dugard, "Semi-active suspension control problem: some new results using an LPV/ $H_\infty$  state feedback input constrained control," in *54th IEEE Conf. on Decision and Control (CDC)*, 2015.
- [70] M. V. Nunes, J. Lopes, H. H. Zörn, U. H. Bezerra, and R. G. Almeida, "Influence of the variable-speed wind generators in transient stability margin of the conventional generators integrated in electrical grids," *Tr. on Energy Conversion*, vol. 19, no. 4, pp. 692–701, 2004.

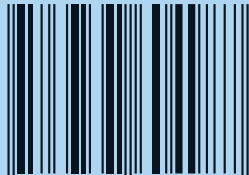
- 
- [71] E. Pouresmaeil, D. Montesinos-Miracle, and O. Gomis-Bellmunt, "Control scheme of three-level NPC inverter for integration of renewable energy resources into AC grid," *IEEE systems journal*, vol. 6, no. 2, pp. 242–253, 2012.
- [72] C. Pousot-Vassal, O. Sename, L. Dugard, P. Gaspar, Z. Szabo, and J. Bokor, "A new semi-active suspension control strategy through lpv technique," *Control Engineering Practice*, vol. 16, no. 12, pp. 1519–1534, 2008.
- [73] W. Qi, J. Liu, X. Chen, and P. D. Christofides, "Supervisory predictive control of standalone wind/solar energy generation systems," *Tr. on control systems technology*, vol. 19, no. 1, pp. 199–207, 2011.
- [74] W. Qiu, V. Vittal, and M. Khammash, "Decentralized power system stabilizer design using linear parameter varying approach," *IEEE Tr. on Power Systems*, vol. 19, no. 4, pp. 1951 – 1960, 2004.
- [75] R. Quirynen, M. Vukov, and M. Diehl, "Auto generation of implicit integrators for embedded NMPC with microsecond sampling times," *IFAC Proceedings Volumes*, vol. 45, no. 17, pp. 175–180, 2012.
- [76] K. Rao and S. Paul, "Design of robust power system stabilizer using mixed sensitivity based  $H_\infty$  output-feedback control in LMI framework," in *Conf. on Sustainable Energy and Intelligent Systems*, 2011, pp. 403–408.
- [77] P. S. Rao and I. Sen, "Robust pole placement stabilizer design using linear matrix inequalities," *IEEE Tr. on Power Systems*, vol. 15, no. 1, pp. 313–319, 2000.
- [78] D. Rotondo, F. Nejjari, and V. Puig, "FTC design for polytopic LPV systems subject to actuator saturations," in *20th Mediterranean Conf. on Control & Automation (MED)*. IEEE, 2012, pp. 524–529.
- [79] D. Rotondo, F. Nejjari, and V. Puig, "A shifting pole placement approach for the design of parameter-scheduled state-feedback controllers," in *Proc. European Control Conf.*, 2013, pp. 1829–1834.
- [80] D. Rotondo, F. Nejjari, V. Puig, and J. Blesa, "Model reference FTC for LPV systems using virtual actuators and set-membership fault estimation," *Int. Journal of Robust and Nonlinear Control*, vol. 25, no. 5, pp. 735–760, 2015.
- [81] K. Schaab and O. Stursberg, "Decentralized robust control of power grids using LPV-models of DAE-systems," in *1<sup>st</sup> IFAC Workshop on Linear-Parameter-Varying Systems*, 2015, pp. 418–423.
- [82] K. Schaab and O. Stursberg, "Robust decentralized LPV control for transient stability of power systems," in *9<sup>th</sup> IFAC Symposium on Control of Power and Energy Systems*, 2015, pp. 566–571.

- [83] K. Schaab, J. Hahn, M. Wolkov, and O. Stursberg, “Robust control for voltage and transient stability of power grids relying on wind power,” *Control Engineering Practice*, vol. 60, pp. 7–17, 2017.
- [84] B. Schürmann, A. El-Guindy, and M. Althoff, “Closed-form expressions of convex combinations,” in *American Control Conf.* IEEE, 2016, pp. 2795–2801.
- [85] M. A. Sehr, A. P. Pandey, and M. C. de Oliveira, “Robust stabilization of linear continuous-time parameter-varying systems without quadratic stability,” in *American Control Conf.* IEEE, 2015, pp. 108–113.
- [86] R. Shah, N. Mithulananthan, R. Bansal, and V. Ramachandaramurthy, “A review of key power system stability challenges for large-scale pv integration,” *Renewable and Sustainable Energy Reviews*, vol. 41, pp. 1423–1436, 2015.
- [87] R. Shah, N. Mithulananthan, and K. Y. Lee, “Large-scale PV plant with a robust controller considering power oscillation damping,” *Tr. on Energy Conversion*, vol. 28, no. 1, pp. 106–116, 2013.
- [88] J. S. Shamma, “Analysis and design of gain scheduled control systems,” Ph.D. dissertation, Massachusetts Institute of Technology, 1988.
- [89] J. S. Shamma and M. Athans, “Guaranteed properties of gain scheduled control for linear parameter-varying plants,” *Automatica*, vol. 27, no. 3, pp. 559–564, 1991.
- [90] H. Shayeghi, H. Shayanfar, S. Jalilzadeh, and A. Safari, “Multi-machine power system stabilizers design using chaotic optimization algorithm,” *Energy Conversion and Management*, vol. 51, no. 7, pp. 1572–1580, 2010.
- [91] J. Sjöberg, R. Findeisen, and F. Allgöwer, “Model predictive control of continuous time nonlinear differential algebraic systems,” *IFAC Proceedings Volumes*, vol. 40, no. 12, pp. 48–53, 2007.
- [92] O. Stursberg and B. H. Krogh, “Efficient representation and computation of reachable sets for hybrid systems,” in *Int. Workshop on Hybrid Systems: Computation and Control.* Springer, 2003, pp. 482–497.
- [93] H. Taheri, O. Akhrif, and A. F. Okou, “Nonlinear frequency and voltage regulation in a PV-battery-diesel microgrid,” *8th Int. Conf. and Exhibition on Ecological Vehicles and Renewable Energies*, pp. 1–6, March 2013.
- [94] S. Tarbouriech, G. Garcia, J. M. G. da Silva Jr, and I. Queinnec, *Stability and stabilization of linear systems with saturating actuators.* Springer Science & Business Media, 2011.

- 
- [95] R. Teodorescu, M. Liserre, and P. Rodriguez, *Grid converters for photovoltaic and wind power systems*. John Wiley & Sons, 2011, vol. 29.
- [96] M. Theißen, K. Schaab, and O. Stursberg, “Voltage stability of power grids with PV plants using robust LPV-control,” in *Control of Transmission and Distribution Smart Grids*, 2016.
- [97] H. N. Tien, C. W. Scherer, J. M. Scherpen, and V. Müller, “Linear parameter varying control of doubly fed induction machines,” *Tr. on Industrial Electronics*, vol. 63, no. 1, pp. 216–224, 2016.
- [98] H. Tien, C. Scherer, and J. M. A. Scherpen, “Robust performance of self-scheduled LPV control of doubly-fed induction generator in wind energy conversion systems,” in *Conf. Power Electronics and Applic.*, 2007, pp. 1–10.
- [99] R. Tóth, *Modeling and identification of linear parameter-varying systems, Vol. 403*. Springer Science & Business Media, 2010.
- [100] N. Van Deelen, A. Jokić, P. Van den Bosch, and R. M. Hermans, “Exploiting inertia of wind turbines in power network frequency control: A model predictive control approach,” in *Int. Conf. on Control Applications*. IEEE, 2011, pp. 1309–1314.
- [101] A. Venkat, I. Hiskens, J. Rawlings, and S. Wright, “Distributed mpc strategies with application to power system automatic generation control,” *IEEE Tr. on Control Systems Technology*, vol. 16, no. 6, pp. 1192–1206, 2008.
- [102] C. Wang and G. Weiss, “Linear parameter varying control of a doubly fed induction generator based wind turbine with primary grid frequency support,” *Int. Journal of Robust and Nonlinear Control*, vol. 24, no. 14, pp. 1927–1946, 2014.
- [103] J. Warren, S. Schaefer, A. N. Hirani, and M. Desbrun, “Barycentric coordinates for convex sets,” *Advances in computational mathematics*, vol. 27, no. 3, pp. 319–338, 2007.
- [104] H. Werner, P. Korba, and T. C. Yang, “Robust tuning of power system stabilizers using LMI-techniques,” *IEEE Tr. on Control Systems Techn.*, vol. 11, no. 1, pp. 147–152, 2003.
- [105] F. Wu, K. M. Grigoriadis, and A. Packard, “Anti-windup controller design using linear parameter-varying control methods,” *Int. Journal of Control*, vol. 73, no. 12, pp. 1104–1114, 2000.
- [106] A. Yazdani and P. Dash, “A control methodology and characterization of dynamics for a photovoltaic (PV) system interfaced with a distribution network,” *Tr. on Power Delivery*, vol. 24, no. 3, pp. 1538–1551, 2009.

- [107] A. Yazdani, A. R. Di Fazio, H. Ghoddami, M. Russo, M. Kazerani, J. Jatskevich, K. Strunz, S. Leva, and J. A. Martinez, “Modeling guidelines and a benchmark for power system simulation studies of three-phase single-stage photovoltaic systems,” *Tr. on Power Delivery*, vol. 26, no. 2, pp. 1247–1264, 2011.
- [108] A. Yazdani and R. Iravani, “An accurate model for the DC-side voltage control of the neutral point diode clamped converter,” *Tr. on Power Delivery*, vol. 21, no. 1, pp. 185–193, 2006.
- [109] S. Yu, C. Böhm, H. Chen, and F. Allgöwer, “Model predictive control of constrained LPV systems,” *Int. Journal of Control*, vol. 85, no. 6, pp. 671–683, 2012.

ISBN 978-3-7376-0498-7



9 783737 604987 >